2014

Stochastic Activation of Enhancers in the Innate Immune Response by the Histone Demethylase JMJD2D

Rohit Chandwani

STOCHASTIC ACTIVATION OF ENHANCERS IN THE INNATE IMMUNE RESPONSE BY THE HISTONE DEMETHYLASE JMJD2D

A Thesis Presented to the Faculty of

The Rockefeller University

in Partial Fulfillment of the Requirements for

the degree of Doctor of Philosophy

by

Rohit Chandwani, M.D.

June 2014

STOCHASTIC ACTIVATION OF ENHANCERS IN THE INNATE IMMUNE RESPONSE BY THE HISTONE DEMETHYLASE JMJD2D

Rohit Chandwani, M.D., Ph.D.

The Rockefeller University 2014

The architecture of chromatin is complex and plays a substantial role in all of the biological processes involving DNA. In particular, transcriptional activation depends on the interplay of dozens of chromatin modifiers to establish an epigenetic landscape permissive of gene transcription. Among the most dynamic histone modifications are the acetylation and methylation at histone 3 lysine 9, but the precise roles of their modifiers in conserved transcriptional programs remain unknown.

Using the poly I:C-induced transcriptional response in MEFs as our model, we find that JMJD2d is a positive regulator of type I interferon responses. siRNA-depletion of the H3K9 demethylase JMJD2d attenuates gene activation and overexpression of JMJD2d potentiates the IFN response. We find that the underlying mechanism involves the activation of enhancers – knockdown of JMJD2d attenuates stimulus-induced enhancer activation, which is normally characterized by the accumulation of acetylated H3K9 and

increased enhancer RNA transcription. In short, JMJD2d appears to control IFN responses by enabling the transition of enhancers from 'poised' (H3K9me^3) to 'active' (H3K9ac) that allows for eRNA production. In support of this hypothesis, we observe that JMJD2d is tightly associated with enhancers in the genome and preferentially binds active enhancer regions. Taken together, JMJD2d represents the first example of a chromatin modifier with enhancer specificity and emerges as a potential therapeutic target in the modulation of IFN responses.

Acknowledgments

First and foremost, my deepest thanks to my advisor, Sasha Tarakhovsky, for the opportunity to embark on this journey five years ago. I will always appreciate the direction, support, and independence I received as I grew as a scientist. In addition to Sasha, it has been an honor to discuss my work over the years with my committee members, Charlie Rice, Sasha Rudensky, and Sarah Schlesinger. I am truly grateful for their unwavering support of my efforts to complete my training. I am also indebted to Dinshaw Patel for serving as a reader for my thesis defense. My warmest thanks to past and present members of the Tarakhovsky laboratory – Marie Chen, Marc Dobenecker, Laura Donlin, Terry Fang, Ron Gejman, Jessica Ho, Kate Jeffrey, Ivan Marazzi, Jonas Marcello, Rebecca Rizzo, Eugene Rudensky, Angela Santana, Uwe Schaefer, and Slava Yurchenko – without whom I would never have learned to do a single experiment. The expertise, advice, and friendship were as integral to my learning experience as anything else. I am thankful to Scott Dewell for his tireless efforts to tackle all the data. I am also grateful to Sid Strickland, Emily Harms, Marta Delgado, and everyone in the Dean's Office for allowing me this unconventional path and for their patience and support. Perhaps most importantly, I am deeply indebted to Barry Coller for both the opportunity to come to Rockefeller in the first place and his ongoing support through the years. And I am indebted to everyone in the Department of Surgery at Columbia for letting me go on this prolonged hiatus. Finally, I owe everything to my parents, Dilip and Sulachni Chandwani, and to my wife, Serre-Yu Wong. They are why I am here.

Table of Contents

List of Figures

List of Tables

Chapter I: Introduction

Host defense and stochastic type I interferon signaling

Host defense is crucial to the survival of a species. In the type I interferon response, which is a central antiviral defense mechanism, IFN-α/β (IFN) is secreted to initiate a complex innate and adaptive immune response against bacterial pathogens and viruses. At the heart of this response is the coordinated activation of a specific transcriptional program.

The first step leading to IFN activation begins with a signal from the cell surface or from the cytoplasm. Typically, the production of IFN is elaborated following recognition of viral nucleic acids by specific receptors that are either membrane-associated (TLR3, TLR 7, TLR9) or cytoplasmic (RIG-I, MDA-5) (Bowie and Unterholzner, 2008). In endosomes and on specialized cells, the Toll-like receptor family consists of receptors with unique specificities. TLR3 recognizes dsRNA, TLR9 recognizes CpG dinucleotides, and TLR7 detects ssRNA. Largely, TLRs are expressed in cells of the immune system, such as macrophages and dendritic cells.

The cytoplasmic pattern recognition receptors (PRRs), by contrast, are ubiquitous, existing in almost all nucleated cells. RIG-I is responsible for the recognition of short dsRNA or ssRNA bearing a 5’ triphosphate group, while MDA-5 recognizes the viral

mimetic poly I:C (Stetson and Medzhitov, 2006). Heterodimers of RIG-I or MDA-5 form with exposure of a CARD domain that interacts with the same motif on IPS-1 on the mitochondrial membrane. Signaling networks downstream of IPS-1 lead to the activation of transcription factors such as IRF3, IRF7, NF-κB, and AP-130 that translocate to the nucleus and together aggregate in the IFN-β enhanceosome (Thanos and Maniatis, 1995; Panne et al, 2007). The coordinated activation of multiple transcription factors leads to the necessary and sufficient enhanceosome constituents, without which transcription of IFN-β will not proceed.

This leads to subsequent docking of the GCN5 histone acetyltransferase complex (Agalioti et al, 2000). GCN5 engagement leads to the acetylation of histone 3 lysines 9 and 14 and of histone 4 lysine 8, all within the nucleosome at the *Ifnb1* promoter. , Nucleosomal remodeling follows, which results in recruitment of CBP-Pol II holoenzyme and subsequent transcription.

Whereas many cells may 'sense' viral RNA, few will end up producing IFN itself. More specifically, the elaboration of type I interferons is known to be stochastic, with only a fraction of infected cells transcribing the gene. This is not a feature of genetic variation – progressive subcloning of IFN-producing cells does not change the frequency of IFN production. Stochasticity is also not due to cell cycle variation, as synchronization experiments still show a minority of cells that respond. It is also not secondary to a failure of adequate sensing, as electroporation experiments with labeled poly I:C

recapitulate a stochastic rather than deterministic response occurring in a small percentage of cells. To date, this feature of the IFN response has been attributed to stochastic assembly of the enhanceosome, owing to the requirement that several transcription factors contemporaneously aggregate on the IFN-β promoter (Apostolou and Thanos, 2008). Recent evidence supports the notion that virtually every factor in the signaling downstream of cytoplasmic sensors is limiting, not just transcription factors. These include sensors for detecting viral nucleic acids (such as RIG-I and MDA-5) and intermediate signaling molecules (such as TRIM25 and IPS-1) (Zhao et al., 2008). It is the natural variation in the levels and activities of these proteins to which stochastic responses to poly I:C and viral infection has been attributed.

Following the production of IFN-β, coordinated activation of a multitude of secondary genes, termed interferon-stimulated genes (ISGs) contribute to antiviral defense. Many of these ISGs are produced in response to transcription factors such as those belonging to the STAT and IRF families that lead to specific SWI/SNF-mediated nucleosomal remodeling at the ISG promoters and subsequent transcription (Ramirez-Carrozzi et al, 2009). The antiviral response that ensues consists of several families of proteins, including the IFITs, the OAS family, and the MX proteins. Each of these IFN-inducible proteins have specialized effector functions.

The Mx1 protein, for instance, has specific antiviral effects on influenza and VSV. A large GTPase that interacts with dynamin, Mx1, inhibits influenza virus infection by blocking

viral transcription and replication. The mechanism of its action is to inhibit the interaction between influenza nucleoprotein (NP) and polymerase basic protein 2 (PB2) (Verhelst et al, 2012). A second key protein is Ccl5, which plays an instrumental role in bridging innate and adaptive responses. Ccl5, also known as RANTES, functions as a chemokine to recruit T cells, eosinophils, and basophils to sites of antigenic challenge (Schall et al, 1990). In a similar vein, IFIT1 – strongly induced in the type I interferon response – acts as an inducible RNA sensor that has specificity for 5' triphosphate ssRNA species (Pichlmair et al, 2011). Together, these examples of antiviral proteins highlight the diverse array of effector functions that IFN-inducible proteins execute. But the coordinated activities of these antiviral proteins in immunity cannot occur without precise transcriptional activation following the initial signal.

Transcriptional activation and chromatin

First articulated in 1958 by Frances Crick, the 'central dogma' of molecular biology describes the flow of sequence information in the cell, beginning with DNA and ending with protein. However, that starting genetic material – DNA – is far more complex than Crick likely envisioned. DNA is wrapped around the nucleosome, an octamer of four histone proteins, and nucleosomes are then densely packed into higher-order fibers that together constitute chromatin. The architecture of chromatin is complex, and it plays a substantial role in all of the processes in which DNA participates, namely replication, recombination, cell division, and transcription.

The complexity of chromatin is reflected both in its spatial organization and in its detailed structure. For a given gene locus, such as that of *Ifnb1*, a number of factors determine whether that small stretch of DNA can be transcribed. First, the type of chromatin it resides in matters. Broadly, chromatin exists as euchromatin or heterochromatin – two functionally distinct regions of the genome. Heterochromatin is tightly packed and inaccessible; euchromatin is less condensed and transcriptionally active. Moreover, these forms of genetic material are essentially segregated within the nucleus. Heterochromatin is restricted to the periphery of the nucleus, where there are extensive interactions with the nuclear lamina. Euchromatin occupies the center, where transcriptional factories can be found.

But for a locus to be transcribed, it is not enough to simply be in located in euchromatin. While broad spatial context within the nucleus is key, local factors are equally critical. Nucleosome density, for one, is crucial, as nucleosomes act as barriers to the RNA polymerase machinery. Alterations to this density are generated by nucleosomal remodeling initiated by complexes belonging to the SWI/SNF family, which modulates the accessibility of nucleosome-associated DNA. How the DNA itself is modified is important, as DNA can itself bear features that determine chromatin usage, such as CpG islands or methylation, both of which act to repress transcription.

Importantly, the local context that determines transcriptional potential is the assortment of histone modifications that are present. The N-terminal histone tails on H3 and H4, which protrude from the surface of chromatin and form ~25% of the histone mass, can be modified in a variety of ways (Strahl and Allis, 2000). To date, several modifications to histone tails have been described, including acetylation, phosphorylation, ubiquitination, ADP-ribosylation, sumoylation, deimination, proline isomerization, and methylation (Kouzarides, 2007). These occur on several different residues, including lysine (K), arginine (R), serine (S), threonine (T), tyrosine (Y), histidine (H), and glutamic acid (E) (Taverna et al, 2007). Together, the combinatorial pattern of these modifications has significant functional consequences, including recruitment of coactivators, eviction of nucleosomes by remodelers, and regulation of the accessibility of the transcriptional machinery.

This epigenetic landscape is dictated by dozens of chromatin-modifying enzymes. Broadly, the histone effector proteins that have been identified, each with their own substrate specificity, can be categorized as 'readers' - such as those containing bromodomains, chromodomains, and PHD fingers that recognize lysine acetylation, lysine 9 or 27 methylation, and lysine 4 methylation, respectively; 'writers' – including various histone acetyltransferases and methyltransferases; and 'erasers' – such as histone deacetylases and histone demethylases (Tarakhovsky, 2010).

Together, these proteins can set and reset the epigenetic context in which a gene locus resides. Alterations to chromatin in the form of histone modifications generated by these readers, writers, and erasers have several consequences. For one, the manner in which histones are modified can directly impact the condensation of chromatin, as histone tails are known to be central to the folding process. The structural impact of histone modification, in turn, impacts the manner in which the central genetic processes involving DNA such as recombination, replication, and transcription proceed (Martin and Zhang, 2005). Specifically, lysine acetylation is known to disrupt the contacts between adjacent nucleosomes in the nucleosomal array by neutralizing the charge of the lysine, creating a chromatin environment wherein DNA is highly accessible (Berger, 2007). The second crucial consequence involves the impact on the 'histone code', wherein the unique pattern of modifications to histones determines its interactions with secondary proteins, which, in turn, mediate specific cellular responses (Jenuwein and Allis, 2001). The presence of histone 3 lysine 9 trimethylation (H3K9me3), for one, leads to the

accumulation of HP1α and HP1β isoforms and the formation of heterochromatin (Bannister and Kouzarides, 2005). By contrast, lysine acetylation of histones is primarily associated with activation of transcription by way of interaction with bromodomain-containing proteins that, in turn, associate with P-TEFb that subsequent phosphorylates Pol II and allows for transcription (Jang et al, 2005). Indeed, each of the myriad histone modifications has an effect on transcription, and often these marks act in concert via engagement of effectors with multiple binding modules (Ruthenburg et al, 2007).

Several associations have been elucidated with respect to the impact of a particular histone modification on transcription. As mentioned earlier, lysine acetylation – most commonly on H3 (K9, K14, K18, and K27) and H4 (K5, K8, K12, K16) – is associated with transcriptional activation. Similarly, serine/threonine phosphorylation, typically occurring in response to a proximal signaling event, is a mark associated with activation of the gene downstream of the promoter. Sumoylation is commonly linked to transcriptional repression, whereas arginine methylation leads to activation. In many instances, the mechanism by which the presence of a specific modification leads to an impact on the transcriptional machinery is unknown. Several possibilities exist, including physical inhibition of binding by either Pol II or other transcriptional components, or by interaction with an unknown corepressor complex (Rosenfeld et al, 2006).

Interestingly, the impact of lysine methylation on transcription is context-dependent, proving to be either an activator or repressor depending on the location of the lysine

residue at which is located and the number of methyl moieties there. Methylation at lysine 4 is invariably associated with transcriptional activation with the H3K4me^3 mark found almost exclusively at the transcriptional start sites of active genes. This mark has been associated several effector molecules through CHD1, which itself is a member of large protein complexes that also feature histone acetyltransferases such as GCN5. This evidence establishes a link between the lysine 4 methyl mark and the transcriptional machinery by way of histone acetylation and its downstream effect on Pol II itself (Pray-Grant et al, 2005).

Both dimethylation and trimethylation of H3K9 are associated with transcriptional repression. H3K9me^3 predominates in heterochromatin and also in the intragenic regions of active genes, whereas H3K9me^2 is primarily located in repressed and silenced promoters. In a similar fashion, multiple methylation at H3K27 is associated with silencing, but is thought to represent a stable mark that remains in the absence of cell division (Tarakhovsky, 2010). Loss of methylation at lysine 27, as in the case of lysine 9, is associated with active promoters as they do not favor the association with the Polycomb chromodomain (PC) and HP1 proteins, respectively (Bannister and Kouzarides, 2005). On the other hand, persistent methylation at these residues is typically associated with transcriptional repression.

Beginning with the identification of the first histone methyltransferase in 2000, several ‘writers’ have been discovered that methylate the lysine and arginine residues on H3. Of

these, G9a, GLP, SUV39h1, SUV39h2, and SETDB1 have been identified as placing methyl groups on histone 3 lysine 9 (H3K9) in mammalian cells. G9a and GLP, are the major H3K9 methyltransferases responsible for placement of methyl groups in euchromatin (Tachibana et al, 2005). Histone methylation was initially thought to be irreversible enzymatically, a belief that was based primarily on observations demonstrating turnover rates of methyl groups on histones no greater than that of histones themselves (Shi and Whetstine, 2007). However, in 2004, lysine-specific demethylase 1 (LSD1) was discovered to have demethylase activity at histone 3 lysine 4, providing evidence for the dynamic regulation of histone methylation (Shi et al, 2004). Since then, several additional demethylases have been discovered, belonging to one of two distinct families. The first group employs an amine-oxidase domain mechanism and consists solely of LSD1, which demethylates H3K4 and H3K9, but the latter only in the context of its association with the androgen receptor (Mossamaparast and Shi, 2010). Moreover, LSD1 is incapable of removing methyl groups from H3K9me^3 (Metzger and Schule, 2007).

The second group of histone demethylases – the Jumonji family -- contains a Jumonji C domain and requires several cofactors, including Fe2+, O2, and α-ketoglutarate to hydroxylate the methyl group (Nottke et al, 2009). Owing to a different mechanism that does not depend on a protonated nitrogen, JmjC domain-containing demethylases can remove any methyl moiety from a given substrate; however, different Jumonji-containing demethylases do bear differing specificities for particular marks. All told,

there are seven members of this group of enzymes (target residues in parentheses), including JMJD1a (H3K9me$^{1/2}$), JMJD1b (H3K9me^{1}), JMJD2a (H3K9me^{3}), JMJD2b (H3K9me^{3}), JMJD2c (H3K9me$^{2/3}$), JMJD2d (H3K9me$^{2/3}$), and PHF8 (H3K9me^{2}) (Yamane et al, 2006; Whetstine et al, 2006; Fodor et al, 2006; Cloos et al, 2006; Shin and Janknecht, 2007; Fortschegger et al, 2010).

To date, several H3K9 demethylases have been implicated in developmental contexts. For example, JMJD1a, which specifically demethylates H3K9me^{2}, is highly expressed during spermatogenesis and is required for chromatin condensation via demethylation of H3K9 at the promoters of Tnp1 and Prm1, two chromatin-packaging genes (Okada et al, 2007). Similarly, JMJD1a and JMJD2c appear to be crucial for the maintenance of embryonic stem cell pluripotency, as both are activated by the transcription Oct4. Stable knockdown of either of these demethylases leads to downregulation of the pluripotency factors Oct4, Sox2, and Nanog, as well as loss of ES cell morphology in culture (Loh et al, 2007). As such, there is considerable evidence implicating the H3K9 demethylases in differentiation and development.

H3K9 demethylases have also been associated with metabolic function, as in the case of JMJD1a. Mice lacking JMJD1a are markedly obese and hyperlipidemic relative to their littermates, a phenotype linked to the nuclear hormone receptors PPAR-γ and RXR-α (Tateishi et al, 2009). The authors show specific demethylation by JMJD1a of the PPAR responsive element of the Ucp1 gene facilitating hormone receptor recruitment. In the

absence of JMJD1a, the expression of metabolic genes is impaired, as is β-oxidation and glycerol release in skeletal muscle. Finally, JMJD2a and JMJD2d interact with the androgen receptor (AR), and in the absence of the latter there is reduction in the transcription of prostate-specific antigen in LNCaP prostate cancer cells (Shin and Janknecht, 2007). Until recently, little else was known about the Jumonji family than these few reports.

How does this complexity of chromatin affect the type I interferon response? The interplay and balance between histone-modifying enzymes of opposing function confers on chromatin an inherent plasticity that can dramatically affect the transcriptional state of a cell. In immune responses, this plasticity is exploited to allow for a vast but precise array of genes to be simultaneously activated or repressed; in other words, the state of chromatin is altered to initiate the transcriptional programs central to innate immunity. This means that all of the coordinated events required for transcription must occur. Histone 'writers' must place active marks, 'erasers' must remove repressive marks, and 'readers' must read the new landscape that has been generated. The changes occurring in the vicinity of promoters and transcriptional start sites (TSSs) were originally thought to primarily determine gene activation. However, recently, considerable data suggest that gene activation is preceded by a similar set of epigenetic events occurring at enhancers.

The role of enhancer chromatin in gene expression

Over the last few years, it has become increasingly clear that c*is*-regulatory elements play a critical role in the activation of gene transcripts. Among the myriad regulatory elements – enhancers, silencers, insulators – enhancers are most noteworthy, as these genomic regions appear to control gene expression of loci that can be great distances removed from the enhancer itself. Like promoters and genes, enhancers are also chromatinized regions but have unique features. They are characterized by high DNase I accessibility, the presence of coactivator proteins, and monomethylation of histone H3 lysine 4 ($H3K4me^1$) (Calo and Wysocka, 2012). Initial profiling of enhancers using ChIP-chip methods revealed a diverse array of regulatory elements in the human genome, more varied across cell types than promoters themselves (Heintzman et al, 2009).

Chromatin states at these enhancers have become increasingly well-characterized beyond the initial finding noting the ubiquitous presence of $H3K4me^1$. $H3K4me^3$ is notably absent from these regions, thereby distinguishing them from promoters. H3K27ac is also frequently associated with enhancer regions, where it is a mark of enhancer activity. Additional histone modifications have since been described as being present, including $H3K27me^3$, H3K9ac, and $H3K9me^3$ (Zentner et al, 2011; Rada-Iglesias et al, 2011). Indeed, the spectrum of histone modifications parallels those observed at promoters.

Nucleosomes are also different at enhancer regions than they are elsewhere. Overall, these regions are relatively nucleosome poor, as indicated by the DNase I hypersensitivity. Second, unique histone variants can be deposited, such as histone H3.3 and H2A.Z – with the double-variant being found primarily at enhancers (Jin et al, 2009). These nucleosome core particles are mobile and highly salt-sensitive such that enhancer DNA is relatively accessible.

Together, the landscape of modifications at enhancers, similar to promoters, is what dictates their functional state. All enhancers are typically associated with H3K4me^{1} and are absent of H3K4me^{3}. The remaining modifications, however, vary with level of enhancer activity. Active enhancers are enriched with the coactivator CBP/p300 and have high levels of H3K27ac, H3K9ac, and H3K36me^{3}), while poised enhancers have H3K27me^{3}, H3K9me^{3}, and lack H3K36me^{3}. These latter enhancers may have lower levels of enrichment with p300 as well. Of note, genes proximal to active enhancers are typically more highly transcribed than those proximal to poised enhancers, suggesting that differences in histone marks at these enhancers correlates with their activity.

Enhancer chromatin is notable in that it too is transcribed. A significant amount of extragenic Pol II has been seen to accumulate at these regulatory elements, specifically in macrophages in response to LPS (De Santa et al, 2010). In another line of evidence, neurons were noted to accumulate enhancer RNA (eRNA) transcripts in response to depolarization with potassium chloride (KCl) (Kim et al, 2010). The amount of eRNA

correlated with nearby mRNA expression, connecting the transcription of enhancers directly with target gene activation. Generally, eRNAs are either short, bidirectionally transcribed, and not polyadenylated or can be longer, unidirectional, and polyadenylated. Transcription proceeds from the enhancer center (at the p300 peak) and proceeds to the termination of the H3K4me^{1} region (Natoli and Andrau, 2012). In sum, we now know that active enhancers, in addition to the histone marks described earlier, are also enriched in Pol II and more frequently transcribed; on the other hand, poised enhancers, with largely repressive marks, have less Pol II and less eRNA.

Active histone marks, Pol II occupancy, and eRNA transcriptions are hallmarks of the active enhancer. These features all correlate with transcription of the nearby gene. But how exactly does an active enhancer facilitate transcription of a gene? Prior to transcription, enhancers first act as an integrated binding platform for upstream signals. Various transcription factors bind to these enhancers at transcription factor binding sites (TFBSs), which is followed by the recruitment of coactivator proteins. These coactivators may include the histone acetyltransferases (such as CBP/p300 or GCN5/PCAF) that generate the 'active' enhancer pattern, the chromatin remodelers (that can evict nucleosomes), and the mediators between enhancer and promoter (such as cohesin and Mediator) (Calo and Wysocka, 2012). Coactivator engagement is followed by recruitment of the polymerase machinery to the enhancer and subsequent transcription.

What follows next remains largely unknown, though the mechanism by which eRNA leads to mRNA is thought to be related to either 'looping' of the DNA or 'tracking'. In either mechanism, enhancers are instrumental in the delivery of both the transcriptional machinery and the chromatin modifiers (such as nucleosome remodelers and coactivators) to the target gene. The 'looping' model posits that the enhancer 'folds' over on to the promoter such that a loop forms thereby excluding the intervening stretch of DNA. The 'tracking' model asserts that the recruited machinery translocates linearly along the DNA. However it occurs, it appears that enhancer activation and transcription are antecedent events that precede and facilitate the transcription of a gene.

Control of transcriptional responses and enhancer activity by H3K9 trimethylation

Given the conserved transcriptional response that occurs in type I interferon signaling, we looked to further our understanding of enhancer chromatin examining nucleic acid sensing in MEFs. Specifically, we sought to determine a role for modifiers of the histone 3 lysine 9 residue in this system, either at promoters or at enhancers. Our hypothesis is that H3K9 enzymes must be central to gene activation, as modifications on the K9 residue on histone H3 are highly dynamic in transcriptional responses.

This hypothesis is rooted in multiple lines of evidence. First, unpublished data from our laboratory suggested a demethylation event might occur at the IFN-β promoter in response to an upstream signal. Second, the Blobel lab had demonstrated that gene bodies dynamically accumulate H3K9me^3 in gene bodies that is cotranscriptionally deposited (Vakoc et al, 2006). This H3K9me^3, despite engagement with HP1γ, is rapidly removed as well. Third, vascular smooth muscle cells from diabetic mice were shown to exhibit a persistent inflammatory phenotype in vitro with continued expression of IL-6, MCP-1, and M-CSF. Subsequent ChIP analysis showed significant reduction in H3K9me^3 at the promoters of these cells compared to cells from wild-type mice. Furthermore, treatment with TNF-α led to an increase in the transcription of these genes that was associated with further demethylation of H3K9me^3 at their promoters (Villeneuve et al, 2008).

Given this evidence, histone 3 lysine 9 modifiers posed a promising avenue for investigation. Our hypothesis at the outset was that one of the H3K9 demethylases would be central to antiviral signaling via demethylation of repressed promoters or poised enhancers.

Chapter II: Stochastic activation of IFN-β and the histone demethylase JMJD2d

Chromatin dynamics and enhancer transcription in the innate immune response

In the antiviral response, key transcriptional programs are activated to effect the expression of genes that are critical for host defense. Expression of innate immune response genes is the outcome of coordinated chromatin events that culminate in initiation and elongation by RNA polymerase II. Some of these chromatin events are well-characterized, such as the accumulation of H3K4me3 and acetylated H3 and H4 residues at nucleosomes in the vicinity of transcribed gene promoters. However, the spectrum of chromatin changes in the innate immune response that occur throughout the epigenome, and specifically at enhancer chromatin, has not yet been described.

To ascertain the modifications that occur at enhancer chromatin, we began by isolating mouse embryonic fibroblasts (MEFs) from wild-type mice and characterizing the transcriptional program that is activated in response to the synthetic dsRNA analog, polyinosinic:polycytidylic acid (poly I:C). Following four hours of *in vitro* stimulation, we detected the expression of 113 genes (Table 1) consisting of several type I interferons and interferon-stimulated genes (ISGs). Several of these gene products detected by gene array were confirmed by reverse transcription-quantitative polymerase chain reaction (RT-qPCR) (Figure 1). *In vitro* stimulation of MEFs with poly I:C was repeated

Table 1. The transcriptional response activated to poly I:C stimulation in MEFs. Wild-type MEFs were stimulated with poly I:C and RNA was isolated after four hours. Microarray analysis was performed; shown are genes upregulated > two-fold. Data are the average of three independent experiments.

Gene	Fold induction	Gene	Fold induction
Cxcl10	31.605846	BC006779	3.122934
Ifnb1	28.197994	Hist1h4i	3.0815237
Mx2	21.680067	Zfp36	3.0594335
Ifit3	17.80783	Slc2a6	3.0403197
Ccl5	15.489736	Dusp8	2.954846
Usp18	13.926942	Phlda1	2.920562
LOC100048346	13.258817	Egr2	2.9192994
Ccl2	10.3806505	Jun	2.9140236
Rsad2	9.976725	Oas1g	2.867266
Gbp3	9.908558	Dhx58	2.8625565
Gbp2	9.564882	Gadd45a	2.8510737
LOC667370	9.257187	Ifi47	2.800076
Tnfaip3	9.252282	LOC100047963	2.7851608
Ifit3	8.9953575	Klf6	2.7642763
Iigp2	8.912015	Hist1h4f	2.7262323
Cxcl1	8.762168	Fos	2.628029
Gbp3	8.508837	Ier3	2.5963612
Igtp	8.133124	Ddx58	2.5943835
Cxcl9	7.614855	Hdc	2.57001
Irf1	6.723368	Slc25a25	2.5684092
Irf1	6.712335	Ripk2	2.5577598
Egr1	6.355163	Ccrl2	2.5141284
Icam1	6.2216988	Josd3	2.4459813
Oasl2	6.16569	Klf2	2.4446518
Ccl7	5.59689	Txnip	2.4422612
LOC100038882	5.524834	Il15	2.4303243
Oasl1	5.513505	Hist1h2ac	2.4291928
Axud1	5.478931	Zc3h6	2.4050522
Tlr2	5.2830234	D14Ertd668e	2.3843863
Irgm1	5.151454	1500012F01Rik	2.3809233
Trim21	5.1163	Trex1	2.340291
Usp18	5.07427	Relb	2.3122492
Parp14	5.0238853	Irf9	2.3026154
Chac1	4.8086157	Klf6	2.2975144
Atf3	4.635319	Eif2ak2	2.2964149

Gene	Fold induction	Gene	Fold induction
Samd9l	4.5879884	Hap1	2.2832747
Cd274	4.513661	Plekha4	2.2785983
BC006779	4.3705626	Hist1h4j	2.2728412
Stat2	4.22059	Ccrn4l	2.2654698
Irf1	4.216204	Ube1l	2.2620642
Apol9b	4.131248	Gadd45a	2.2534916
Irf1	4.1279507	Ccrn4l	2.2346642
Hist1h2bj	4.1037383	Irf7	2.2253335
Junb	4.0334687	Daxx	2.2144337
Gbp6	3.9819858	LOC100046232	2.1916113
Gadd45g	3.976631	Ppm1k	2.1887937
Hist1h2bh	3.916566	Cish	2.1771824
Myd116	3.9051251	Apobec1	2.166548
Nfkbie	3.8878582	4930599N23Rik	2.1636698
Gadd45b	3.8755217	Casp4	2.1571677
Tyki	3.8577104	D14Ertd668e	2.1451836
Oasl1	3.6770806	Ch25h	2.1433632
Hist1h2bf	3.6752925	Rhob	2.1350336
Map3k14	3.601361	Stat1	2.099436
Hist1h2bc	3.5996723	AA467197	2.0968196
Irf9	3.5742452	Adar	2.0962126
Oas1b	3.5114527	Zfp119	2.0928428
Hist1h2bm	3.499247	Birc2	2.0871625
Hist1h2bn	3.4989486	Dusp6	2.0710497
Taf15	3.478466	Hist1h2bg	2.0666418
Ifit2	3.4701445	Fbxw17	2.065485
LOC100047963	3.4637952	Trex1	2.0468059
Nfkbia	3.3646343	Trib3	2.0466084
Gadd45g	3.3426063	Bhlhb2	2.0411756
Ifit2	3.3320348	Rbm43	2.0352569
Hist1h2bk	3.3153229	Edn1	2.0242689
Clec2d	3.2698836	Pim3	2.0188584
Hist1h1c	3.1748059	Arc	2.01379
Oas1b	3.1642835	Hist1h2be	2.0041735
Stat1	3.1558104	Napb	2.000367
Errfi1	3.155		

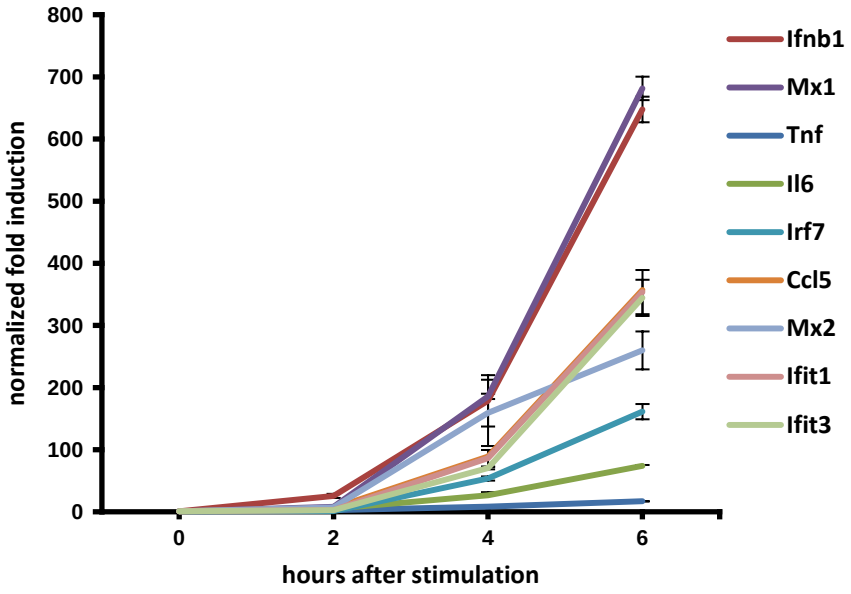

Figure 1. Poly I:C stimulation is associated with the induction of IFN-β and pro-inflammatory and antiviral gene targets. Following poly I:C stimulation for four hours, RNA was isolated from MEFs and quantitative PCR was performed. Shown is the fold induction above unstimulated cells, normalized to hypoxanthine-guanine phosphoribosyltransferase (HPRT). Error bars represent variance of data from three independent transfections.

with subsequent fixation and chromatin isolation. We then performed chromatin immunoprecipitation for several histone marks followed by next-generation sequencing. Transcriptional activation of poly I:C induced genes were notable for the accumulation of active histone marks at induced but not random promoters (Figure 2). Specifically, inducible genes showed substantial increases in H3K4me^3, H3K9ac, H4ac, and Pol II.

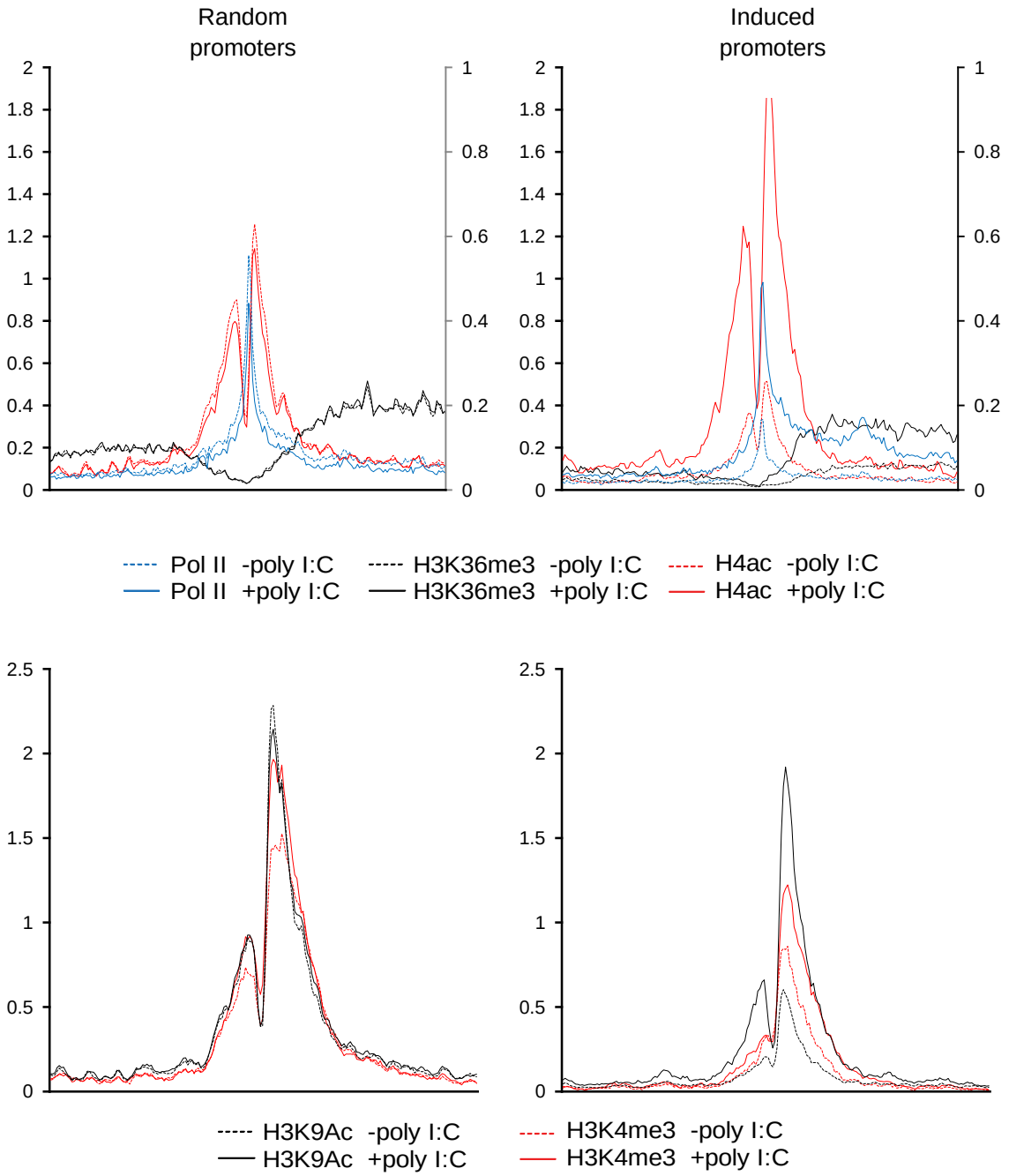

Figure 2. Transcriptional activation by poly I:C is accompanied by dynamic changes in histone marks at promoters. ChIP-sequencing was performed with integrated profile plots generated corresponding to the average Pol II / H3K36me3 / H4ac / H3K9ac / H3K4me3 signal (in FPKM, as indicated) among either the 113 poly I:C-induced or 113 random genes in the region +/- 5 kb from the transcriptional start site.

We observed in our data that dynamic regions also occurred outside of promoter regions. Specifically, our examination of the poly I:C-induced chromatin changes at the *Ifnb* and *Ccl5* loci yielded a few noteworthy regions that displayed similar accumulation of active acetylated histones not present prior to stimulation. We suspected these regions might correspond to regulatory elements, which prompted sequencing for both H3K4me^{1} and p300 – both of which are found in regulatory regions. Indeed, we found that the vicinity of *Ifnb* and *Ccl5* is populated by areas of dynamic chromatin that bear enhancer features (Figure 3).

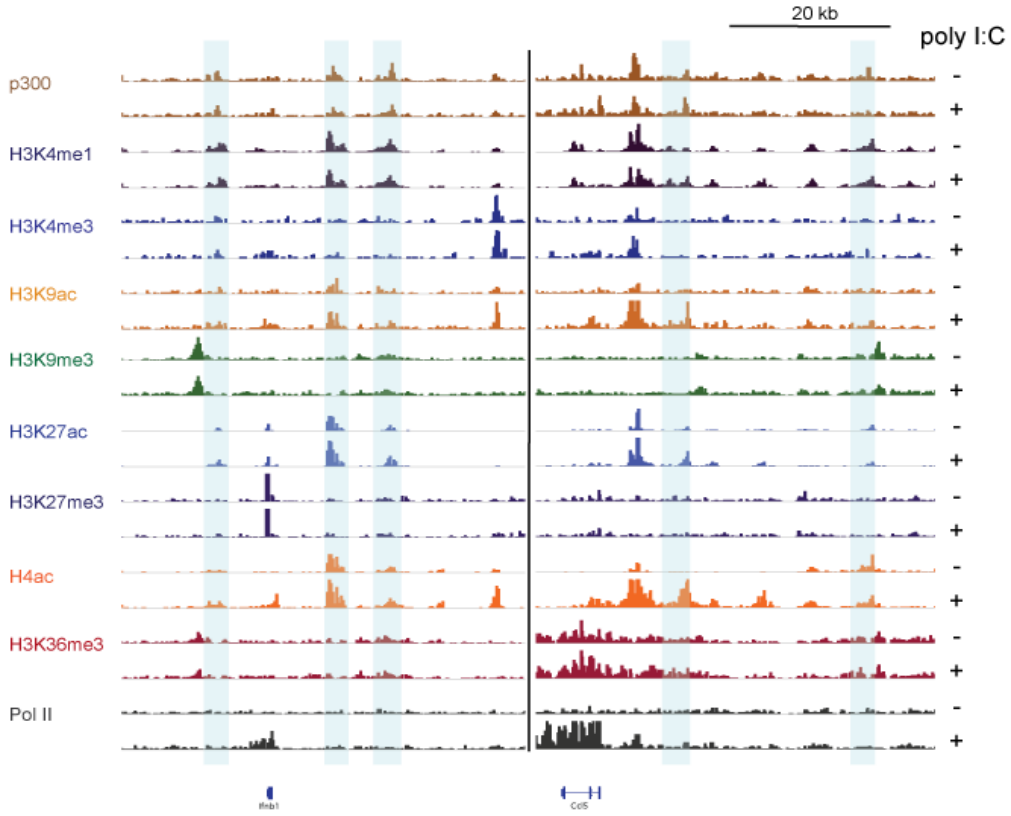

Figure 3. Histone marks are dynamic at the enhancers of inducible genes. ChIP-sequencing tracks corresponding to the antibodies listed on the left; blue rectangles denote areas of H3K4me^{1} and p300 enrichment in the absence of H3K4me^{3} indicative of a putative enhancer region.

In light of this finding, we turned our attention to the identification of enhancer elements throughout the genome, as defined by the presence of H3K4me^1 and the absence of H3K4me^3 (Heintzman and Ren, 2009). This revealed over 200,000 putative regulatory elements in the mouse genome, of which approximately 22,000 were simultaneously bound by the transcriptional coactivator p300. Among this set of global distal regulatory elements, we sought to identify those enhancers activated in the innate immune response. We first employed an unbiased approach to find enhancers displaying dynamic regulation; using a two-fold cutoff, we detected 632 enhancers with an increase in H3K9ac, 869 with an increase in H4ac, and >2000 with an increase in Pol II binding. The accumulation of permissive marks and RNA polymerase at enhancers suggested a transition among a subset to increased enhancer activity. Whether these regulatory elements displaying dynamic regulation were in any way associated with poly I:C-induced genes was unclear – despite having noted proximity of these elements in the case of *Ifnb1* and *Ccl5.*

We therefore took an alternate approach to dynamic regulation of chromatin modifications at enhancers by first identifying those enhancers 'belonging' to poly I:C-induced genes. This required an appropriate assignment of enhancers identified in sequencing data to annotated genes. Recently, the Ren lab described genome-wide annotation of enhancer-promoter units (EPUs) as an improvement over previous attempts at assignment (such as those based on proximity or within blocks between insulators [CTCF-bound]) (Shen et al, 2012). We used mouse EPU data to identify all

enhancers to a given promoter and examined the dynamics of marks at enhancer chromatin. As before, this analysis revealed an accumulation of active histone marks such as H4ac and H3K9ac at the enhancers of poly I:C-inducible genes paralleling the events at corresponding promoters (Figure 4).

Figure 4. The transcriptional response to poly I:C is accompanied by broad activation of the enhancers of transcribed genes. ChIP-sequencing was performed with integrated profile plots generated corresponding to the average H3K4me^3 / H3K4me^1 / H3K27ac / H3K27me^3 / Pol II / H3K36me^3 / H4ac / H3K9me^3 / H3K9ac signal (in fragments per kilobase of exon per million reads [FPKM], as indicated) among either the 113 poly I:C induced gene promoters (left column; TSS +/- 5 kb) or at the extragenic enhancers within the EPUs of these genes (right column; p300 peak +/- 3 kb).

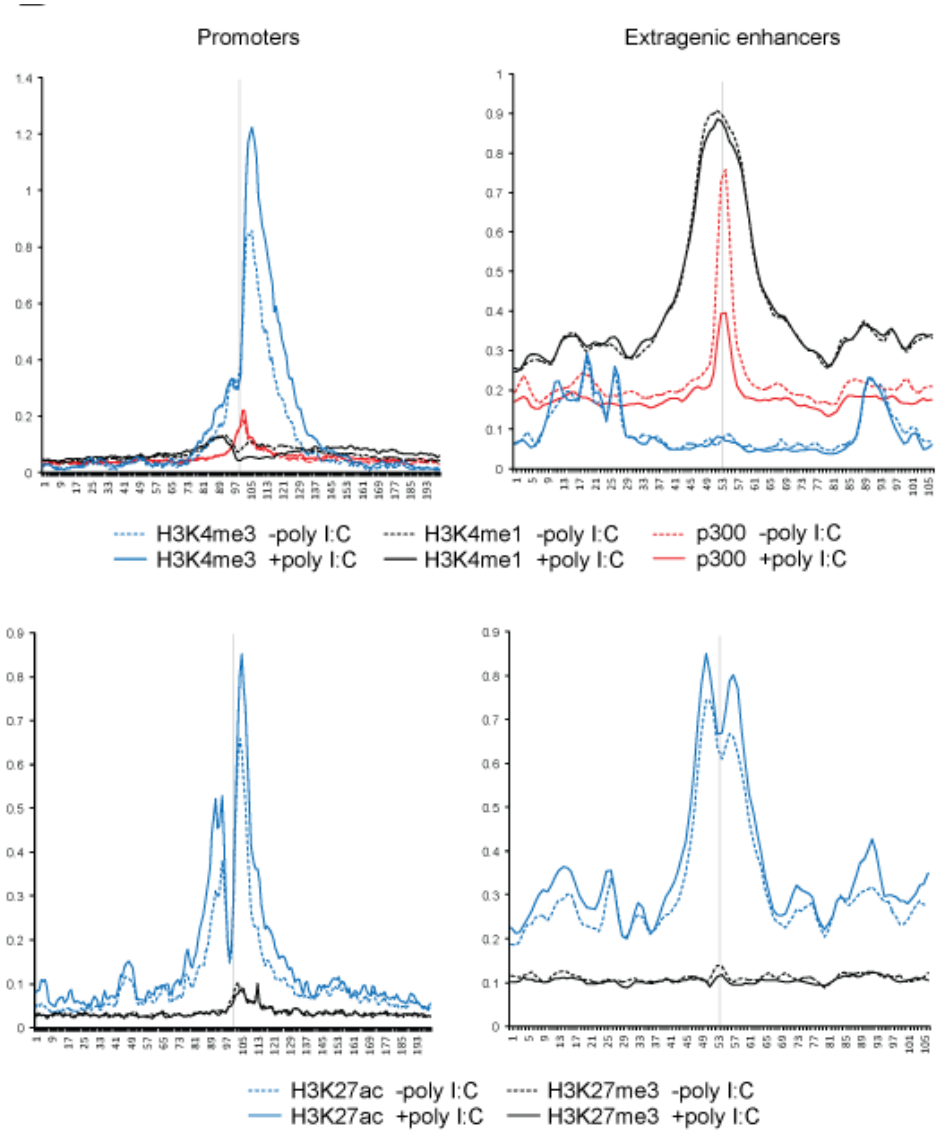
Promoters
Extragenic enhancers
H3K4me3 -poly I:C
H3K4me3 +poly I:C
H3K4me1 -poly I:C
H3K4me1 +poly I:C
p300 -poly I:C
p300 +poly I:C
H3K27ac -poly I:C
H3K27ac +poly I:C
H3K27me3 -poly I:C
H3K27me3 +poly I:C

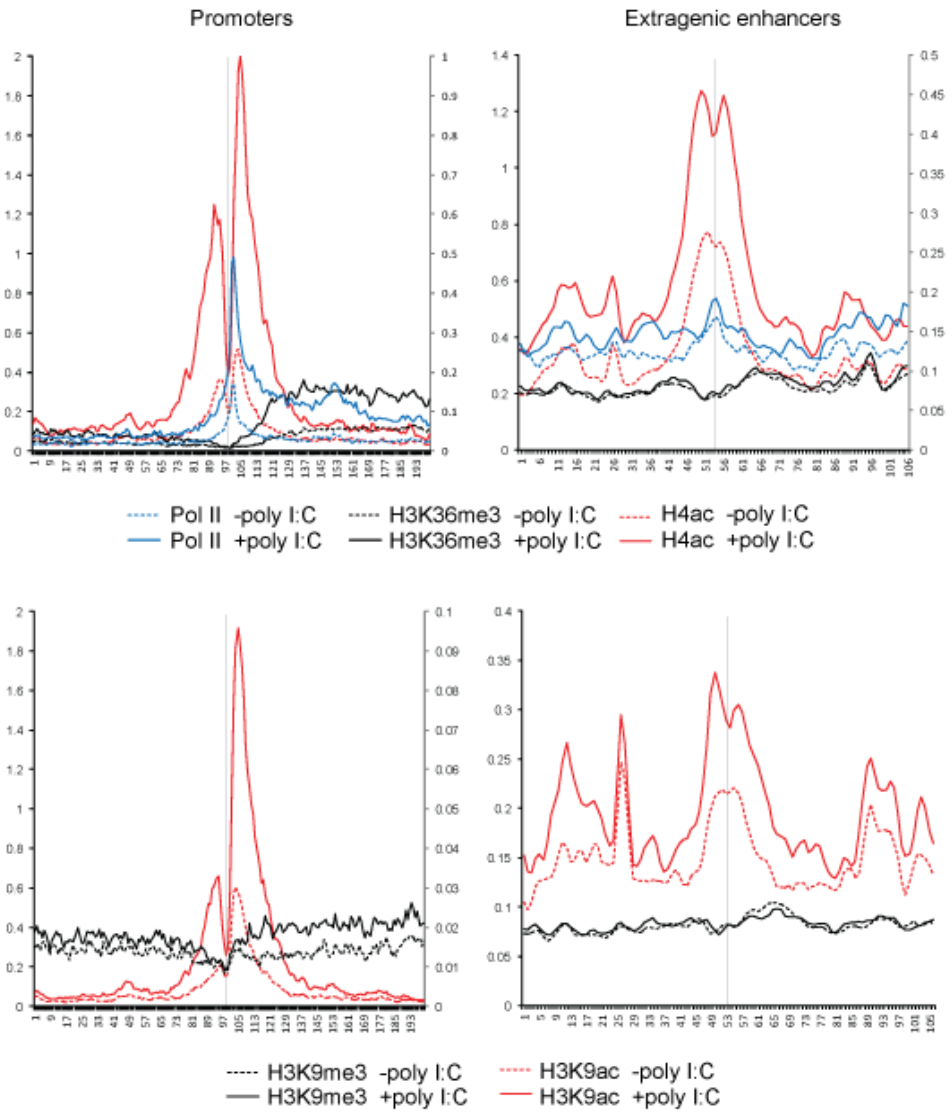
Promoters
Extragenic enhancers
Pol II -poly I:C
Pol II +poly I:C
H3K36me3 -poly I:C
H3K36me3 +poly I:C
H4ac -poly I:C
H4ac +poly I:C
H3K9me3 -poly I:C
H3K9me3 +poly I:C
H3K9ac -poly I:C
H3K9ac +poly I:C

When examined broadly among the enhancers of inducible genes, we did not detect a discernible reduction in repressive marks, such as H3K9me^3 or H3K27me^3. Furthermore, an observable increase in Pol II was observed, suggesting that these enhancers may be newly transcribed. In this way, we uncovered a transition to enhancer activity specifically among those regulatory elements within EPUs of newly transcribed genes.

Given the accumulation of permissive chromatin modifications at this group of enhancers, we next asked if these changes were associated with enhancer transcription. Using strand-specific RNA-sequencing of ribosomal RNA-depleted RNA, we were able to quantify transcripts of enhancer RNA (eRNA). Enhancer RNA within EPUs of poly I:C-inducible genes were also induced, whereas enhancers in random EPUs were not similarly activated (Figure 5).

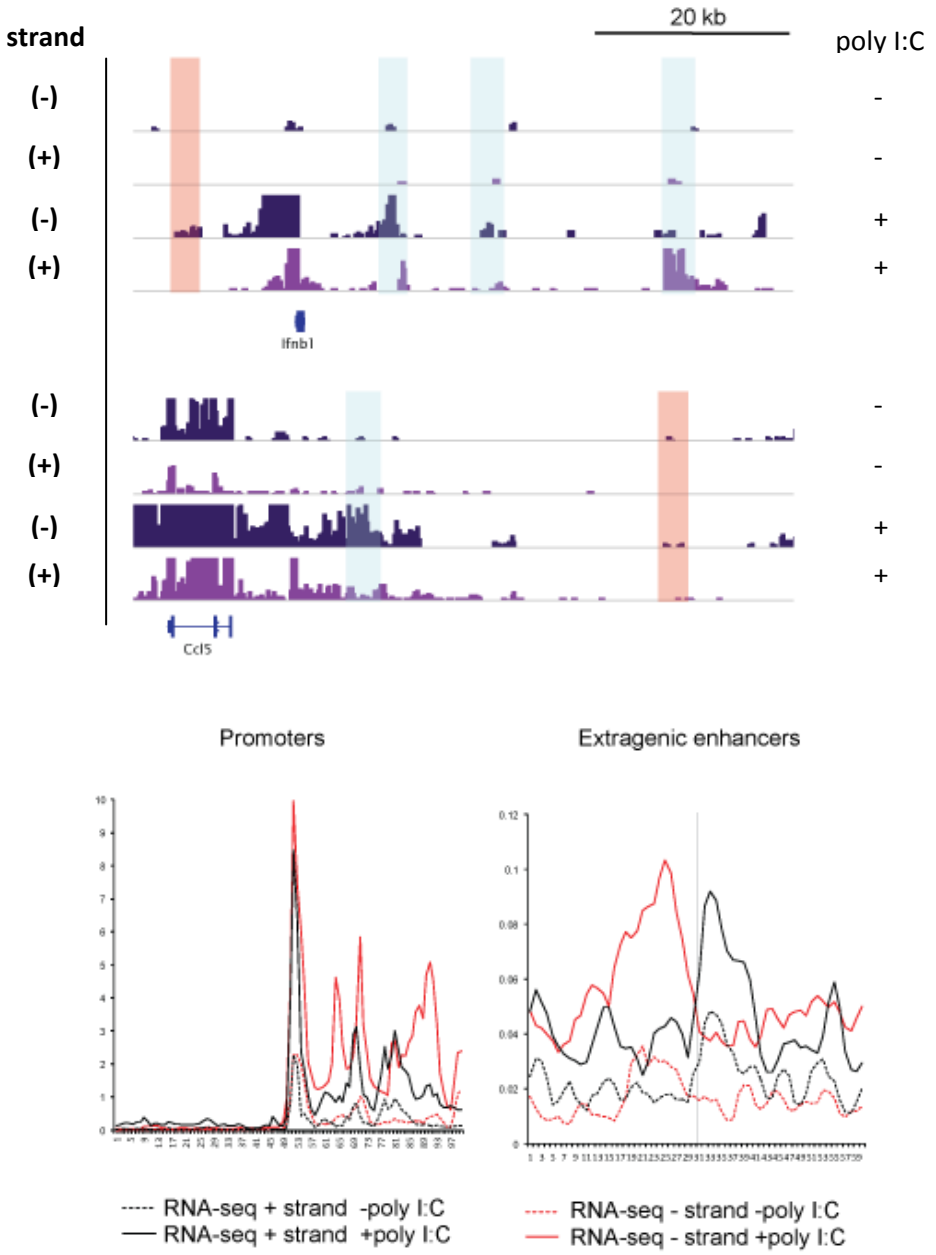

Figure 5. Enhancer transcription occurs broadly as part of the response to poly I:C. (A) Strand-specific RNA-sequencing tracks showing the upregulation of transcripts at (+) strand enhancers (red boxes) and (-) strand enhancers (blue boxes). (B) Profile plots of RNA-seq FPKM integrated for all promoters and their corresponding extragenic enhancers (within EPU) for same entities as in Figure 4.

As has been described previously, these eRNA transcripts appeared to originate from the enhancer 'center', as defined by the p300 peak and the center of the H3K4me[1] region, and extend bidirectionally (Kim et al, 2010). We were also able to detect the upregulation of specific eRNAs by RT-qPCR using random hexamers to prime the reverse transcription reaction, as eRNAs are not necessarily poly-adenylated. We saw specific increases in the transcription of several eRNAs at enhancers in proximity to the *Ifnb1, Ccl5, and Mx2* genes, but not at a control enhancer belonging to *Actb* (Figure 6).

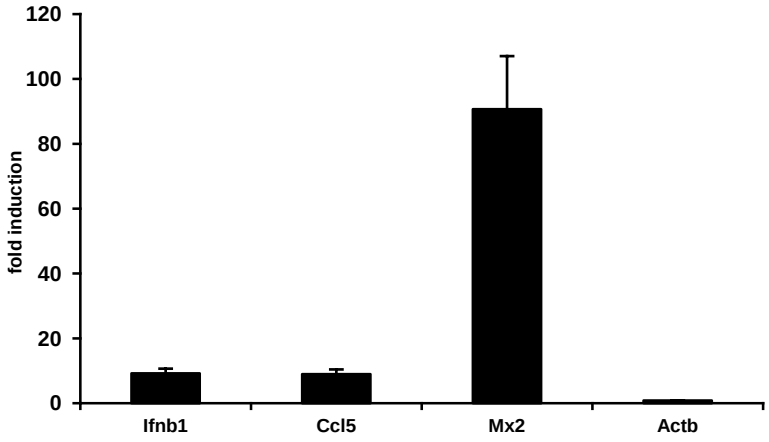

Figure 6. Dynamic enhancers frequently belong to dynamic genes. Fold induction in enhancer RNA (eRNA) levels with 4 hours poly I:C stimulation, as measured by RT-qPCR with random hexamers to prime the cDNA reaction (to detect non-polyadenylated eRNA species). Data shown reflect three independent experiments; Y-axis reflects fold induction over unstimulated cells.

Recently, enhancers have been classified according to their functional status as active, intermediate, or poised. Enhancers that are active are characterized by high levels of H3K9ac, H3K27ac, Pol II, and eRNA production; poised enhancers have H3K9me[3],

H3K27me^3, and low levels of Pol II and eRNA (Calo and Wysocka, 2012). Intermediate enhancers are thought to be unmodified at both H3K27 and H3K9. We then asked if poly I:C-induced enhancers were active enhancers with increased levels of activity or intermediate/poised enhancers that have become active. To answer this question, we determined the presence or absence of H3K9ac/H3K9me^3 and H3K27ac/H3K27me^3 prior to stimulation to divide enhancers into active, intermediate, and poised groups. We observed that the majority of regulatory elements are active or intermediate by H3K27 status, but are intermediate or poised by H3K9me^3 status. This controverts previous data that suggested that enhancers cluster similarly when K9 and K27 status are used (Zentner et al, 2011). When divided into active/intermediate/poised groups, intermediate or poised (by H3K9) poly-I:C-induced enhancers were more dynamic than active (H3K9ac) enhancers (Figure 7).

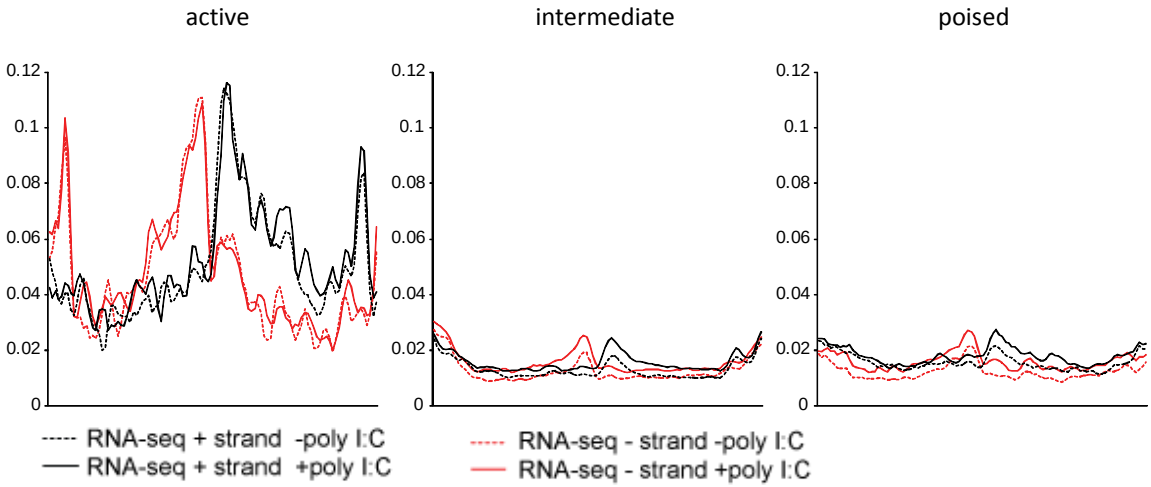

Figure 7. Poised and intermediate enhancers are more dynamic than active enhancers in the poly I:C transcriptional response. Integrated profile plots reflecting RNA-seq data for extragenic enhancers of inducible genes, divided on the basis of H3K9me^3+ (poised), H3K9- (intermediate), and H3K9ac+ (active).

That these H3K9me^3/H3K9- enhancers show dynamic gain of transcriptional activity with poly I:C suggested that enhancer activation in the innate immune response involves a transition between enhancer states rather than an increase in the activity of already transcribed enhancers.

We next asked if enhancer activation was a broad feature of the innate immune response. MEFs were cultured as previously but stimulated with either 500U/mL recombinant IFN-β or infected with Sendai virus (MOI = 10). Both stimuli elicited a similar transcriptional response (data not shown); chromatin changes at promoters and enhancers were as seen with poly I:C.

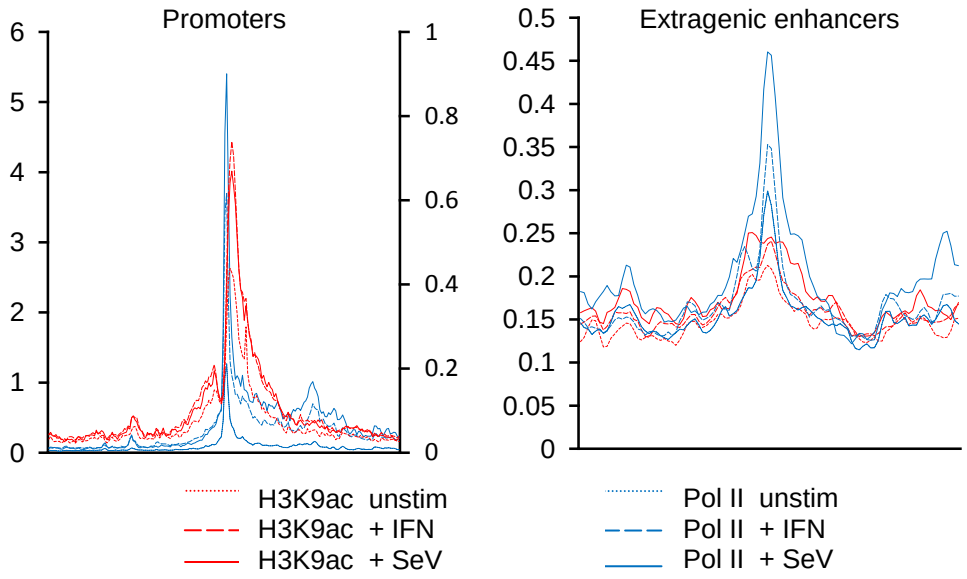

Figure 8. Dynamic chromatin changes at transcriptional start sites and enhancer centers can be observed in response to other innate immune stimuli. Integrated profile plots reflecting ChIP-seq data following IFN-β stimulation (4 hours) or Sendai infection (6 hours) for the set of promoters and extragenic enhancers obtained from poly I:C stimulation.

Specifically, we observed both increases in H3K9ac and Pol II at promoters and enhancers (Figure 8) as well as increases in eRNA in the same group of EPUs of poly I:C-inducible genes (Figure 9).

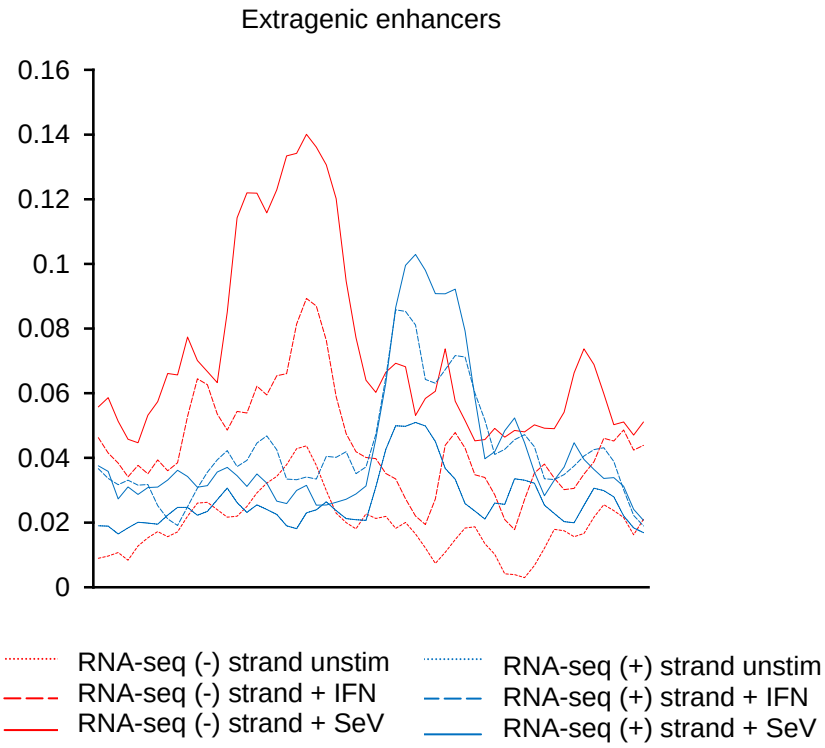

Figure 9. Enhancer activation is a broad feature of the innate immune response. Integrated profile plots reflecting RNA-seq FPKM for the enhancers induced by poly: I:C, here showed before and after IFN stimulation (4 hours) or Sendai virus infection (6 hours).

These findings suggest that enhancer activation is indeed a broad feature of the type I interferon response and typically features a relatively conserved set of chromatin targets, as they can be observed at the same enhancers as for poly I:C. Finally, our data

suggest that poised and intermediate enhancers are most transcriptionally dynamic in the innate immune response.

Stochastic activation of enhancers in the innate immune response

In the foregoing section, we were able to determine that there are global changes to chromatin in the type I interferon response. These changes consist of the accumulation of active histone modifications and RNA Pol II at the promoters of activated genes and their associated enhancers, which are accompanied by corresponding increases in the presence of eRNA transcripts. These findings are based on analyses of large cell populations; however, cellular activation in the type I interferon response is known to be heterogeneous.

We next sought to determine if stochastic activation of the IFN-β gene is accompanied by stochastic activation of enhancer transcripts. To this end, we generated MEFs from IFN-YFP reporter mice generated by the Locksley lab (Scheu et al, 2008). MEFs were immortalized and subsequently stimulated with poly I:C. Using single-color flow cytometry, we recapitulated stochastic IFN-β activation with about ~15% of cells positive for YFP expression (data not shown). We sorted these cells for YFP and detected 10-fold greater IFN-YFP transcript in YFP+ cells as compared to YFP- cells (Figure 10). To eliminate the contribution of IFN-dependent IFN-activation, we blocked the effects of secreted IFN-β with the addition of the IFN receptor antibody. In the absence of IFN-β signaling, stochastic activation persisted with a 10-fold difference in IFN-β transcript between YFP- and YFP+ cells. (Figure 11).

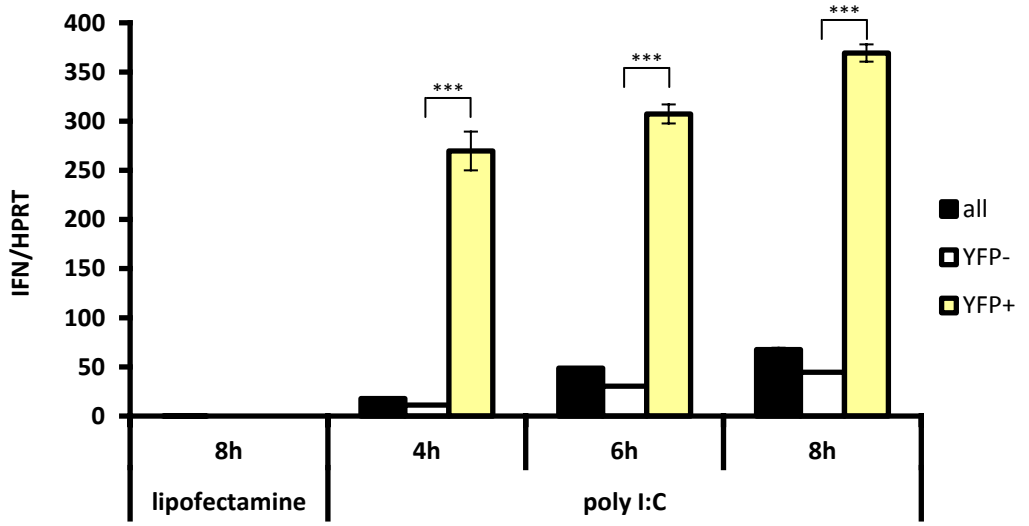

Figure 10. Expression of IFN-β in response to poly I:C exhibits stochastic features. qPCR results of normalized IFN-β expression in IFN-YFP MEFs stimulated with poly I:C for the times indicated and sorted on the basis of YFP. Data shown are representative of four independent experiments with Student's T-test performed for analysis (***p<0.001).

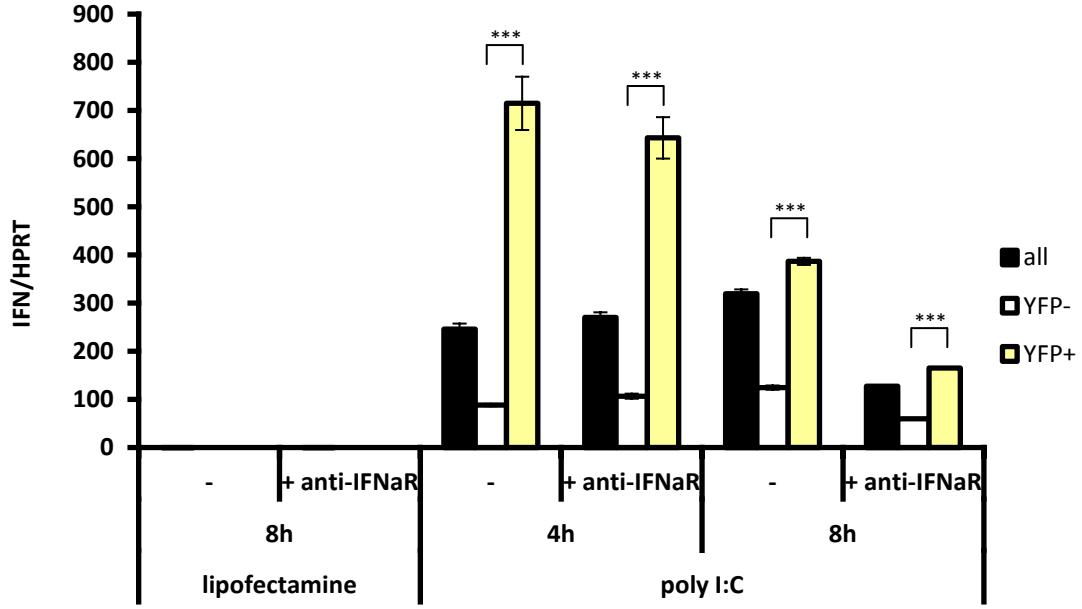

Figure 11. Stochastic activation of IFN-β occurs independently of the signaling effects of IFN. Quantitative PCR results showing normalized IFN-β expression in IFN-YFP MEFs either pre-treated with vehicle or anti-IFNαR antibody and stimulated with poly I:C and sorted on the basis of YFP expression. Data shown are representative of three experiments; Student's T-test performed for statistical analysis (***p<0.001).

Having demonstrated that gene transcripts are heterogeneously activated in a minority of cells, we hypothesized that the enhancer transcripts we found upregulated by poly I:C (Figure 6) would be detectable primarily in YFP+ cells. However, using primers generated to detect specific inducible eRNA transcripts and RT-qPCR, we found that poly I:C-induced eRNAs predominate in YFP- cells (Figure 12).

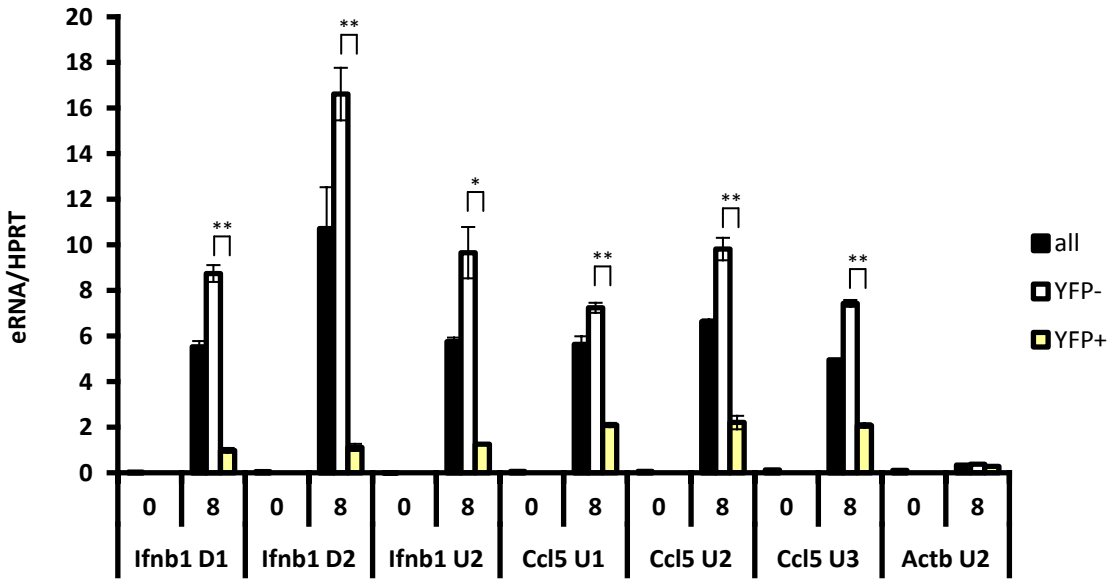

Figure 12. Enhancer RNAs are also activated in a stochastic manner primarily in the cells that do not activate gene targets. Quantitative PCR was performed on IFN-YFP MEFS sorted following stimulation with poly I:C. Primers were designed against enhancers located either downstream (D) or upstream (U) of the gene listed. Data shown are representative of three independent experiments; Student's T-test performed for analysis (**p<0.01; *p<0.05).

Much to our surprise, this was reproducible with several eRNAs in multiple independent experiments. This result suggests that (1) eRNAs are short-lived, and may be rapidly degraded in cells that make productive gene transcripts, or (2) eRNAs never accumulate in YFP+ cells. To confirm these findings, we subjected isolated RNA to whole-

transcriptome ribosomal-depleted RNA sequencing. Though target gene transcription was substantially higher in YFP+ cells, we again noted a greater abundance of related eRNAs in YFP- cells (Figure 13). Taken together, these findings suggested a stochastic activation of enhancers in a distinct subpopulation from that which responds with successful target gene activation.

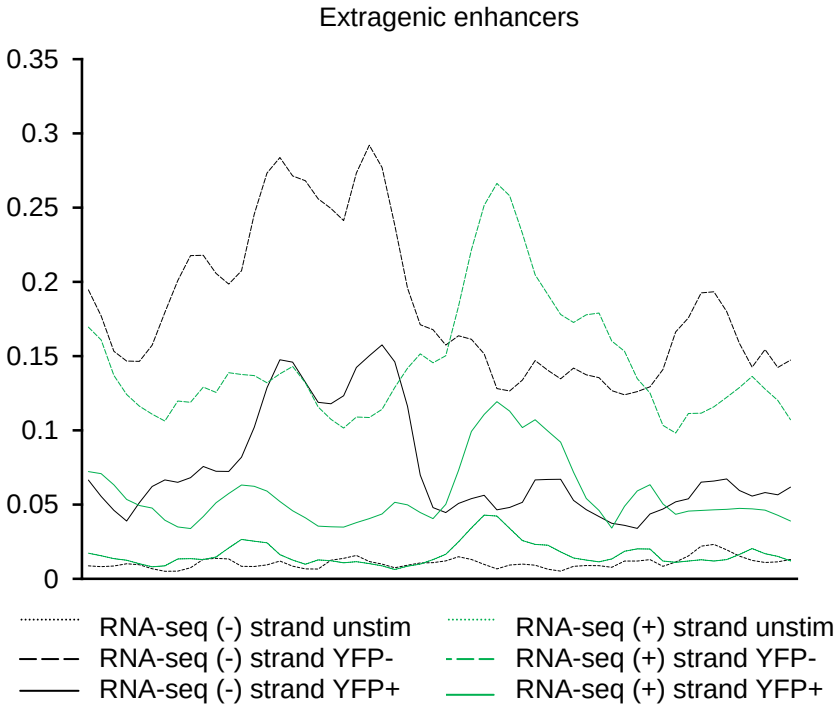

Figure 13. Widespread transcription of enhancers is detectable primarily in cells without gene activation. Integrated profile plots showing the eRNA detectable by strand-specific RNA-seq of extragenic enhancers in IFN-YFP cells either unstimulated (dotted lines) or stimulated and sorted into YFP- (dashed lines) and YFP+ (solid lines) populations.

In vitro modulation of JMJD2d in MEFs affects the magnitude of the innate immune response

We observed in our chromatin analysis that the bulk of newly transcribed enhancers were H3K9me^3 or H3K9-. While we saw greater inducibility in H3K9ac than in any other chromatin mark (other than Pol II), we suspected that this represented a transition of poised and intermediate enhancers to active ones, as these are the ones that become transcribed. This led us to believe that H3K9 demethylases could be implicated in enhancer activation in the innate immune response. We searched for H3K9 modifiers that were transcriptionally induced by poly I:C. No specific acetyltransferase was inducible (data not shown); however, we did see that the mRNA transcript of the histone lysine demethylase JMJD2d was induced 10-fold to the exclusion of other H3K9 demethylases (Figure 14).

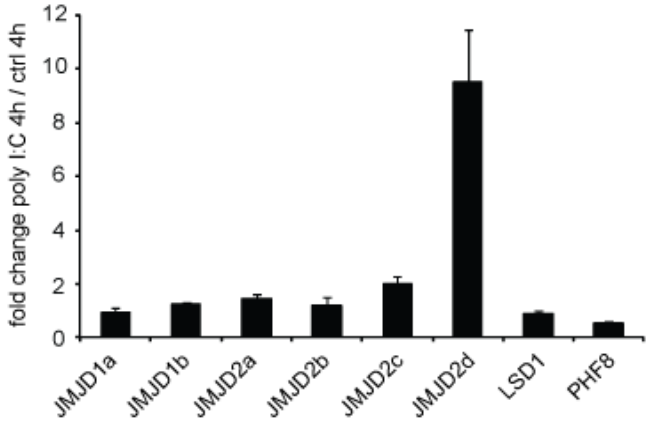

Figure 14. JMJD2d is transcriptionally activated by poly I:C. Quantitative PCR was performed on MEFs four hours following stimulation with poly I:C; primers were designed to detect transcripts corresponding to each of the demethylase genes above. Data shown are the average of three independent transfections.

That JMJD2d was specifically upregulated in this context suggested a role for the enzyme in the innate immune response that we investigated further.

To determine if JMJD2d has an effect on poly I:C-induced responses, we performed *in vitro* knockdown of JMJD2d in MEFs using specific siRNAs (generated by collaborators at Alnylam Pharmaceuticals). Following stimulation with poly I:C 48 hours after knockdown, we saw a ~50% reduction in IFN-β expression as compared to control siRNA (Figure 15), with a similar attenuation of expression seen with several interferon-stimulated genes (ISGs).

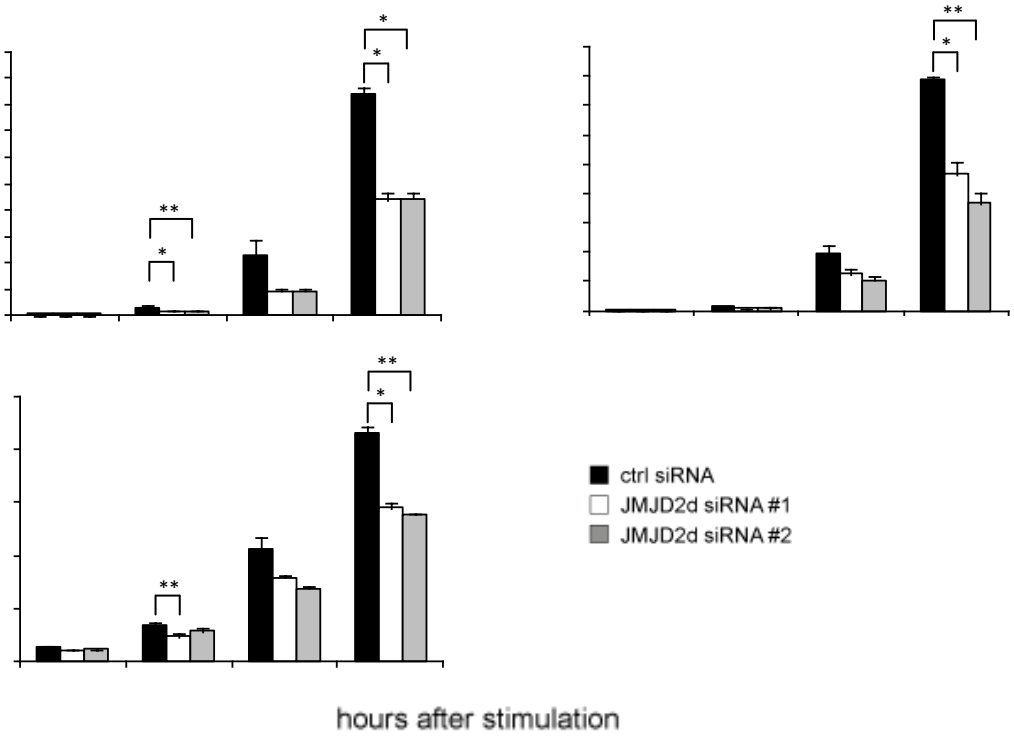

Figure 15. Knockdown of JMJD2d attenuates Ifnb1 and ISG activation in response to poly I:C. MEFs were transfected with either ctrl or JMJD2d siRNA for 48 hours and then stimulated with poly I:C. Shown are normalized expressions of the indicated genes at the indicated times after poly I:C stimulation. Data shown are the average of three independent transfections; paired T-test used for analysis (*p<0.05; **p<0.01).

We analyzed RNA extracts by microarray analysis, which revealed a significant decrease in ~30% of poly I:C stimulated genes, suggesting a broad effect on the type I interferon response (Figure 16).

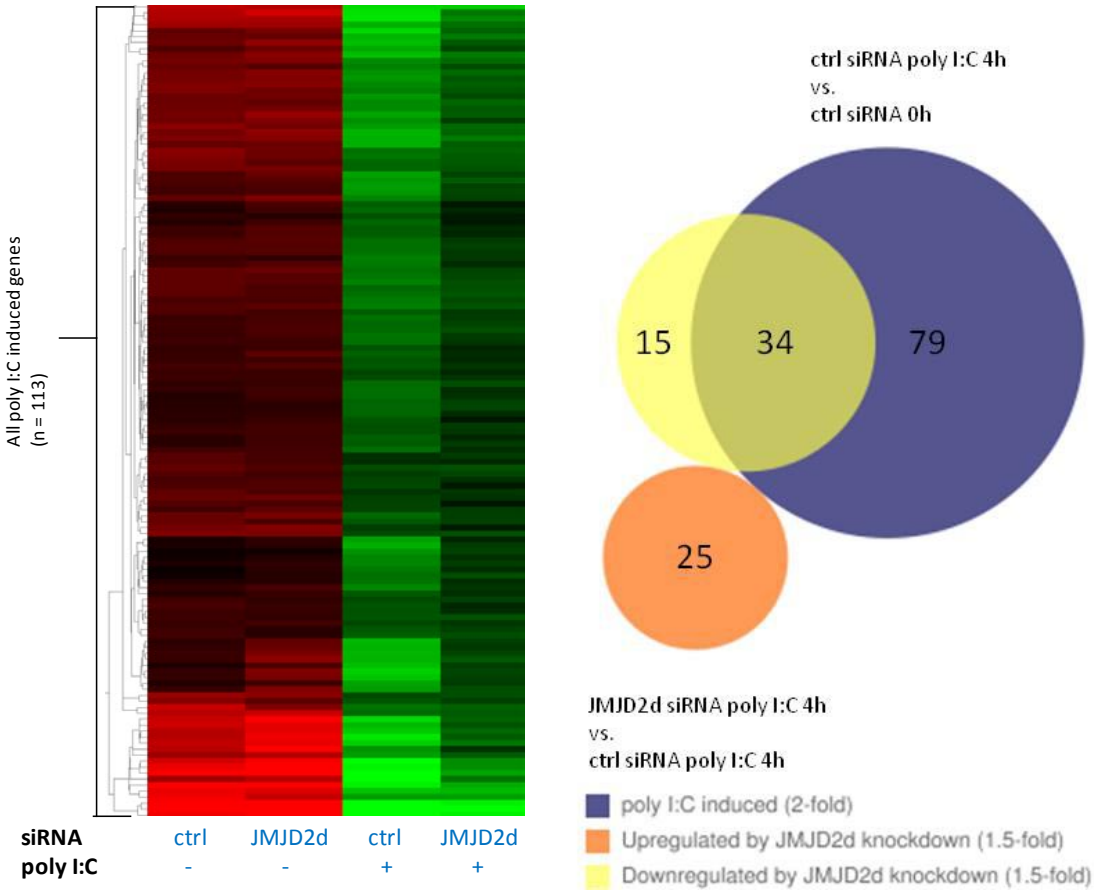

Figure 16. JMJD2d knockdown has a broad impact on the upregulation of several innate immune response genes. (A) Heat map showing decreased gene upregulation with JMJD2d knockdown in the 113 genes induced by poly I:C. (B) Venn diagram showing the proportion of poly I:C inducible genes downregulated and upregulated by JMJD2d knockdown. Data shown are the average of 3-4 independent samples subjected to microarray.

We then sought to determine if overexpression of JMJD2d would have the opposite effect. Cell lines stably overexpressing JMJD2d were generated and stimulated with poly I:C; here we observed a significant increase in the expression of IFN-β (Figure 17).

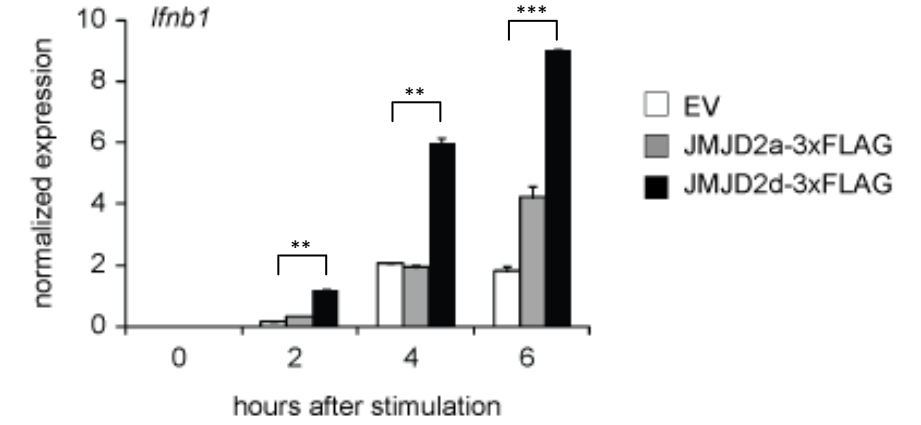

Figure 17. Overexpression of JMJD2d increases expression of IFN-β in response to poly I:C. Stable cell lines overexpressing empty vector (EV), FLAG-tagged JMJD2a, or FLAG-tagged JMJD2d were stimulated with poly I:C and collected at the time points indicated. Shown is normalized *Ifnb1* expression by qPCR. Data are representative of three independent experiments, with paired T-test used for analysis (**p<0.01; ***p<0.001).

Overexpression of JMJD2a did not have the same effect. Together, our knockdown and overexpression data implicate JMJD2d as a modulator of the poly I:C-induced activation of IFN-β.

To determine if these findings could be generalized to physiologic type I interferon signaling, JMJD2d knockdown and overexpression experiments were performed with subsequent virus infection. In response to infection with vesicular stomatitis virus (VSV), JMJD2d-knockdown MEFS expressed less IFN-β than control siRNA treated cells (Figure

18). Similarly, the response to VSV was moderately enhanced by the overexpression of JMJD2d (Figure 19).

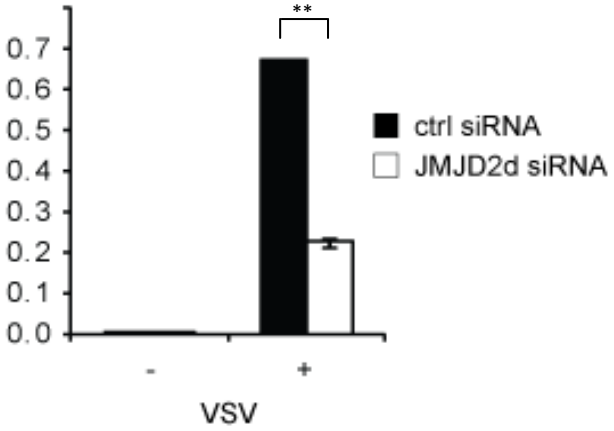

Figure 18. Knockdown of JMJD2d affects the IFN response to virus. MEFs were transfected with either control or JMJD2d siRNA and infected with VSV (MOI = 1). Cells were collected after 16 hours and RNA extracted; shown are the results of qPCR on triplicate infections where the Y-axis represents normalized *Ifnb1* expression; student's T-test performed for statistical analysis (**p<0.01).

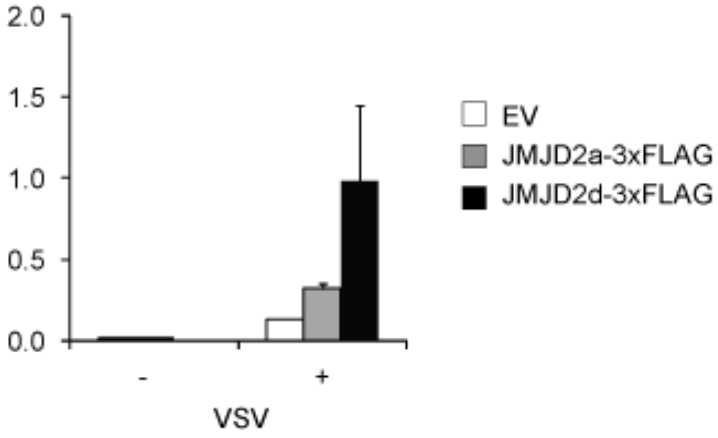

Figure 19. Overexpression of JMJD2d potentiates the IFN response to virus. Stable cell lines overexpressing empty vector (EV), FLAG-tagged JMJD2a, or FLAG-tagged JMJD2d were infected with VSV (MOI = 1). Cells were collected after 16 hours and RNA extracted. The Y-axis represents normalized *Ifnb1* expression; shown are the results of qPCR on triplicate infections; Student's T-test performed (no significant p-values).

These findings also extended to the frequency of viral infection using fluorescently-labeled virus. Knockdown and overexpression of JMJD2d conferred viral susceptibility to VSV-GFP and resistance to sindbis virus (with mCherry fluorophore), respectively (Figure 20). Taken together, these findings confirm a robust role for JMJD2d in broader type I interferon responses.

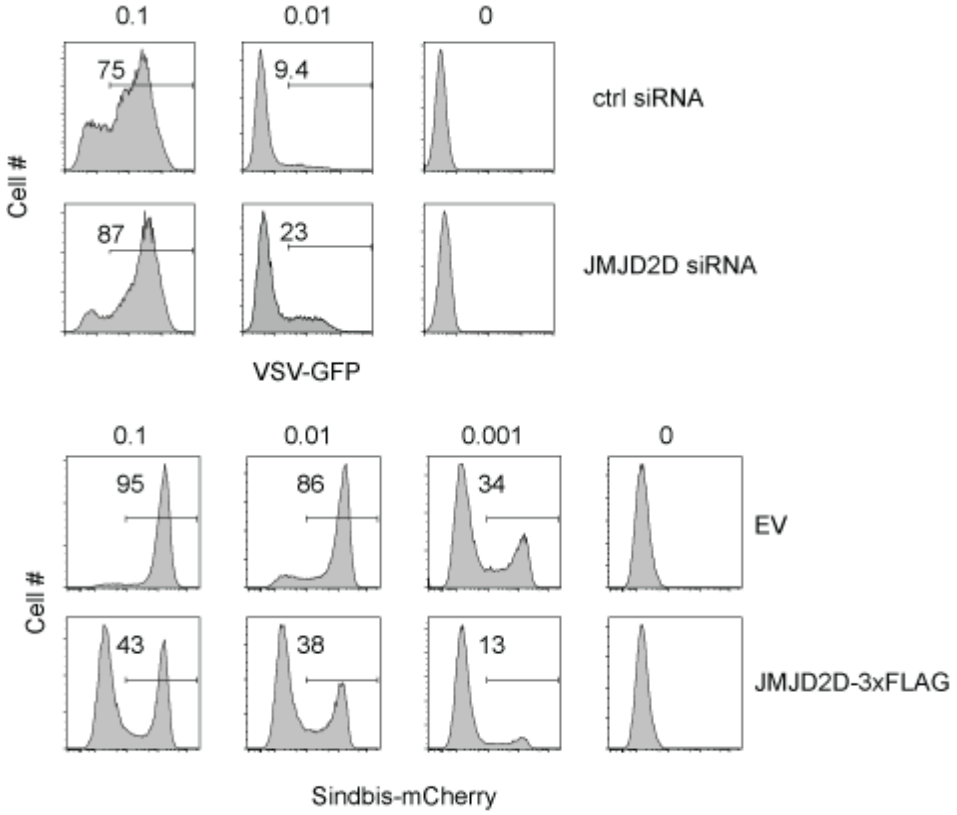

Figure 20. Viral susceptibility and resistance are conferred by knockdown and overexpression of JMJD2d, respectively. (A) MEFs were transfected with control or JMJD2d siRNA and infected with GFP-expressing VSV at the MOI indicated. After 16 hours, cells were subjected to flow cytometry and the percentage of GFP+ cells were calculated. (B) Stable cell lines overexpressing empty vector or FLAG-tagged JMJD2d were infected with mCherry-expressing Sindbis at the MOI indicated. After 16 hours, cells were subjected to flow cytometry and the percentage mCherry+ cells was determined.

In vitro modulation of JMJD2d in MEFs impacts stochastic activation of IFN-β

We next inquired if the effects of JMJD2d on IFN-β activation also extend to the stochastic features as well. Using the IFN-YFP fibroblasts described previously, we found that siRNA-mediated knockdown of JMJD2d decreased the percentage of YFP+ cells generated in response to poly I:C by approximately 30-50% (Figure 21). This finding was replicated across several time points, two different siRNAs, and multiple experiments.

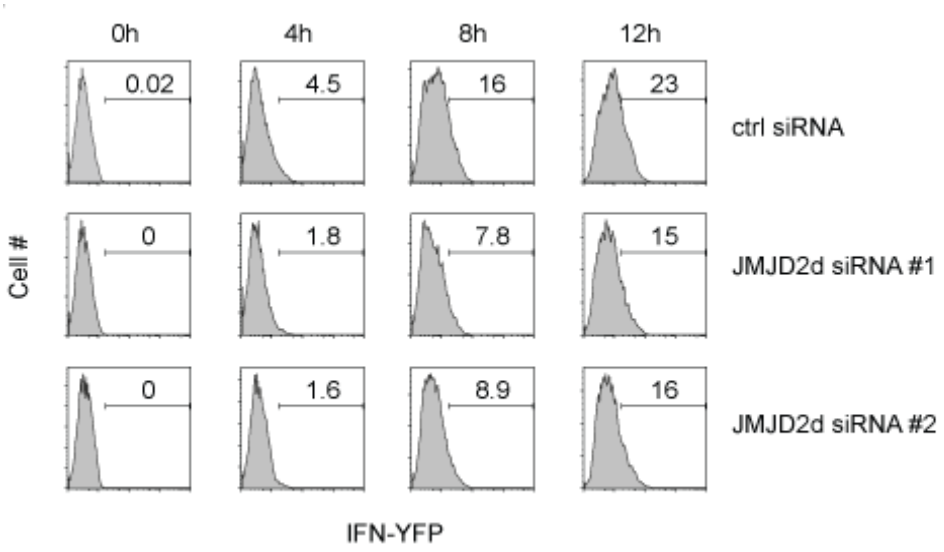

Figure 21. Knockdown of JMJD2d decreases the percentage of IFN+ cells in response to poly I:C. IFN-YFP MEFs were transfected with control or one of two JMJD2d-directed siRNAs and stimulated with poly I:C for the indicated times. Cells were collected and subjected to flow-cytometry to determine the percentage of YFP+ (IFN-expressing cells). Data shown are representative of three independent experiments.

We observed a similar phenomenon in the context of virus infection with substantial abrogation in %YFP+ cells following JMJD2d knockdown and subsequent infection with Sendai virus (Figure 22).

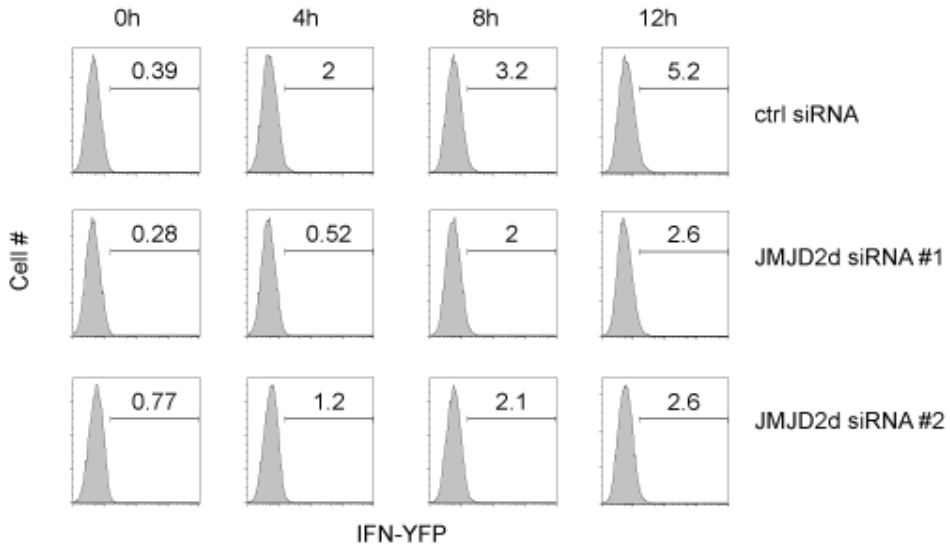

Figure 22. Knockdown of JMJD2d decreases the percentage of IFN+ cells following infection with Sendai virus. IFN-YFP MEFs were transfected with control or one of two JMJD2d-directed siRNAs and infected with SeV for the indicated times. Cells were collected and subjected to flow-cytometry to determine the percentage of YFP+ (IFN-expressing cells). Data shown are representative of three independent infections (conducted in parallel).

In the case of poly I:C stimulation, overexpression of JMJD2d in IFN-YFP cells yielded the opposite result, with an increase in the percentage of YFP+ cells by approximately 25-50% (Figure 23).

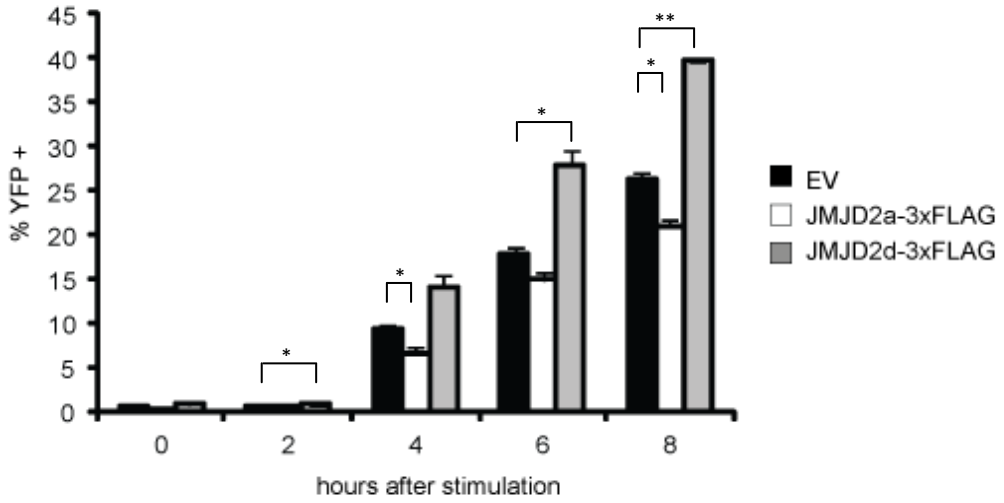

Figure 23. Overexpression of JMJD2d increases the percentage of IFN-producing cells in response to poly I:C. Stable cell lines overexpressing empty vector, JMJD2a, or JMJD2d were stimulated with poly I:C and subjected to flow cytometry at the times indicated. Data reflect the average of three independent transfections with paired T-test used for statistical analysis (*$p<0.05$, **$p<0.01$).

Having shown a robust impact of JMJD2d on the frequency and extent of innate immune responses, we next asked what is required for the effect of JMJD2d. In previous studies, JMJD2d has been described as an H3K9me^3 demethylase with enzymatic activity dependent on a critical histidine residue within its binding pocket (H192). We asked if this residue is important to our observed effects. To that end, we mutated the histidine residue to alanine (H192A) to determine if the effect of JMJD2d on type I interferon responses depends on its enzymatic activity. We subsequently overexpressed enzymatically-dead JMJD2d in MEFs and stimulated these cells with poly I:C. In contrast to wild-type JMJD2d, we found no effect on the frequency of IFN-β producing cells, suggesting the effect depends on the catalytic activity of the enzyme (Figure 24).

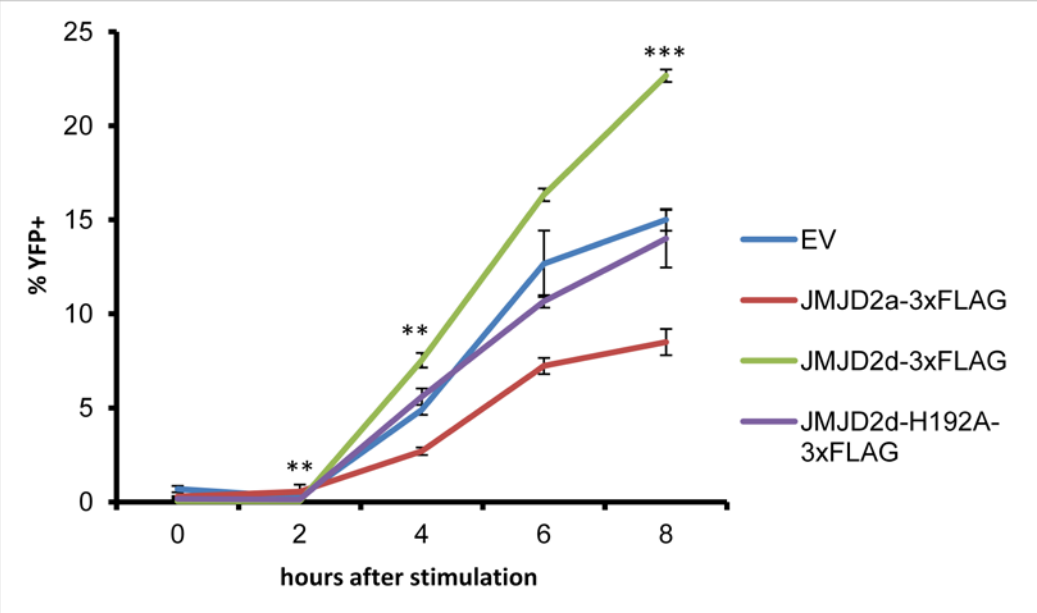

Figure 24. The catalytic activity of JMJD2d is required for the effect of JMJD2d overexpression on the frequency of IFN-producing cells. Stable cell lines overexpressing empty vector, JMJD2a, JMJD2d, or JMJD2d with the H192A mutation were regenerated and stimulated with poly I:C and subjected to flow cytometry at the times indicated. Data reflect the average of three independent transfections; Student's T-test performed for statistical analysis (**p<0.01; ***p<0.001).

Interestingly, the magnitude of the change in the frequency of YFP+ cells with knockdown and overexpression in these experiments nearly recapitulated the change in the quantity of transcript (see Figure 16/17). Of note, the mean fluorescence intensity in both knockdown and overexpression experiments was equivalent between control siRNA and JMJD2d siRNA samples and empty vector, JMJD2A overexpression, JMJD2D overexpression and JMJD2D-H192A overexpression samples, respectively. This suggests a role for JMJD2d in determining whether or not a cell activates IFN-β and not the extent to which it is transcribed in each cell. This data raised the possibility of JMJD2d as

a factor that not only modulates the type I interferon response but also helps to generate its stochasticity.

If JMJD2d positively contributes to stochastic IFN-β gene activation, it follows to reason that JMJD2d would be most enriched in IFN-producing cells. In our previous sorting experiments, we had observed increased IFN expression in sorted YFP+ populations, but lower levels of inducible eRNA. YFP- cells had high levels of eRNA but low levels of activated genes. We next asked which sortable population, if any, would display JMJD2d enrichment. Much to our surprise, YFP- cells displayed a substantial enrichment of JMJD2d (~5-fold higher than YFP+ cells) (Figure 25).

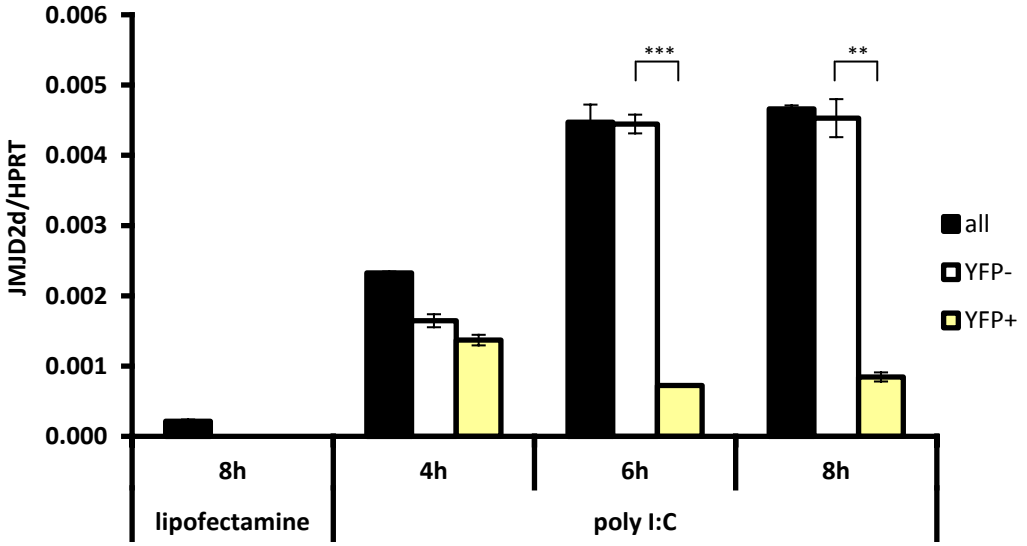

Figure 25. JMJD2d is preferentially expressed in cells that have high levels of enhancer RNA but low levels of gene activation. Quantitative PCR results of normalized *Jmjd2d* expression in IFN-YFP MEFs stimulated with poly I:C for the times indicated and subsequently sorted for YFP expression. Data shown are representative of three independent experiments, with a Student's T-test used for statistical analysis (**p<0.01; ***p<0.001).

In fact, the inducibility of JMJD2d with poly I:C stimulation observed previously occurred entirely in the YFP- population, with little difference in JMJD2d expression between poly I:C-stimulated IFN-producing (YFP+) cells and unstimulated cells. This result persisted in spite of blockade of any effects of IFN-signaling with the IFN-receptor antibody (Figure 26).

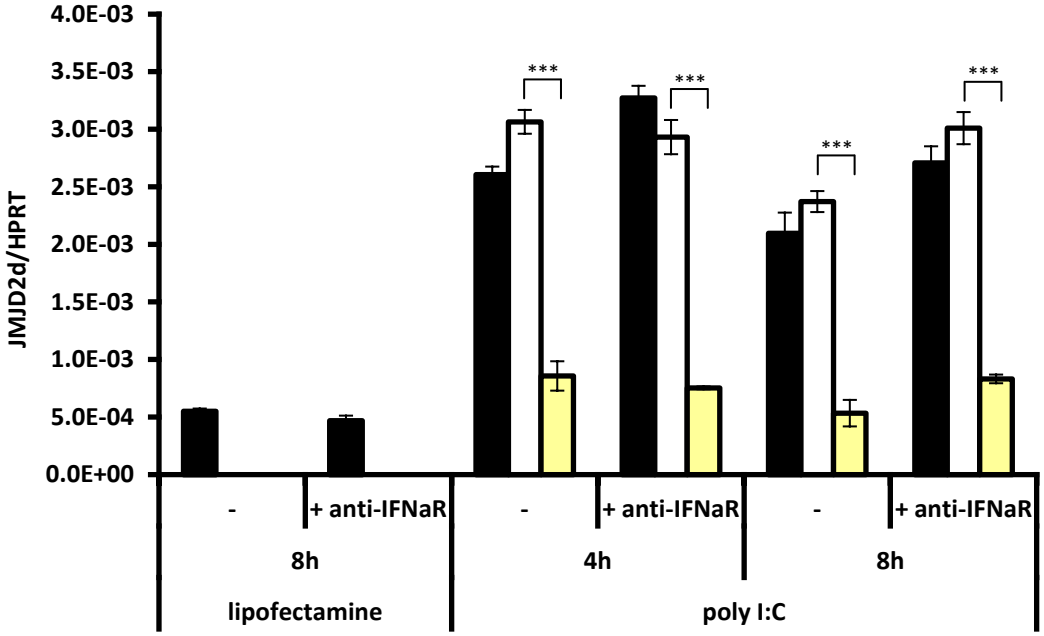

Figure 26. **Preferential expression of JMJD2d in YFP- cells occurs independently of the signaling effects of IFN.** Quantitative PCR results showing normalized *Jmjd2d* expression in IFN-YFP MEFs either pre-treated with vehicle or anti-IFNαR antibody and stimulated with poly I:C and sorted on the basis of YFP expression. Data shown are representative of three experiments, with statistical analysis conducted using a Student's T-test (***$p<0.001$).

At first glance, this constellation of results appears puzzling. JMJD2d displays a robust effect on the overall magnitude of IFN responses largely by affecting the percentage of responding cells which themselves are not enriched for JMJD2d. Because IFN responses are characterized by enhancer activation and JMJD2d upregulation is seemingly detectable only in YFP- cells, we postulate that both eRNA and JMJD2d upregulation are transient and necessary events required for IFN-β activation. What remains unclear is why both eRNAs and JMJD2d are lost in IFN-producing cells.

Knockout of JMJD2d does not reveal a clear phenotype

Having implicated JMJD2d in control of stochastic IFN responses, we sought to determine if a JMJD2d knockout mouse would recapitulate the *in vitro* findings. In mice, the JMJD2d gene consists of two exons, only the second of which contains the protein coding sequence. We generated a conditional targeting strategy employing *Cre* recombinase technology with loxP sites flanking exon 2 (Figure 27).

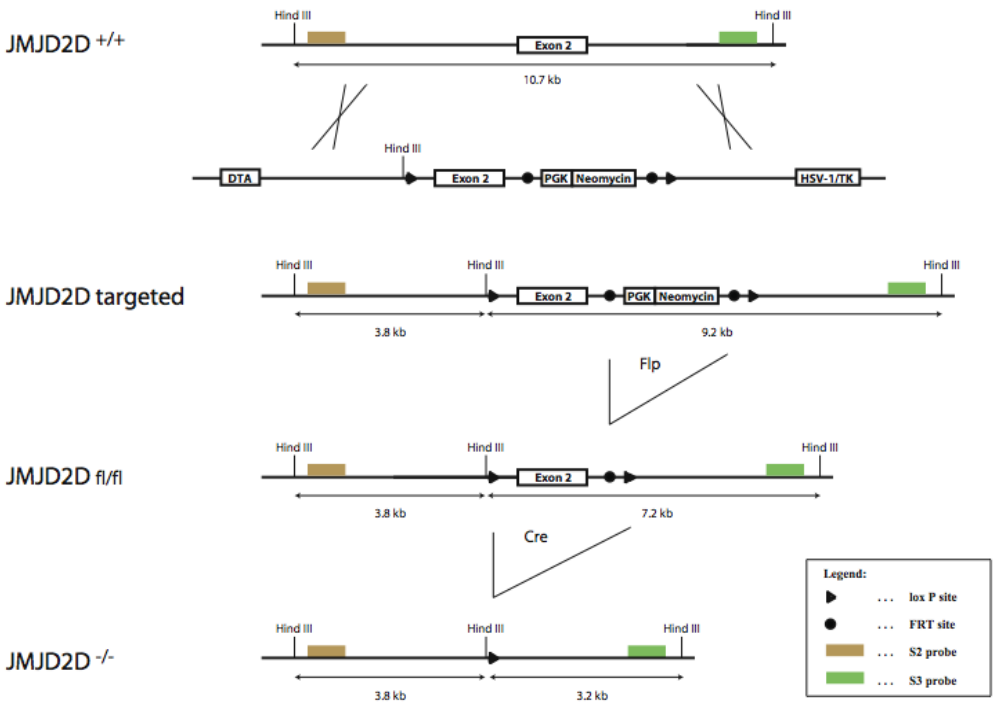

Figure 27. Targeting strategy for conditional knockout of JMJD2d. Exon 2 of mJMJD2d was targeted with insertion of a PGK/Neomycin antibiotic selection cassette and *loxP* sites as shown above. Probes were designed for Southern blotting as indicated by S2 and S3 probes in tan and green, respectively.

Following successful targeting, recombinant clones were confirmed by Southern blot analysis (Figure 28). After generation of JMJD2d$^{floxed/floxed}$ mice, two different *Cre* lines were used to delete in various cell types. Specifically, EIIA-Cre was used to generate germline knockout mice (JMJD2d$^{-/-}$) from which MEFs were derived and Vav-Cre was used to generate conditional deletion in hematopoietic cell lineages.

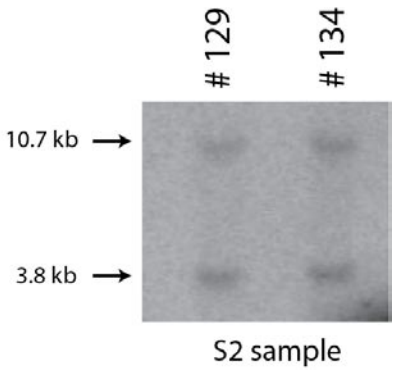

Figure 28. Evaluation of JMJD2d targeting by Southern blot. Genomic DNA was digested with Hind III. Using the S2 probe, 3.8kb and 10.7kb products corresponding to targeted and wild-type alleles, respectively, were identified. Clones were numbered #129 and #134 and were used to generate JMJD2d$^{-/-}$ mice used in the subsequent analysis.

JMJD2d$^{-/-}$ MEFs were isolated cultured, and immortalized as described previously. We confirmed the absence of any JMJD2d transcript; however, they did not clearly display any difference in poly I:C-induced IFN expression (Figure 29). Of note, the MEF cell lines – derived from separate embryos – displayed considerable heterogeneity in the amount of IFN expressed before stimulation, which persisted after poly I:C was administered.

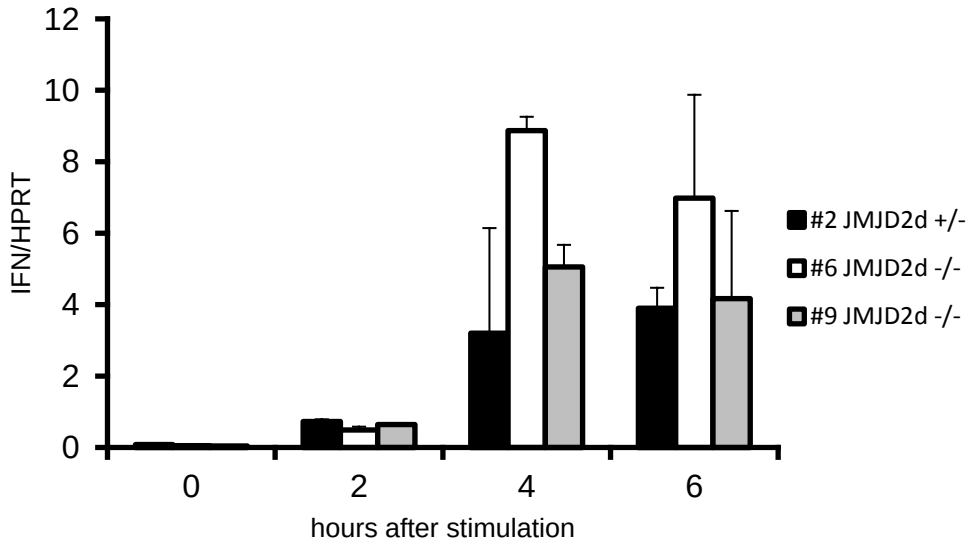

Figure 29. JMJD2d knockout MEFs do not display a consistent difference in poly I:C-induced IFN-β activation. Three independently derived MEF lines corresponding to JMJD2d$^{+/-}$ (#2) and JMJD2d$^{-/-}$ (#6, #9) genotypes were cultured and stimulated with poly I:C for the indicated times. Shown is the normalized *Ifnb1* expression. Data are from three independent experiments.

In a similar fashion, JMJD2d$^{-/-}$ bone marrow-derived macrophages were stimulated with poly I:C; no difference in IFN-β activation was observed (Figure 30). JMJD2d$^{floxed/floxed}$ Vav-cre^{+} mice were injected with Flt3 ligand to induce the maturation of splenic DCs. DCs were harvested and cultured and stimulated with poly I:C; in concordance with our other knockout data, no difference in IFN-β was elicited (Figure 31). Finally, JMJD2d$^{-/-}$ mice and age-matched littermates were injected with poly I:C. We again did not detect a difference in IFN-β accumulation in either the spleen or in serum (Figure 32). These experiments simply failed to extend the findings in MEFs with JMJD2d knockdown/overexpression to other cell types lacking JMJD2d entirely.

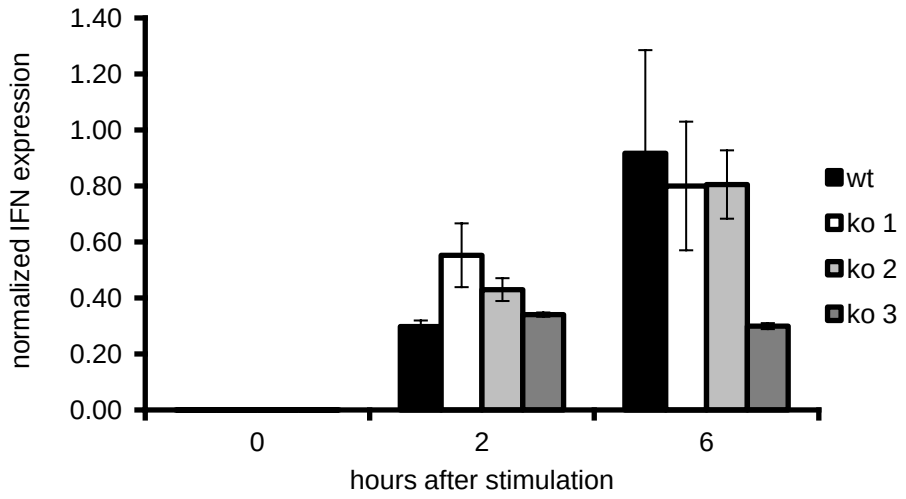

Figure 30. JMJD2d knockout macrophages do not display a consistent difference in poly I:C induced IFN-β activation. Bone marrow-derived macrophages from either JMJD2d$^{+/+}$ (wt) or JMJD2d$^{-/-}$ (ko) mice were generated and directly stimulated on day 7 with poly I:C (not transfected); shown is the normalized *Ifnb1* expression after the times indicated.

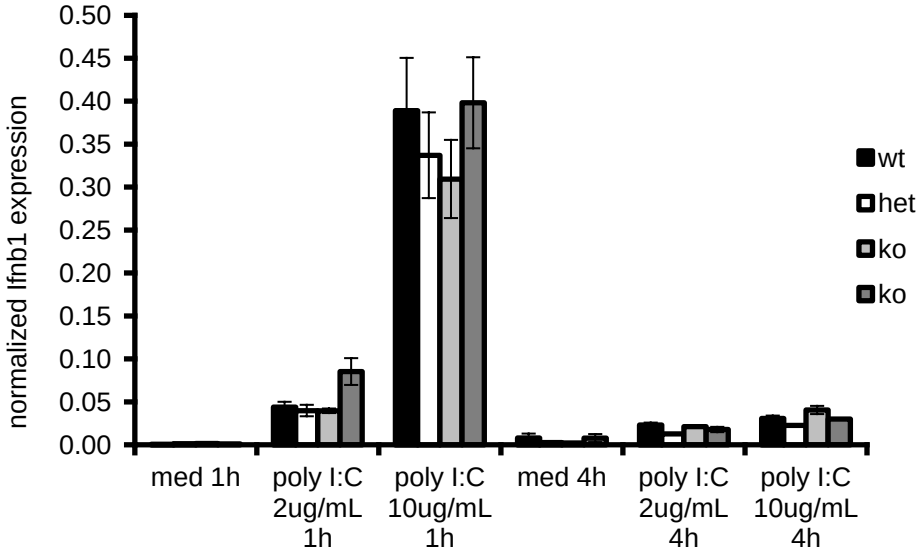

Figure 31. JMJD2d knockout splenic dendritic cells do not display a consistent difference in poly I:C induced IFN-β activation. Splenic dendritic cells (DCs) derived from either JMJD2d$^{fl/fl}$ (wt), JMJD2d$^{fl/+}$ Vav-cre^{+} (het) or JMJD2d$^{fl/fl}$ Vav-cre (ko) mice were injected with Flt3-L were cultured and stimulated with poly I:C for the times indicated; shown is the normalized *Ifnb1* expression.

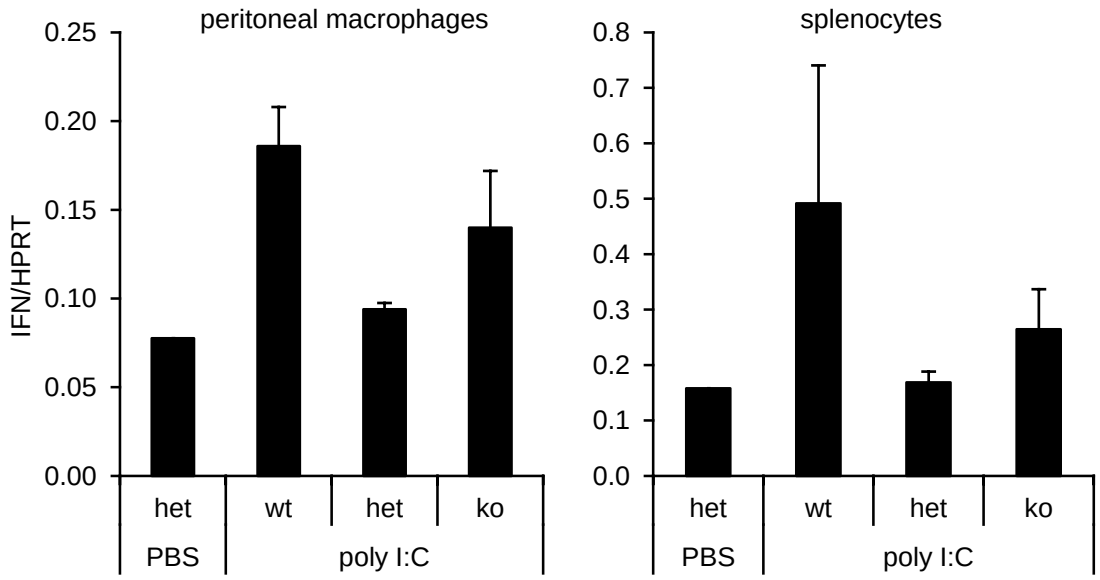

Figure 32. Systemic injection of poly I:C in JMJD2d$^{-/-}$ mice shows no type I interferon signaling defect. Three to five mice of each indicated genotype were injected with either PBS or 200 μg poly I:C as indicated. with subsequent harvesting of peritoneal macrophages or splenocytes after 8 hours. Quantitative PCR was performed on isolated cDNA; shown is normalized expression of *Ifnb1*.

The absence of IFN signaling effects with in vivo deletion of JMJD2D led us to be concerned that the findings with *in vitro* modulation of JMJD2d might represent non-specific effects of siRNA-mediated knockdown and retrovirally-transduced overexpression plasmids. To rule out artifact in these experiments, JMJD2d wild-type and knockout MEFs were transfected with JMJD2d siRNA. We observed that wild-type and JMJD2d heterozygous MEFs displayed any attenuation of IFN-β expression, while JMJD2d$^{-/-}$ MEFs were resistant to the effects of JMJD2d siRNA (Figure 33). In other words, the effect of JMJD2d siRNAs on IFN responses required the presence of JMJD2d in the cell, making a non-specific or off-target phenomenon less likely.

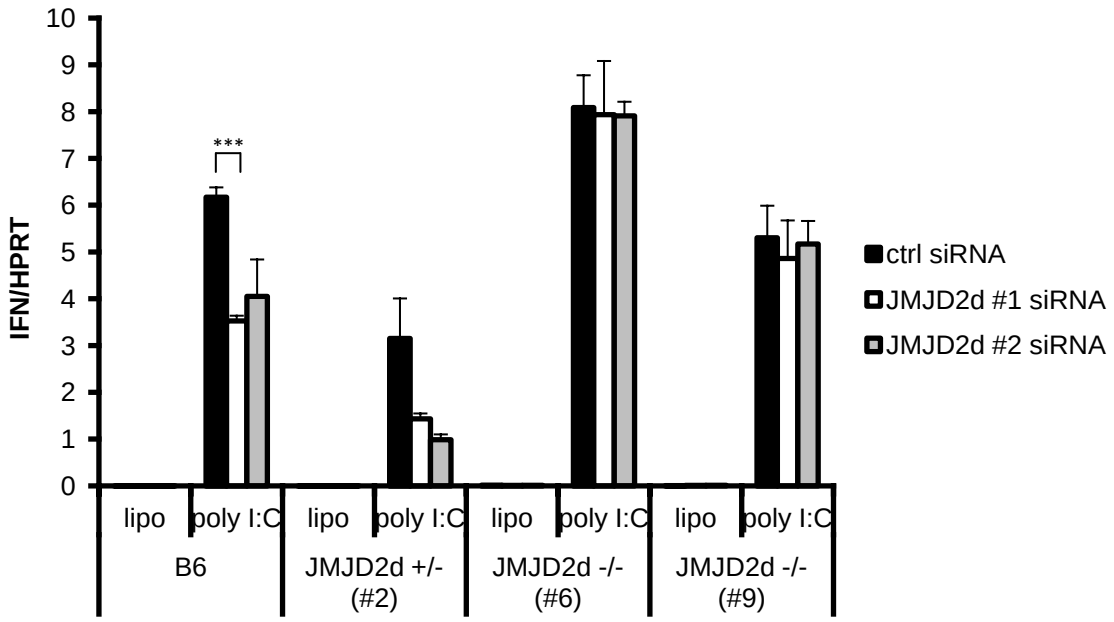

Figure 33. The effects of JMJD2d knockdown on poly I:C-induced IFN-β activation require the presence of JMJD2d. Wild-type (B6), heterozygous (#2) and JMJD2d$^{-/-}$ MEFs (#6, #9) were transfected with either control or JMJD2d siRNA and stimulated with poly I:C for 4 hours; shown is the normalized expression of *Ifnb1*. Student's T-test performed for statistical analysis (***p<0.001).

We concluded from the foregoing that JMJD2d modulation has a discernible, robust, and reproducible effect with a few caveats. First, it seems to be most defined in MEFs and does not occur in cells of other lineages. Second, knockout cells of the same type also do not display a relationship between JMJD2d and IFN-β – perhaps this is owing to compensation by another demethylase. Regardless, we concluded that JMJD2d modulation is indeed a specific phenomenon insofar as we observed the same phenomenon in multiple wild-type fibroblasts cell lines and not in those lacking JMJD2d.

Chapter III: Control of enhancer transcription by JMJD2d

The impact of JMJD2d modulation on chromatin

Heretofore we have described a central role for JMJD2d in the modulation of type I interferon responses in MEFs. This role apparently depends on the presence of a key histidine residue central to the enzyme's demethylase activity, a finding that led us to search for a role for JMJD2d on chromatin. At the outset, however, we sought to exclude the possibility that JMJD2d has a non-chromatin substrate for which its enzymatic activity is required. To answer this question, we transfected luciferase reporter constructs conjugated to the IFN-β promoter (IFN-luc) or to an IFN-sensitive response element (ISRE-luc) into MEFs. This provided a non-chromatinized IFN-β substrate responsive to the same upstream signaling elements and transcription factors as the endogenous IFN-β gene, but without the chromatin context (including any H3K9me$^{1/2/3}$). MEFs were transfected with JMJD2d-directed siRNA to mediate knockdown of JMJD2d mRNA, followed by transfection of either luciferase reporter 24 hours later. These cells were subjected to poly I:C stimulation with subsequent quantification of luciferase expression. We observed that siRNA-mediated knockdown of JMJD2d did not attenuate activation of the IFN- or ISRE-luciferase reporter in response to poly I:C (Figure 34), suggesting that the effects of JMJD2d depletion are not due to an impact on signaling.

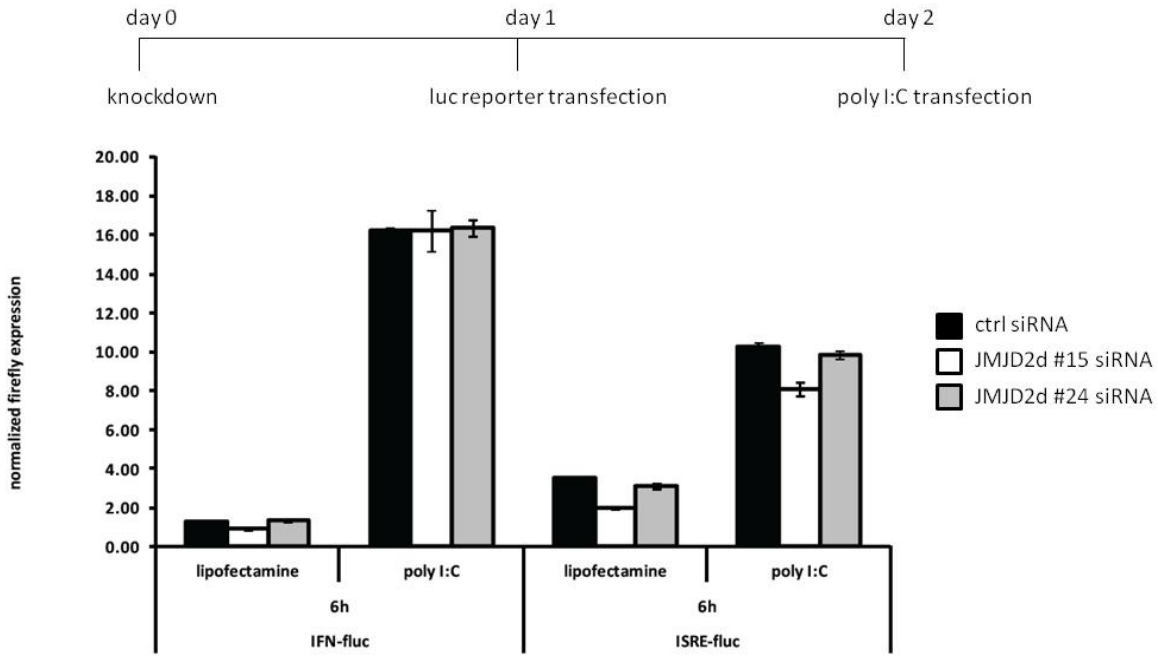

Figure 34. Chromatin is required for the effect of JMJD2d knockdown on poly I:C-induced IFN-β expression. MEFs were transfected with either control or JMJD2d siRNA as indicated, then transfected 24h later with either an IFN-luc or ISRE-luc reporter (non-chromatinized). Cells were stimulated 24h later with poly I:C and luciferase expression was measured; normalized firefly luciferase expression (using *Renilla* as control) is shown.

We conclude that JMJD2d is a positive regulator of IFN responses whose effect requires the presence of chromatin. Because type I interferon responses feature dynamic changes to chromatin leading to enhancer activation, we asked if JMJD2d knockdown interfered with these epigenetic events. MEFs were transfected with either control or JMJD2d-directed siRNA and stimulated with poly I:C 48 hours later. Cells were fixed and chromatin prepared for sequencing as described previously. Consistent with the broad effect on gene expression described previously, we observed a reduction with JMJD2d

knockdown in the amount of H3K4me^3, H3K9ac, H4ac, and Pol II at the 107 poly I:C-induced genes (Figure 35). While the overall magnitude reductions in each of these chromatin marks with JMJD2d knockdown were quite small, this result was highly significant given the number of genes integrated into each curve.

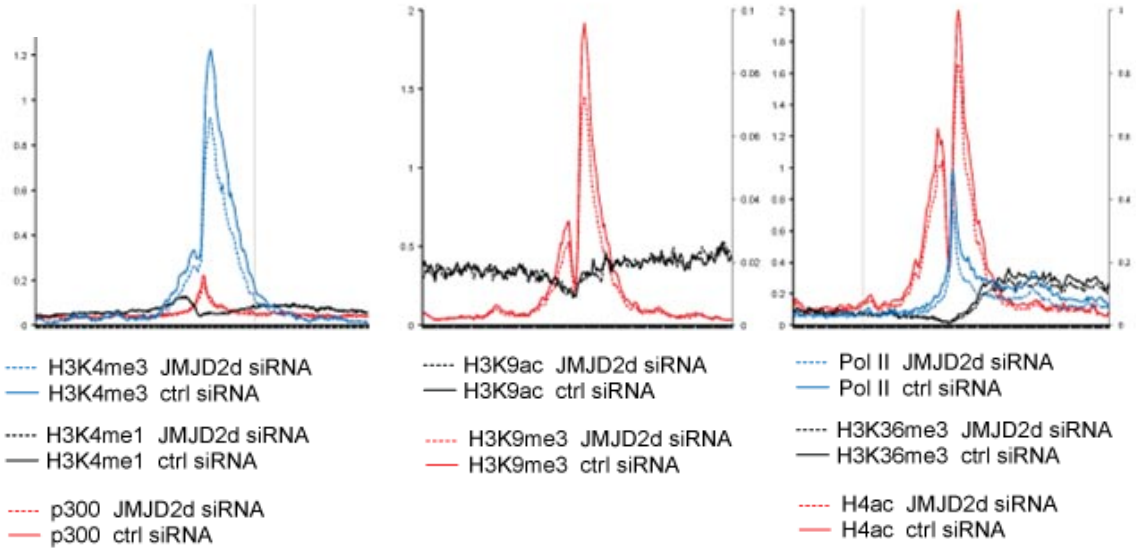

Figure 35. Diminished accumulation of active marks at promoters induced by poly I:C with JMJD2d knockdown. Integrated profile plots showing the average enrichment of the indicated marks by ChIP-sequencing in MEFs at promoters induced by poly I:C. Chromatin was harvested from cells treated with control or JMJD2d siRNA and stimulated with poly I:C.

The reduction of active histone modifications and Pol II was reflected in decreased transcription of poly I:C-induced genes in JMJD2d knockdown cells, as determined by RNA-sequencing (Figure 36). No reductions with JMJD2d knockdown in either chromatin marks or RNA transcripts were detected in a set of 107 random genes (data not shown).

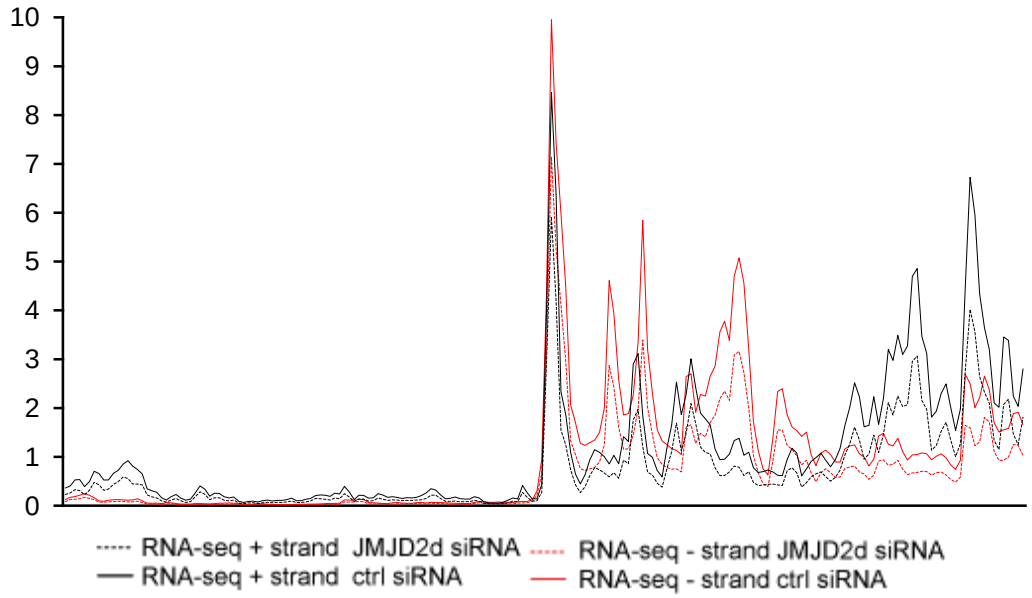

Figure 36. JMJD2d knockdown leads to diminished antiviral gene transcription. Integrated profile plots showing the average FPKM by RNA-seq of poly I:C-induced genes after 4h stimulation following pretreatment with either control or JMJD2d-directed siRNA as indicated.

These findings in the ChIP-sequencing data recapitulate what we previously described: a small but broad reduction in the expression of poly I:C inducible genes and active promoter marks typically associated with gene expression level. We next asked if similar differences could be observed at enhancer locations. Because our data pointed to a key role for dynamic H3K9 at enhancers in IFN signaling, we reasoned that JMJD2d knockdown might interfere with the accumulation of H3K9ac. Using our previous set of extragenic enhancers assigned to inducible genes, we found that JMJD2d knockdown did affect H4ac and Pol II accumulation at enhancers (Figure 37).

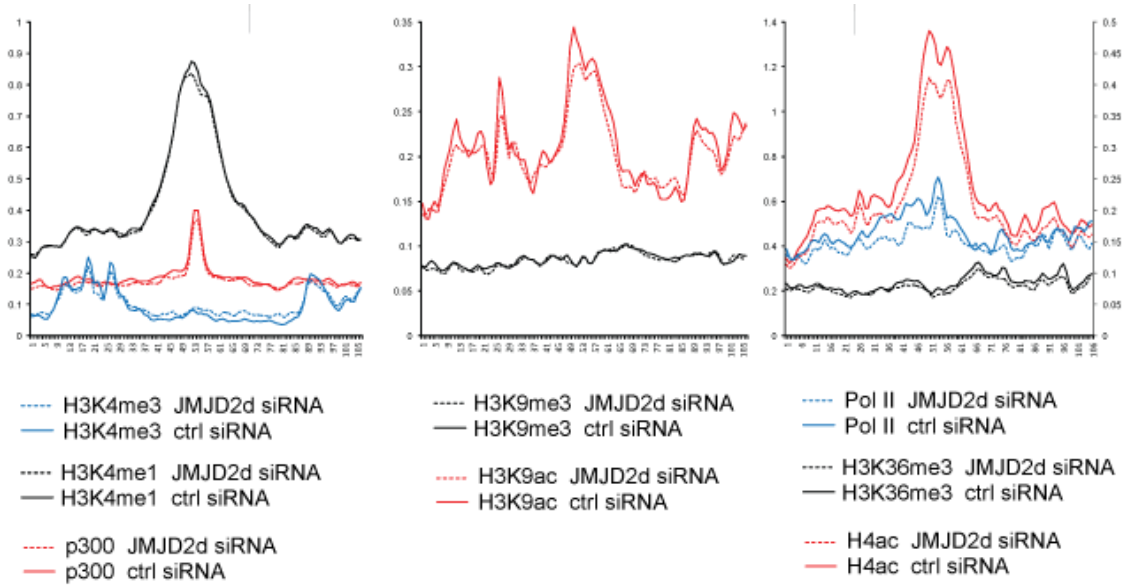

Figure 37. Altered dynamics of chromatin marks at enhancers also occurs with depletion of JMJD2d. Integrated profile plots showing the accumulation of the indicated marks as detected by ChIP-seq in MEFs at extragenic enhancers induced by poly I:C. Chromatin was obtained from cells stimulated with poly I:C after either treatment with control or JMJD2d siRNA.

A much smaller effect was discerned for H3K9ac, but this was magnified by restricting the group of extragenic enhancers to a smaller set in which poly I:C stimulation resulted in an H3K9ac increase (Figure 38). In other words, H3K9ac was induced to a lesser extent at enhancers in the setting of JMJD2d depletion.

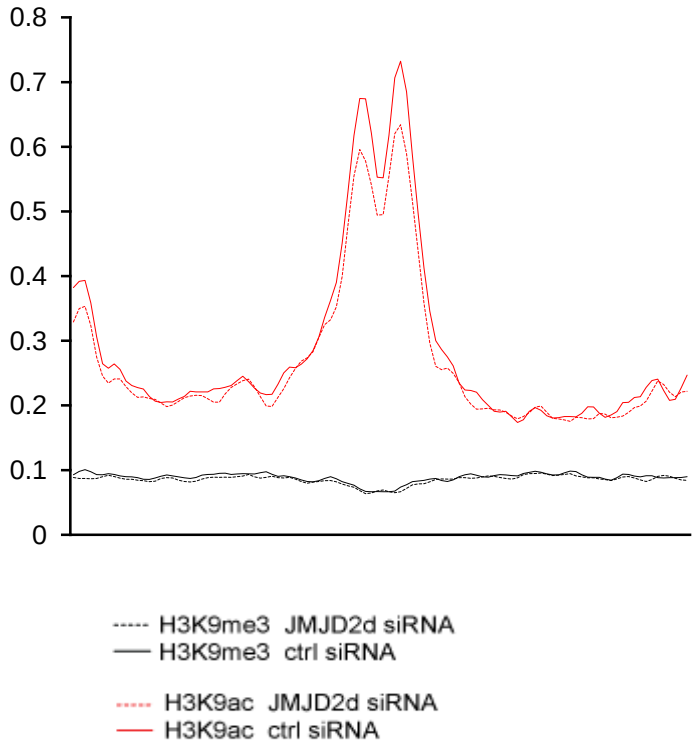

Figure 38. Diminished H3K9ac accumulation at enhancers that normally induce H3K9ac in the poly I:C-induced transcriptional response. Integrated profile plots showing the accumulation of H3K9ac and H3K9me^3 at extragenic enhancers in MEFs stimulated with poly I:C following pretreatment with control or JMJD2d siRNA.

We next asked if poly I:C-induced extragenic enhancers display altered transcription with JMJD2d knockdown. Using ribosomal-depleted RNA sequencing, we observed a small but perceptible reduction in eRNA transcripts with JMJD2d knockdown (Figure 39). This reduction occurred primarily among the transcripts that displayed H3K9ac inducibility with stimulation, suggesting that JMJD2d only affects those enhancers that are dynamic at lysine 9. In order to validate this result, we designed primers for key

inducible enhancers in the type I interferon response and performed qPCR for these eRNAs.

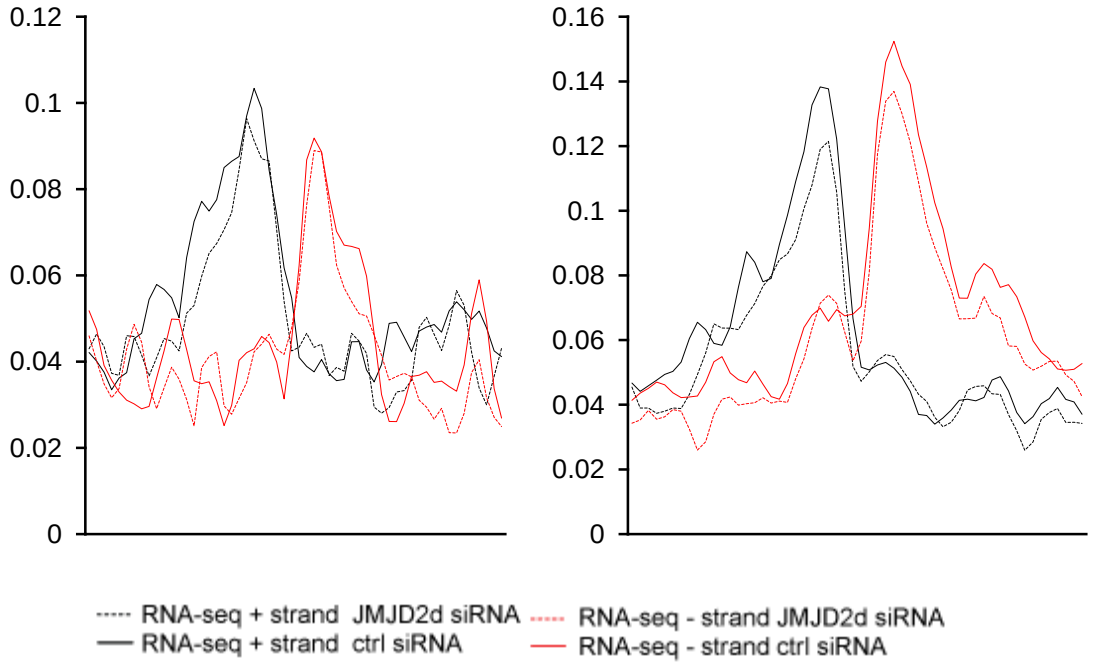

Figure 39. Diminished enhancer transcription is most notable among extragenic enhancers that induce H3K9ac. Integrated profile plots showing the FPKM of RNA transcripts as measured by RNA-seq in MEFs stimulated with poly I:C following pretreatment with either control or JMJD2d siRNA. All induced extragenic enhancers (left panel) and the subset of H3K9-inducible extragenic enhancers (right panel) are shown.

Specifically, we found that JMJD2d knockdown significantly diminished eRNA expression at enhancers downstream of *Ifnb1*, *Ccl5,* and *Mx2* without affecting any control enhancers at *Actb* (Figure 40).

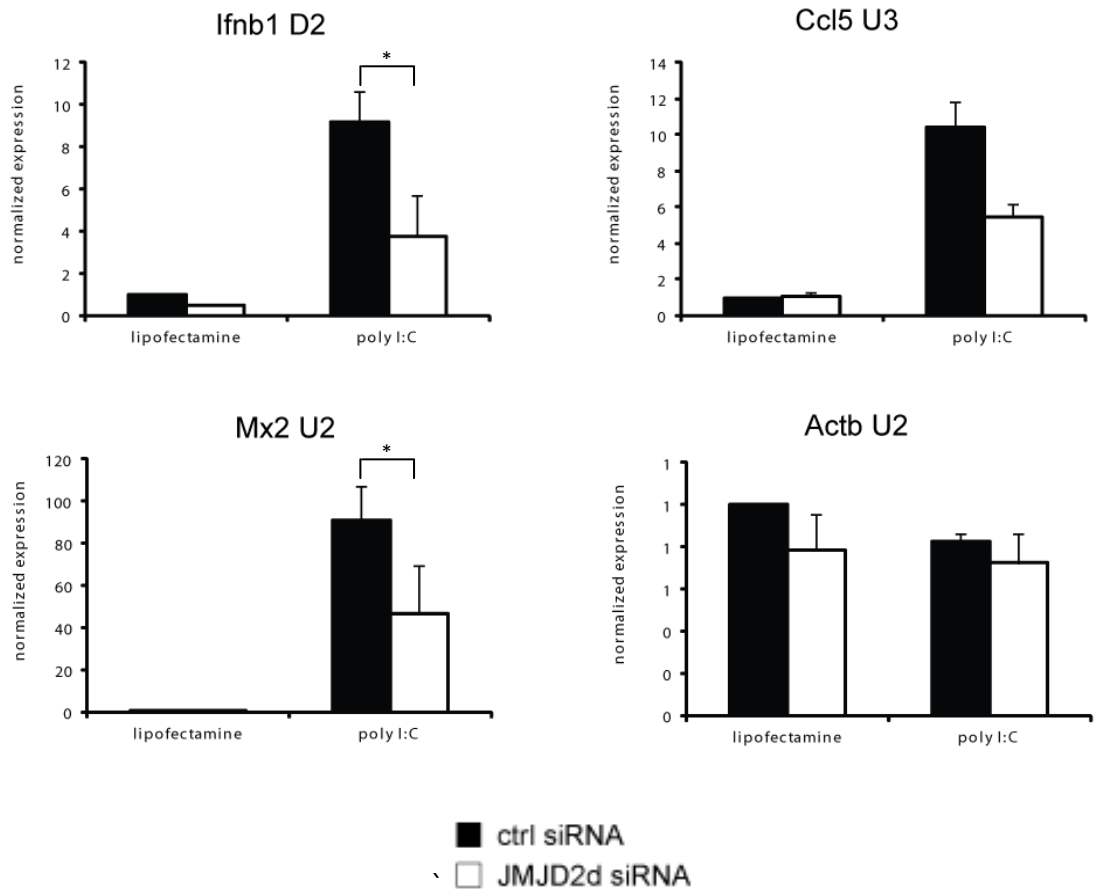

Figure 40. Enhancer RNA transcription is attenuated by the knockdown of JMJD2d. Quantitative PCR showing the reduction in detectable enhancer RNA transcripts with JMJD2d knockdown in MEFs stimulated by poly I:C following pretreatment with either control or JMJD2d siRNA. Student's T-test employed for statistical analysis (*p<0.05).

Our results clearly show a role for JMJD2d in chromatin dynamics as well as transcription at induced enhancers. Because JMJD2d is a H3K9 demethylase, we looked for a corresponding change in H3K9me^3, typically found at either end of the enhancer region as defined by the area of H3K4 monomethylation. In multiple experiments, we

did not observe any consistent change in this 'flanking' H3K9me^3, though enhancers with H3K9me^3 were the most dynamic in terms of both new H3K9 acetylation and Pol II accumulation. We attribute this finding to one of two possibilities: (1) a change in H3K9me^3 is in fact present, but ChIP-sequencing was not sensitive enough to elucidate it, or (2) no change in H3K9me^3 occurs and that JMJD2d functions instead to maintain a demethylated lysine 9 to facilitate acetylation (from H3K9me^1 or H3K9me^2 species) rather than to actively transition fully inactive or poised H3K9me^3 to an active state.

JMD2d is tightly associated with actively transcribed enhancers on chromatin

To this point, we have described a role for JMJD2d in the control of type I interferon responses. JMJD2d affects the frequency of IFN-producing cells presumably by regulating the activation and transcription of enhancers. JMJD2d is most highly enriched in those cells that have high levels of eRNA; when cells transition from enhancer transcription to gene transcription, JMJD2d is reduced to resting levels. Despite this circumstantial data, we did not yet have evidence to directly implicate JMJD2d in the control of enhancer chromatin. We therefore asked – what is the chromatin occupancy of JMJD2d?

We initially sought to perform ChIP-sequencing for endogenous JMJD2d in MEFs. Unfortunately, no commercially available antibody displayed any enrichment for JMJD2d in multiple immunoprecipitations; Western blot analysis using these antibodies failed to adequately detect endogenous JMJD2d (data not shown). As a result, we examined stable JMJD2d-3xFLAG overexpressing cell lines against empty vector controls to determine the occupancy of JMJD2d. Chromatin was prepared as before and immunoprecipitation was performed with Flag antibody coupled to magnetic beads. In genome browser alignments, we recognized a significant enrichment in JMJD2d at enhancer positions that was not present at promoters (Figure 41). Of note, the binding pattern of JMJD2d was relatively broad, occurring over multiple kilobases. Across the genome, we further noted substantial enrichment in FLAG signal in JMJD2d-3xFLAG

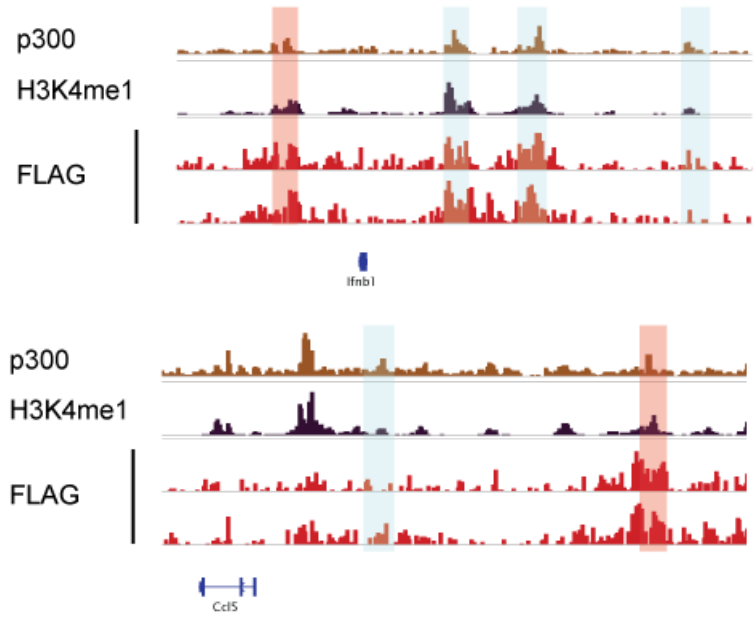

Figure 41. JMJD2d occupancy aligns with enhancer locations in the genome. Genome browser tracks showing the colocalization of JMJD2d (as detected by FLAG ChIP-seq) with p300 / H3K4me1 regions (blue boxes highlight (+) strand enhancers / red boxes highlight (-) strand enhancers) in regions surrounding the *Ifnb1* and *Ccl5* genes.

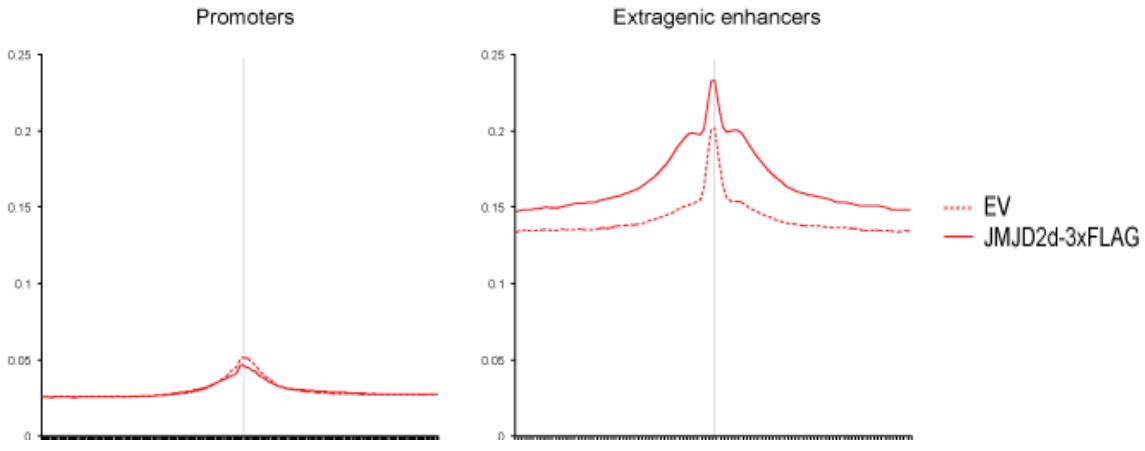

Figure 42. JMJD2d is enriched at enhancer chromatin genome-wide. Integrated profile plots showing the enrichment of FLAG in JMJD2d-3xFLAG or empty vector (EV) MEFs at either promoters (left panel) or extragenic enhancers (right panel) as determined by ChIP-seq data. Data shown are representative of three independent experiments in two independently derived cell lines.

chromatin samples relative to empty vector samples primarily at enhancers and not promoters (Figure 42). We subsequently took great care in peak-calling using algorithms optimized for the broad-type enrichment that we observed (see Materials and methods). After setting a false-discovery rate to <2.5%, we identified 4821 discrete JMJD2d-binding sites throughout the genome in unstimulated JMJD2d overexpressing MEFs; of these binding sites, approximately 70% colocalized with enhancer positions, while only 19% overlapped with promoters (Figure 43). Of the top 1000 JMJD2d binding sites in the genome, 85% overlapped with enhancers.

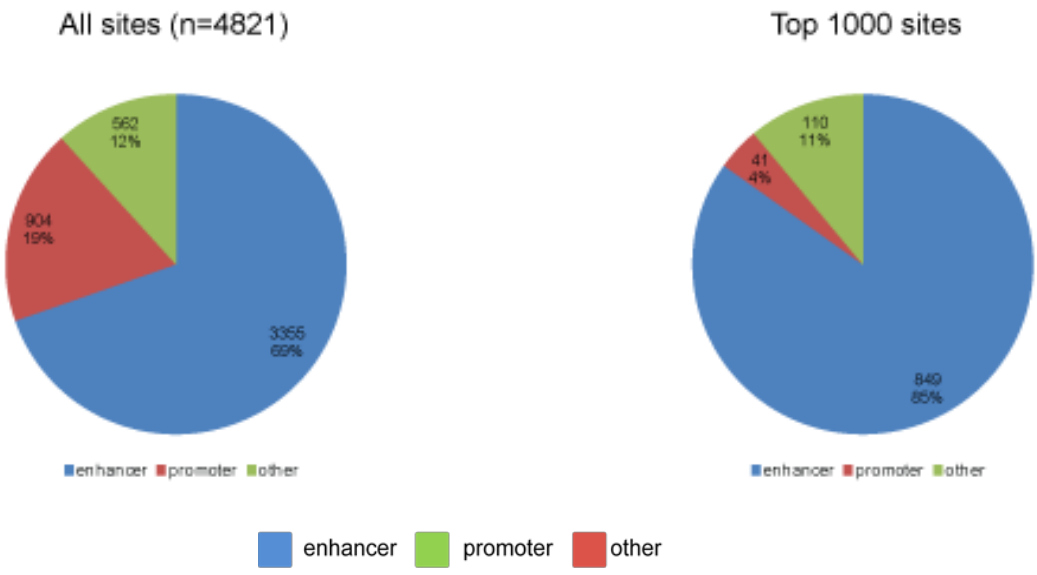

Figure 43. The majority of JMJD2d binding sites in the genome colocalize with enhancers. Pie charts showing the percentage of JMJD2d binding sites overlapping with promoters (red), enhancers (blue), or other chromatin regions (green) for all binding sites with FDR<0.25 (n=4821) (left) or for the top 1000 sites (right).

Given the strong association between JMJD2d and enhancers, we next asked if JMJD2d is specifically enriched at particular subtypes of enhancers (i.e. active, intermediate, or poised). By H3K27 status, JMJD2d-bound enhancers were more likely to be active rather than intermediate or poised. We suspected that JMJD2d might be bound to active (H3K9ac) or intermediate (H3K9-) enhancers rather than poised (H3K9me^3) enhancers because the enzyme would be unlikely to be bound without having catalyzed its target residue. Consistent with this hypothesis, we found that active enhancers were much more likely to be bound by JMJD2d than either poised or intermediate ones (Figure 44).

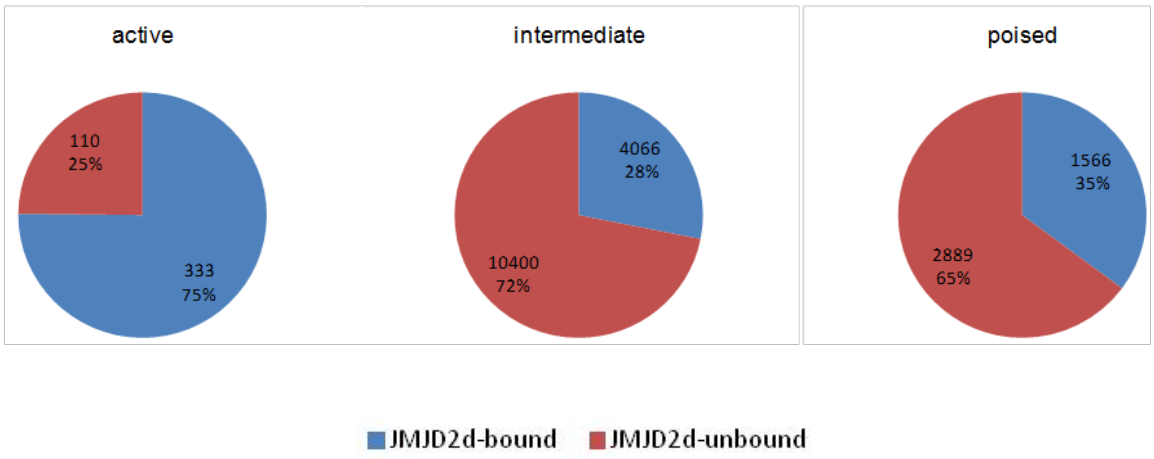

Figure 44. Active enhancers are more frequently bound by JMJD2d than poised or intermediate enhancers. Pie charts indicating the percentage of JMJD2d-bound (blue) or JMJD2d-unbound (red) enhancers belonging to extragenic enhancers of each type: active (H3K9ac+), intermediate (H3K9-), or poised (H3K9me^3 within 7.5 kb of enhancer center)

This data suggests that JMJD2d remains bound to enhancers where it has presumably demethylated K9 lysine residues. This observation fits nicely with our previous finding that enhancers with inducible H3K9ac are the most impacted by JMJD2d depletion, given that H3K9 acetylated enhancers are those bound by JMJD2d. In other words, JMJD2d – a demethylase that appears to potentiate enhancer activity – localizes precisely on those enhancers that are most active.

Next, we asked if the chromatin occupancy of JMJD2d also displays dynamic features. JMJD2d-3xFLAG-overexpressing MEFs were stimulated with poly I:C and chromatin prepared as described previously. After 4 hours of poly I:C stimulation, JMJD2d binding was substantially altered. Though JMJD2d remained bound primarily to enhancers, we found substantial changes to binding sites corresponding to the locations of enhancers of nearby induced genes, with many sites either gaining or losing JMJD2d occupancy (Figure 45).

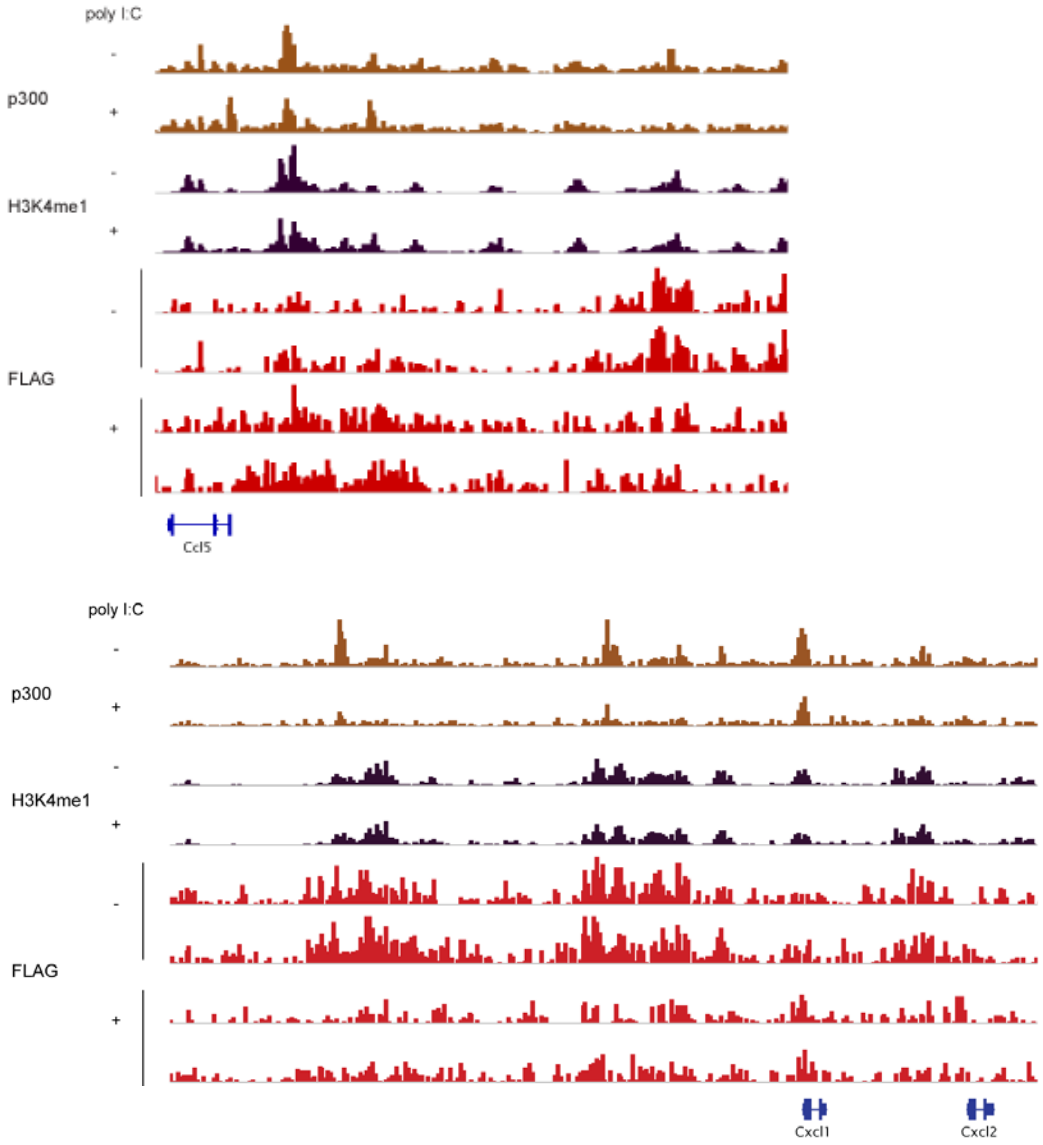

Figure 45. The localization of JMJD2d is dynamic with poly I:C stimulation. Genome browser tracks showing the enrichment of FLAG in duplicate samples either before (top 2 red tracks) or after (bottom 2 red tracks) poly I:C stimulation, in regions surrounding the *Ccl5* (top) and *Cxcl1/Cxcl2* (bottom) chromatin regions.

This provides another piece of evidence to support JMJD2d as an enzyme crucial to enhancer activation. If JMJD2d in fact participates in this process, we hypothesized that its binding would positively correlate with other marks of active enhancers, such as p300 and eRNA expression. Though we saw changes in the enrichment of p300 at a given enhancer accompanied by a corresponding change in the amount of JMJD2d, we could not identify a significant genome-wide correlation. But when we restricted our analysis to enhancers dynamic in the innate immune response, we saw a modest correlation (r = 0.57) between the change in p300 and the change in JMJD2d with stimulation (Figure 46).

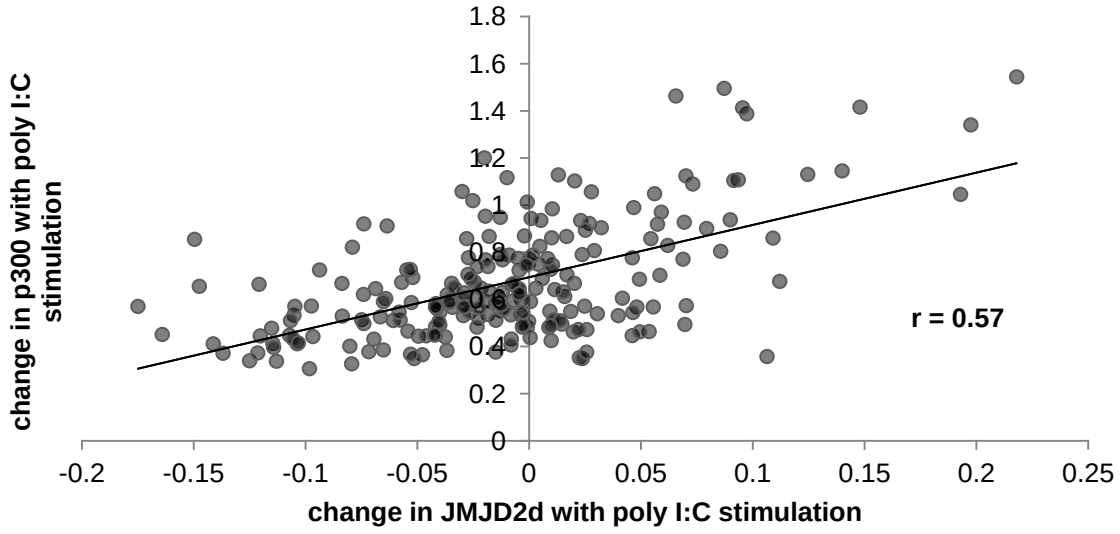

Figure 46. Mild correlation between the change in JMJD2d occupancy and the change in p300 enrichment with poly I:C stimulation. The changes in enrichment of JMJD2d and p300 at H3K9c-inducible extragenic enhancers between unstimulated and poly I:C stimulated samples was calculated and plotted as above. Shown is the Pearson correlation coefficient.

Because p300 is also a marker of enhancer activity, we suspected that enhancer transcription might correlate with JMJD2d binding, but no discernible correlation could be identified.

As we were unable to identify a strong genome-wide correlation between JMJD2d and enhancer transcription and p300 coactivator occupancy, we turned to a chromatin state model to parse out these relationships. Such analyses have formed the backbone of chromatin annotation of both human and *Drosophila* genomes, respectively (Ernst et al, 2011; Kharchenko et al. 2011). Specifically, using a hidden Markov model, we were able to identify 29 unique chromatin states that capture the complexity of chromatin profiles, using the combinatorial data provided by our set of ChIP-seq and RNA-seq data (Figure 47). Each state is defined by a relative enrichment of each of the marks used to train the data set.

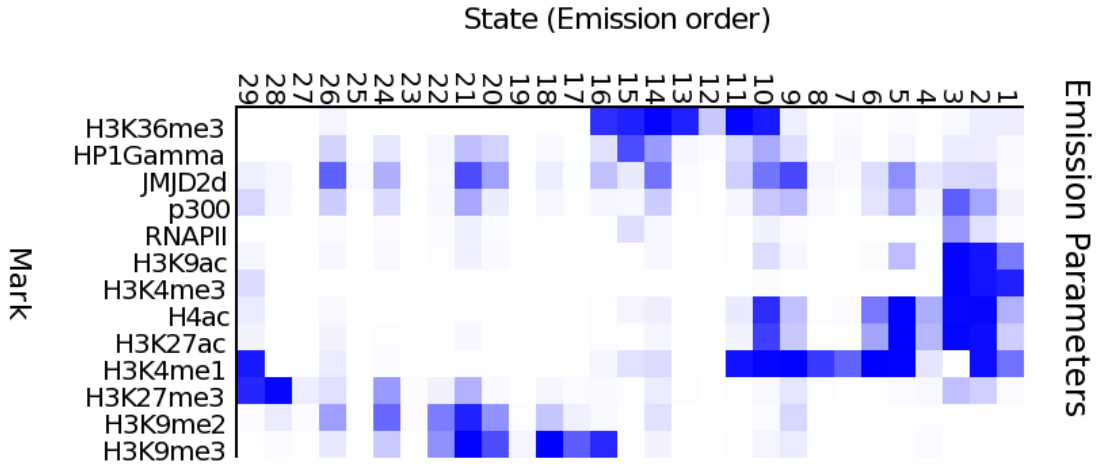

Figure 47. Chromatin state analysis reveals JMJD2d strongly associated with enhancer chromatin. Multivariate hidden Markov model emission showing 29 chromatin states based on ChIP-seq for the marks as indicated on the left. Intensity of each box indicates the frequency with which each state is accompanied by a given histone mark.

We pursued this type of analysis to capture the association between JMJD2d and regulatory elements and their associated marks with the greater precision and robustness as has been described. As in previous studies, our 29 states could be subdivided into those associated with promoters, enhancers, transcribed, or inactive states. We did not have here the data with which to parse out insulator states (i.e. CTCF ChIP-seq).

In our analysis, we found that JMJD2d was most enriched in states 9, 21, and 26 and to a lesser extent in 5, 10, and 14. In keeping with our speculation, states 9, 21, and 26 were notable for higher enrichment of p300 than states 5, 10, and 14. More broadly, states 5-

11 displayed enrichment of H3K4me^1 without H3K4me^3, suggesting these as potential enhancers. In these states, there are varying degrees of enrichment of p300, H3K9ac, H4ac, and H27ac – all markers of enhancer activity – with which the state enrichments of JMJD2d appear to closely correlate. JMJD2d was also notably largely absent from promoter/TSS states (1-3) and likely heterochromatin states (17-18, 27-28); this confirms the idea that JMJD2d is most highly associated with enhancer chromatin. Whereas genome-wide correlations could not be generated, these findings further reinforce our view that JMJD2d is a key regulator of enhancer transcription as its enrichment closely follows other markers of active distal regulatory elements.

To this point, we have outlined a role for JMJD2d in the control of type I interferon responses. Our data points to an effect of JMJD2d modulation on gene activation that is accompanied by an impact on the activation of enhancers – both in terms of the accumulation of active chromatin marks and the upregulation of enhancer transcription. Because enhancer activation temporally precedes gene transcription and there is no upstream signaling defect, we argue that the effects seen with JMJD2d depletion and overexpression arise directly from its effect on enhancers, which is precisely where the enzyme is bound on chromatin.

JMJD2d associates with chromatin remodelers and DNA repair machinery

Our final question is whether JMJD2d engages in its activities on enhancer chromatin alone or as part of multimeric protein complex. We hypothesized that JMJD2d would require interactors because its structure is unique among the Jumonji family of demethylases in that it lacks both PHD and Tudor domains that interact with methylated histones. Because JMJD2d lacks such structural domains with which to cooperatively engage both H3K9me$^{2/3}$ and a second residue (say H3K4me^{1}), we suspected that it would require binding partners to 'find' enhancers.

Table 2. JMJD2d associates with several DNA repair proteins and histone remodelers. Mass spectrometry results indicating the most highly enriched peptides with at least four unique spectra following immunoprecipitation of JMJD2d using FLAG antibody.

Protein	Function	Enrichment
PARP2	ADP-ribosylase	11.53
JMJD2D	Histone demethylase	10.70
RAD23B	XPC complex	10.27
RPS8	RPA & synthesome complexes	8.07
LTV1	Ligase	7.61
XRCC6	RAP1 complex	7.31
RPS24	RPA & synthesome complexes	7.29
AHCYL1	Homocysteinase	6.65
XRCC5	RAP1 complex	6.18
HIST1H2AD	Histone	6.02
SSRP1	FACT dimer subunit	5.55
CBX3	Heterochromatin protein	5.55
HIST1H4A	Histone	5.37
PNO1	RNA-binding protein	5.26
EMD	Nuclear membrane protein	5.22
KLHL26	Unknown	5.20
USP9X	Transcription co-activator	4.94
HIST3H2BB	Histone	4.72
RPA1	DNA-binding protein	4.69
TSR1	Transcription co-activator	4.69

To determine if such interactors exist, we performed immunoprecipitation of JMJD2d-3xFLAG with M2 beads followed by mass spectrometric (MS) analysis. Trypsin digests revealed several DNA repair proteins and chromatin remodelers, including FACT complex members (SSRP1, SUPT16H) and RAP1 complex members (XRCC5, PARP1) (Table 2). We confirmed by Flag-IP followed by Western blotting that XRCC5 and PARP1 immunoprecipitate with JMJD2d (Figure 48).

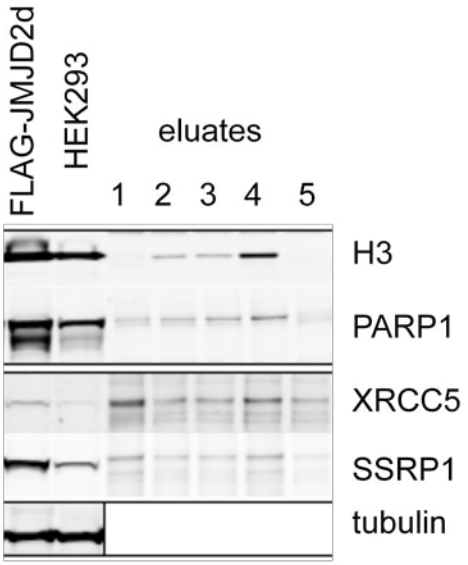

Figure 48. JMJD2d appears to interact with PARP-1, XRCC5, and SSRP1. Immunoprecipitation of JMJD2d in stably transfected HEK293 cells using FLAG antibody followed by Western blotting as shown.

Interestingly, PARP1 has been previously linked to enhancer binding through its DNA-binding domains and appears to promote the recruitment of transcriptional coactivators (Kraus, 2008). Of note, PARP-1 interacts with enhancers in a sequence-specific fashion, suggesting the possibility that PARP-1 recruits JMJD2d to specific enhancer positions.

Because a clear model of the regulation of gene expression by PARP-1 has yet to be elucidated, the significance of the JMJD2d-PARP1 interaction remains unknown.

Chapter IV: Discussion

In the last few years, there have been significant advances in our understanding of enhancer chromatin. We know now that distal regulatory elements are typically annotated with specific histone marks, such as the preponderance of H3K4me^{1} and the absence of H3K4me^{3}. Enhancers also feature many of the same combinatorial histone marks initially described for transcriptional start sites and promoters, such as H4ac and H3K9ac. Indeed, the epigenetic landscape at enhancer positions closely mirrors that of promoters because they too are transcribed, with detectable enrichments of the RNA polymerase machinery and enhancer RNA transcripts. These findings have made clear that not all regulatory elements are equal; the pattern of histone marks and coactivator binding make some enhancers active and others inactive. As before, the active enhancers are frequently transcribed and feature 'active' histone marks, while poised enhancers are less commonly transcribed and can feature 'repressive' histone marks. Functionally, enhancers serve as platforms for the engagement of transcription factors and therefore serve to integrate upstream signal with downstream gene transcription.

To date, little is known about how these enhancers and associated chromatin environments are controlled. Several studies have shown that transcription factors can 'license' enhancers ('pioneer' factors) or bind cooperatively to enhancer chromatin. Moreover, the histone acetyltransferase complexes p300/CBP and Gcn5/PCAF likely modulate the acetylated lysine 27 and lysine 9 histones seen at active enhancer

chromatin. But the factors that modulate methylated histone marks at enhancer chromatin and determine the patterning of active versus poised are largely unknown, as are the natural dynamics of enhancer chromatin in transcriptional contexts.

In the preceding analysis, we describe a novel role for the histone 3 lysine 9 demethylase JMD2d in the modulation of enhancer activity in innate immune responses. We have shown that type I interferon signaling is typically characterized by the activation of enhancer transcription and the accumulation of acetylated histones at enhancers with poised enhancers being the most dynamic. JMJD2d is also induced in the response to poly I:C and is a positive regulator of the extent of IFN-β production and the frequency of IFN-β producing cells. At the level of chromatin, JMJD2d is found at enhancers, primarily those that are active, and its occupancy covaries with the amount of p300. Presumably, in its binding to enhancers, JMJD2d seems to have an effect on the induction of active histone marks at enhancers and on the extent of eRNA upregulation. Finally, the downstream effect on IFN-β production appears to require the catalytic activity of JMJD2d.

Contemporaneous with our work, Zhu and colleagues published data supporting a role for H3K9me^3 in the control of enhancer function. They showed that enhancer regions with flanking H3K9me^3 regions were associated with inactive genes. Artificial targeting of H3K9 trimethylation at the *Mdc* and *Il12b* enhancer regions was able to abrogate TNF-α-induced expression of the *Mdc* and *Il12b* genes. Similarly, demethylation of

H3K9me^3 by overexpression of JMJD2d permitted expression in fibroblasts. Their data point to a central role of H3K9me^3 in repressing enhancer function and describe JMJD2d as an enzyme that can remove this repressive mark to permit expression of two genes. In their analysis, they find as we have that JMJD2d colocalizes with enhancers and suggest that the H3K9me^3 serves to give cell-type-specificity to otherwise broadly functional enhancers (Zhu et al, 2012).

Taken together, the constellation of findings in our work represents the first description of a histone demethylase that acts in the transition of enhancers from 'poised' to 'active', as we show a role for JMJD2d in enhancer transcription and in subsequent gene activation. H3K9me^3 demethylation – undetectable in our experimentation – is a focal chromatin event catalyzed by JMJD2d that allows for the acetylation of nearby histones. This acetylation leads to eRNA transcription by Pol II, which either by tracking or by DNA looping or by an unknown mechanism involving the transcript itself (perhaps acting as a scaffold) leads in turn to initiation of transcription or relief of proximal-promoter pausing at nearby genes. JMJD2d appears instrumental in this process, given that it tightly associates with enhancers, modulates their transcription, and is found in subpopulations of cells producing eRNA but not mRNA. Our data, in conjunction with that of Zhu and colleagues, provides a strong body of evidence to support a central role for JMJD2d in enhancer activation.

Stochastic features of JMJD2d and enhancer RNA transcription

Our analysis highlights features of IFN-β that are unique to a non-deterministic system. As has been described by Maniatis and colleagues, IFN-β expression occurs in a minority of cells despite activation with a signal that ubiquitously enters and activates cells. The stochasticity observed in this system has been attributed to limiting levels of the upstream signaling molecules, such that overexpression of RIG-I and TRIM25 augments the percentage of cells responding to ssRNA and increases in MDA5 and IRF7 enables responses to dsRNA (such as poly I:C). In our studies, we observed an interesting ability of JMJD2d to positively regulate the frequency of IFN-producing cells. This suggests that JMJD2d might also be limiting, a notion reinforced by the consistently low levels of absolute transcript observed in MEFs.

Interestingly, our cell sorting experiments revealed a series of unexpected findings. As expected, *Ifnb1* transcripts were higher in YFP+ cells yet this was accompanied by a lack of enhancer RNA. On the other hand, enhancer RNAs, even those 'belonging' to the *Ifnb1* locus, predominated in YFP- cells despite limited activation of target genes in these cells. The presence of eRNA upregulation in YFP- cells suggests that transcription factors are not limiting, because eRNA activity likely requires TF engagement on enhancer DNA prior to transcription. Instead, the presence of eRNA without mRNA suggests two possibilities: (1) enhancer transcription is simply noise unrelated to gene transcription or (2) stochasticity is imparted by a block between enhancer activation and

gene activation. As to the first possibility, our data suggests that JMJD2d positively regulates both enhancer transcription and downstream gene activation - making it unlikely that they are unrelated. Furthermore, there is quite a bit of data to support a correlation between enhancer activity and nearby gene transcription (Kim et al, 2010; De Santa et al, 2010). The second possibility – that of a block between eRNA and mRNA at the root of stochasticity – is an intriguing one. It suggests that the means by which eRNA and mRNA transcription are connected is the step at which the bulk of poly I:C-transfected cells remain confined.

What are the steps between eRNA activation and mRNA production? A variety of chromatin barriers need to be overcome in order to mediate this connection. One is looping of the DNA between enhancer and promoter, facilitating the dissemination of information encoded in the enhancer-proximal landscape to the promoter. This looping requires the actions of Mediator and cohesin (Ong and Corces, 2011), as well as the displacement of nucleosomes by chromatin remodelers. Recruitment and assembly of the transcription complex is another key step leading to mRNA transcription beginning with the docking of TFIID and the pre-initiation complex (PIC). Where the PIC is already formed, enhancer chromatin may still be necessary for the release of promoter-proximal pausing that requires acetylation of H4K16 and multimeric engagement by bromodomain-containing proteins (BRDs). Any one of these molecular events may represent the key step at which YFP- cells in our system are blocked from becoming YFP+. That we can distinguish in our experimental model a set of cells able to generate

eRNA without subsequent mRNA is intriguing, as it is may serve as a tool to elucidate the precise sequence of events that bridges the two transcriptional events.

Enhancer specificity of JMJD2d

Coupled with the phenotype we observed with JMJD2d modulation is a strong association of JMJD2d with enhancers on chromatin. One of the questions that emerges from this finding is what are the mechanisms that give JMJD2d its specific occupancy?

JMJD2d itself differs the other Jumonji family demethylases insofar as it lacks both PhD and Tudor domains, both of which are modules that engage methylated histones. Without these domains, JMJD2d is restricted to engagement of histones via only its JmjN and JmjC domains and does not have the ability to participate in multivalent engagement of histones. Two distinct observations raise the likelihood that JMJD2d requires interacting proteins to mediate its binding to enhancers. First, H3K9me^3, the residue that JMJD2d catalyzes, is present in heterochromatin and in gene bodies as well as enhancers. JMJD2d is excluded entirely from heterochromatin – though it is possible that compaction of this chromatin precludes JMJD2d binding. Transcribed gene bodies, however, are euchromatic and have significant H3K9me^3 without JMJD2d, suggesting a layer of specificity. If JMJD2d has no interacting partners, it follows that it would be found ubiquitously on H3K9me^3 territories, as it lacks any other domains for further discrimination. Second, JMJD2d is frequently bound to enhancers that lack H3K9me^3 altogether – approximately two-thirds of active enhancers in our analyses were engaged by JMJD2d – suggesting that there is a mechanism that maintains JMJD2d occupancy long after the presumed demethylation event.

Our immunoprecipitation experiments raise the possibility that JMJD2d interacts with histone remodelers such as SSRP1, a member of the FACT complex. FACT, however, is relatively ubiquitous and heretofore has been described as a chromatin remodeler that facilitates nucleosome exchange to permit passage of active RNA polymerase II through transcribed genes (Kwon et al, 2010). How such a protein may recruit JMJD2d to enhancers is unclear. Certainly, chromatin remodeling may be crucial to maintenance of open chromatin at enhancers, but there is no data yet to describe the presence of FACT in these regions.

PARP-1, involved in the polymerization of ADP-ribose, is another candidate interactor that emerged in our analysis. Like SSRP1, PARP-1 localization in the genome has been primarily at transcribed promoters, where it localizes just upstream of the transcriptional start site (Kraus, 2008). No enhancer function or occupancy has been described to date. PARP-1, unlike JMJD2d, directly interacts with genomic DNA via an amino-terminal DNA-binding domain containing two zinc finger motifs, and appears to preferential bind to double-strand breaks or crossovers rather than specific sequence motifs.

In the absence of clear interactors with JMJD2d, the most parsimonious explanation for how JMJD2d is recruited to enhancers is that it interacts with a protein that has enhancer specificity. Candidates would include transcription factors, as the underlying enhancer DNA will have the transcription factor-binding site (TFBS) in question, or other

coactivators that engage enhancers (such as p300 or GCN5). Whatever the constituent members, JMJD2d likely is a subunit in a macromolecular complex that acts cooperatively to activate enhancers.

Cell-type specific activation of enhancers by JMJD2d

In our analysis, we observed that the effects of JMJD2d on poly I:C-induced transcriptional responses were restricted to mouse embryonic fibroblasts (MEFs). Our attempts to extend the findings to macrophages and dendritic cells (DCs) proved futile, as did our efforts with systemic poly I:C injection in the JMJD2d knockout mouse. While the failure of these efforts might suggest that the knockdown and overexpression data might be artifactual, we had sufficient robustness imparted by the reproducibility of the data, the use of multiple siRNAs in multiple cell lines, and a specificity arising from the failure of the knockdown to have any effect in knockout cells. What might explain the absence of a phenotype in other cell types?

In the work of Zhu et al., it was noted that the expression of the *Mdc* and *Il12b* genes in response to TNF-α is cell-type specific. The failure of these genes to be expressed in 3T3 fibroblasts was attributed to the presence of H3K9me^3-rich regions flanking the enhancers, which are absent in *Mdc* and *Il12b* DCs. Indeed, our analysis produced a similar finding with respect to the effects of JMJD2d; sequencing of multiple histone marks including H3K9me^3 in macrophages showed an altogether different pattern of histone marks at enhancers (data not shown). Notable in our data was the relative absence of H3K9me^3 at poly I:C-inducible enhancers in macrophages, suggesting a lack of any enzymatic substrate for JMJD2d to have a role. One might expect this finding, as macrophages and DCs are so-called 'professional' IFN-producers and should intuitively

lack barriers to antiviral gene transcription. As such, our JMJD2d knockdown experiments in macrophages and knockout experiments in macrophages and dendritic cells showed no effect, we believe, because enhancer chromatin in these cell types is not identical to that in MEFs.

In a similar vein, our inability to recapitulate the IFN phenotype in JMJD2d$^{-/-}$ MEFs may be explained by a difference in steady-state chromatin landscape between JMJD2d$^{-/-}$ and wild-type cells. It is entirely plausible that JMJD2d$^{-/-}$ MEFs may have an altogether different patterning of histone marks dictated by the absence of the demethylase during differentiation. Alternatively, a different demethylase may compensate for the lack of JMJD2d. Chief among the potential explanations, it should be noted, is that the JMJD2d wild-type and knockout MEFs were generated from different embryos (rather than conditionally deleted in MEFs following isolation and generation); in our hands, different MEF cell lines derived from different embryos (and of the same genotype) produce different amounts of IFN that appears to be an inherent property of the line that perpetuates with passaging. Naturally, conditional deletion using an ERT2-Cre system post-derivation of the line would have been ideal, but our repeated efforts to delete JMJD2d with tamoxifen never yielded complete deletion of the floxed allele.

To conclude, that the modulation of enhancer activity by JMJD2d was observed strictly in MEFs most likely reflects the cell-type specificity of enhancer chromatin. This bears directly on the likely settings in which JMJD2d would play a role. Specifically, JMJD2d

may function differently depending on cell type and signaling context; while macrophages and DCs may not have any defect in IFN responses, there are likely other transcriptional responses for which there would be cell-type specific control imposed by JMJD2d. For example, Zhu et al. describe the JMJD2d-dependency of *Il12b* and *Mdc* mRNA expression downstream of TNF-α in DCs. We suspect that myriad as yet unknown JMJD2d-dependent combinations of cell type and target genes exist, all controlled by JMJD2d, but as of yet unknown.

JMJD2d as a potential therapeutic target

In vivo, cell type-specific responses are a consequence of lineage specification, which is dictated by gene expression, which is, in turn, the result of the interplay between promoters, insulators, and enhancers. As Ren et al. have shown, enhancers, more so than the target genes they activate, are cell type-specific. In their analysis of five different human cell types, chromatin modifications at promoters are cell-type invariant, while they are highly varied at enhancers. Given that underlying DNA sequences are the same, variations in enhancer chromatin may contribute greatly to cell-type heterogeneity. This means that all the properties of enhancer chromatin are likely to be fundamentally different from one cell to the next. The DNA, on the other hand, is likely to be exactly the same, absent a mutation. Molecular targets that control enhancer chromatin are intriguing then because they can be expected to behave very differently depending on the cell type.

JMJD2d, as a modifier of enhancer chromatin, may be a compelling therapeutic target. Plainly, drugs targeting JMJD2d could be used to treat autoimmune disease, for instance, but not carry with it potential side effects as the enzyme has a limited or altogether different effect on other cell types. More broadly, the presence of other modifiers of enhancer chromatin unearths a resource of targets that may have precise effects in a limited number of cell type/signal combinations. One might suspect that therapeutics directed against enzymes with such circumscribed effects would have

excellent pharmacologic properties. Whether the possibilities exist for targeting JMJD2d or histone-modifying enzymes like it remains to be explored.

Chapter V: Materials and methods

Cell lines and culture. MEFs were generated from d13.5 embryos from C57/B6, JMJD2d$^{+/+}$, JMJD2d$^{-/-}$ and IFN-YFP mice by trypsinization of the embryonic body and culture of adherent cells. Immortalization was performed with SV40 latent T antigen administered via retroviral transduction. All MEFs were cultured in DMEM with 15% fetal bovine serum (FBS), 1% L-Glutamine (L-glut), 1% penicillin-streptomycin (P/S), 1% non-essential amino acids (NEAA), and 0.1% 2-mercaptoethanol (2-Me) (GIBCO). MEFs from passage number 12-15 were used for all experimentation. Bone-marrow derived macrophages (BMDMs) were cultured in DMEM with 10% FBS, 1% L-glut, 1% P/S, 1% NEAA, 0.1% 2-Me and supplemented with 5 ng/mL IL-3 (Peprotech) and 5 ng/mL M-CSF (Peprotech). Splenic dendritic cells (DCs) were cultured in RPMI 1640 with 10% FBS, 1% L-glut, 1% P/S, 1% NEAA, 10mM HEPES, 1mM sodium pyruvate, and 0.1% 2-Me, supplemented with 100 ng/mL of Flt3-L (R&D Systems).

Mice. C57Bl/6 mice were obtained from Charles River Laboratories. EIIA-Cre and Vav-Cre mice were obtained from Jackson Labs. IFN-YFP mice were obtained from Richard Locksley. JMJD2d$^{fl/fl}$ mice were generated in the Tarakhovsky laboratory by Georg Busslinger. All mice were bred onto a C57Bl/6 background and mice were housed under specific pathogen free conditions. Experimental protocols were approved by the Rockefeller University Institutional Animal Care and Use Committee. Genotyping was performed by overnight digestion of clipped mouse tails in tail lysis buffer (10 mM Tris-

HCl pH 8.5, 200 mM NaCl, 5 mM EDTA pH 8.0, 0.2% SDS and 100 µg/ml Proteinase K (Roche)) and subsequent ethanol precipitation to isolate DNA. Primers used are summarized in Table 1.

Isolation of bone marrow-derived macrophages. Six to ten week-old female JMJD2d$^{+/+}$ and JMJD2d$^{-/-}$ mice were euthanized and bone marrow cells isolated from the femur and tibia of both hind legs by flushing with 1x balanced salt solution (1xBSS). Bone marrow cells were cultured for 7 days, with BMDMs subsequently collected on day 7 by serial pipetting after incubation in PBS containing 2% FBS and 5 mM EDTA for 15 min. Cell viability was determined using Trypan Blue exclusion in a Neubauer hemocytometer. BMDMs were subsequently cultured in medium as described above.

Isolation of splenic dendritic cells (DCs). Six to ten week-old female JMJD2d$^{fl/fl}$ and JMJD2d$^{fl/fl}$ Vav-Cre^{+} mice were injected subcutaneously with 5 x 10^6 BL6-Flt3L cells to expand the splenic dendritic cell compartment. Mice were euthanized two weeks later and splenocytes isolated in 1x BSS following 0.375U/mL collagenase D (Sigma) digestion of splenic fragments. Cell suspensions were passed through a 100 µM cell strainer, followed by lysis of erythrocytes. Enrichment of CD11c^{+} cells was then performed with initial Fc receptor blockade using (5 µg/mL anti-CD16/CD32) followed by CD11c MACS beads (Miltenyi Biotec). Conventional DCs were further purified by cell sorting (FACSAria; BD Bioscience) by gating on the B220^{-} CD11b^{+} CD11c^{+} mPDCA-1^{-} population.

cDCs were subsequently cultured in medium as described above, with replacement of medium on day 4 and collection of non-adherent cells on day 9.

Cell transfections and stimulations. All knockdown experiments were performed using the Lipofectamine RNAiMAX transfection reagent (Invitrogen) with siRNA delivered at a concentration of either 20 or 50 nM in serum-depleted medium (OptiMEM; Invitrogen) as per the manufacturer's instructions. Reverse transfections were employed with cells added to preformed siRNA:lipofectamine complexes pre-incubated for 20 minutes. Subsequent cell stimulations or viral infections were performed 48 hours after initial siRNA knockdown. Reporter constructs were transfected using the Lipofectamine 2000 transfection reagent (Invitrogen) according to the manufacturer's instructions.

MEFs were stimulated by transfection of 2 μg/ml poly(I:C) into the cells using Lipofectamine 2000 transfection reagent (Invitrogen) following the manufacturer's instructions. Alternatively, MEFs were stimulated with 500 U/ml recombinant IFN-β (R&D Systems) for the indicated times. To block IFN-β-induced signaling, MEFs were pre-incubated with 10 μg/ml IFNαR1 antibody (MAR1-5A3, eBioscience, catalogue number 16-5945).

Retroviral transduction. Retrovirus was generated by transfecting BHK cells (ATCC) or Phoenix cells (laboratory stocks) with 1-4 μg plasmid using the Lipofectamine 2000 Transfection Reagent (Invitrogen). Supernatants were collected at 24 and 48 hours post-

transfection and added to MEFs pre-cultured in six-well plates. Polybrene (Sigma) was added at a concentration of 8 μg/mL. Six well plates were then centrifuged at RT for 90 min and incubated at 37°C overnight; efficiency of transduction was measured by flow cytometry 48 hours following spin infection.

Viruses and viral infections. Viruses were obtained as follows. Stocks of GFP-expressing VSV (designated VSV-GFP M51R), mCherry-expressing Sindbis virus, as well as influenza A (Puerto Rico/8/34 (H1N1)), amplified in 8-day old embryonated chicken eggs and titered by plaque assay on Madin-Darby canine kidney cells) were kindly provided by Adolfo Garcia-Sastre. Wild type VSV Indiana serotype (San Juan), originally a gift from Milton Schlesinger, was grown and titered on BHK-21 cells as previously described (Bick et al., 2003).

MEFs were infected with individual viruses with a multiplicity of infection (MOI) between 0 and 1 by diluting the virus stock in PBS containing 0.5% to 1% FBS. Infection was allowed to proceed for 1 h. After removal of the virus containing supernatant, cells were incubated in fresh medium. For detection of infected cells via FACS, cells were infected with a reporter virus that leads to the expression of GFP in the infected cells (VSV-GFP, sindbis-mCherry). Cells were analyzed for GFP or mCherry expression at the indicated times.

Plasmids and cloning. Plasmids expressing mJMJD2A and mJMJD2d were generated by cloning PCR- amplified constructs containing the endogenous *Jmjd2a* and *Jmjd2d* loci conjugated to 3xFLAG into the MigR1 plasmid backbone. MigR1-JMJD2d-3xFLAG was subsequently subjected to site-directed mutagenesis using the GeneArt kit (Invitrogen) to generated the MigR1-JMJD2d-H192A-3xFLAG plasmid. All plasmids were transformed into competent *E.coli* at 42°C and subjected to antibiotic selection. Overnight bacterial cultures were grown, plasmids purified via maxiprep (Qiagen), and quantified on a NanoDrop spectrophotometer (Agilent).

Flow cytometry and cell sorting. For flow cytometry, cells were collected and fixed in PBS containing 1% paraformaldehyde and analyzed on a FACSCalibur flow cytometer (BD) using CellQuest software. For cell sorting, cells were collected and fixed in the same fashion but analyzed on a FACSAria (BD) cell sorter to divide into YFP+ and YFP- populations.

Primers. Primers used for mouse genotyping are listed in Table 3. Primers used for quantitative RT-PCR are summarized in Table 4. JMJD2d, Mx2, IRF7, Ifit1, and Ifit3 TaqMan probes obtained from Applied Biosystems Primer for enhancer RNA qPCR are listed in Table 5. All forward and reverse primers were mixed to a final concentration of 50 µM for qPCR primers and 20 µM for genotyping primers.

Table 3. Primers used for mouse genotyping. Indicated are the sequences of primers used in the genotyping of JMJD2d, EIIA-Cre, and Vav-Cre.

JMJD2d F	CATTCCCAGCACCCTAACAG
JMJD2d R1	CTGGTCCTACACAGCCCAGT
JMJD2d R2	AGGCCTGGAGCCACTTTATC
EIIA-Cre F	AAGGGCGCGAAACTAGTCCTTAAG
EIIA-Cre R	CGCATAACCAGTGAAACAGCAT
Vav-cre F	AGATGCCAGGACATCAGGAACCTG
Vav-cre R	ATCAGCCACACCAGACACAGAGAT

Table 4. Primers used for mRNA RT-qPCR. Indicated are the sequences of primers used to detect transcripts as listed.

HPRT F	CTCCTCAGACCGCTTTTTGC
HPRT R	TAACCTGGTTCATCATCGCTAATC
Cxcl1 F1	CTTGAAGGTGTTGCCCTCAG
Cxcl1 F2	GCACCCAAACCGAAGTCATA
Cxcl1 R	AGGTGCCATCAGAGCAGTCT
Cxcl2 F1	GCCAAGGGTTGACTTCAAGA
Cxcl2 R1	CTTCAGGGTCAAGGCAAACTT
Cxcl2 F2	CTCCAGACTCCAGCCACACT
Cxcl2 R2	AGGGTCTTCAGGCATTGACA
IFN F	TCAGAATGAGTGGTGGTTGC
IFN R	GACCTTTCAAATGCAGTAGATT
Mx1 F	GTGGTAGTCCCCAGCAATGT
Mx1 R	AGCACCTCTGTCCACCAGAT
TNF F	CCCCAAAGGGATGAGAAGTT
TNF R	CTCCTCCACTTGGTGGTTTG
IL-6 F	TGGGAAATCGTGGAAATGAG
IL-6 R	CCAGTTTGGTAGCATCCATCA

Table 5. Primers used for eRNA RT-qPCR. Indicated are the sequences of primers used to detect enhancer RNAs as listed.

Ifnb1 D1 F	TCAAAGAAGGGCACCACCTA
Ifnb1 D1 R	GTGCTGGAGGAAGGAACAACT
Ifnb1 D2 F	ACTGCACGCAGAGAGGTTTC
Ifnb1 D2 R	GGAGGTAACTGGTTGCACTGA
Ifnb1 U1 F	CCATCCTGTCCCTGACAGAC
Ifnb1 U1 R	ATGAACGAGAAAGCAGCTGTG
Ifnb1 U2 F	TAGAACAAACGGGGCAAAGA
Ifnb1 U2 R	AGATCCTGCAGTTGTGCTCAG
Ifnb1 D3 F	TTCAAACATTGGCCATCTGA
Ifnb1 D3 R	CAAGACTGAGGGTGCGTATGT
Mx2 U1 F	ATCAGAGCACTGGGTGTCATC
Mx2 U1 R	TGGTTCCTGGCATACAATGTT
Mx2 U2 F	ACCCTTCCACCCATCCTCTA
Mx2 U2 R	TCCTTGCCTCTGCAGTGTTT
Ccl5 U1 F	CCAACCACATTCAGACCAGAG
Ccl5 U1 R	TCAGAGAGCAAGTGGGTGTG
Ccl5 U2 F	ACCTCTGGGACAGCAAGTAGC
Ccl5 U2 R	AGGGCAGGCAACTAGAGACA
Ccl5 U3 F	CCATGGTCACAGGGTAACAAC
Ccl5 U3 R	CCCAGCCCTTGCTTGTATTA
Ccl5 U4 F	TGCCTGTCTCTGCAACAAGA
Ccl5 U4 R	AACCCCCTGACTCCACCTAC
Cxcl1 U1 F	GGCCACAGCTTCATTAAAACA
Cxcl1 U1 R	AAAGTGGAATCCTGGGAGACA
Cxcl1 U2 F	CATTCAACCTCAGTCCCATGA
Cxcl1 U2 R	TTGTCACAGATCCGGAGAAAG
Ifitm3 D1 F	GGAATGGAAGATGGGGAACT
Ifitm3 D1 R	CTTCCACTTAGCCCCAGTCA
Ifitm3 D2 F	AGCCGCAGTTTTATCCATCAT
Ifitm3 D2 R	TCAATTCACTCGCCTTCACA
Irf1 U1 F	AAGGAAAAGAGCGAGCAAAGA
Irf1 U1 R	CCTGGACCTCAGGATCTTCTC
Irf1 U2 F	TGCGTGCCATGAGATACAAG
Irf1 U2 R	AACTGAAGGGACAGGCAGTG
Actb U1 F	ACGGAAGGGAAAGGAAAGAA
Actb U1 R	CCCCAGACAGTTACCACACAA
Actb U2 F	AAAACAAGCCAGGCACACAT
Actb U2 R	TAGCTGCCCTGGAACTCACT
Actb U3 F	TCTCTCCAGGCCCTGTTAAGT
Actb U3 R	CCTCTCGAGTGCTGGGATTA

Quantitative reverse-transcribed PCR. RNA was isolated with the RNeasy mini kit (Qiagen) or by the High Pure RNA isolation kit (Roche) and subsequently quantified using the NanoDrop 8000 spectrophotometer (Agilent). RNA was reversed transcribed using the Transcriptor First Strand Kit (Roche). qPCR was carried out using SYBR Green and products were quantified with a standard curve. Gene expression was displayed relative to Tbp or HPRT or GAPDH as indicated.

Microarray analysis. 1-5 µg of total RNA from 2-3 MEF samples per group was used to prepare biotinylated RNA using the Ambion Illumina TotalPrep RNA Amplification Kit (Applied Biosystems) according to the manufacturer's instructions. This RNA was hybridized to Illumina MouseRef-8 v2.0 expression BeadChip kits, with chips then scanned using the Illumina BeadArray Reader followed by analysis using Genespring (Affymetrix). The raw expression data was quality assessed and subjected to background adjustment and quantile normalization. The individual gene expression levels were compared by using an unpaired Student's T-test ($P<0.05$) and by pairwise comparison.

Immunoprecipitation. HEK293 cells were stably transfected with empty vector (MigR1) or FLAG-tagged JMJD2d (MigR1-JMJD2d-3xFLAG) constructs. Immunoprecipitation was performed using M2 beads on a rotator overnight at 4°C.

Southern blotting. DNA was electrophoresed on 0.8% (for genomic DNA) agarose gels and rotated in transfer buffer (0.6 M NaCl, 0.4 M NaOH) for 45 min. DNA was

transferred by upward capillary transfer onto Hybond-N membrane (Amersham) overnight. Blots were rotated in neutralization buffer [0.5 M Tris-HCl (pH 7.0), 1 M NaCl] for 15 min and crosslinked in a Stratalinker (Stratagene) on “auto” mode.

Blots were incubated briefly in 2X SSC, and transferred into pre-warmed hybridization buffer [50 mM Tris-HCl (pH 7.5), 1 M NaCl, 1% SDS, 10% dextran sulfate, 300 ug/ml sonicated salmon sperm DNA] and pre-hybridized for 3 hours at 65°C. Probes were PCR amplified from BAC DNA and gel purified (Qiagen). DNA (50 ng) was labeled with 5 µL 32P-α-dCTP using Ready-to-Go labeling beads (Amersham) and purified over ProbeQuant G50 spin columns per manufacturers protocol. Eluted DNA was boiled for 5 min and iced for 5 min prior to addition to prehybridized blot. Hybridization was carried out overnight with blots subsequently washed in 2X SSC/0.1% SDS, 1X SSC/0.1% SDS and 0.5X SSC/0.1% SDS, wrapped in clear plastic wrap and exposed to film (Kodak XAR).

Antibodies. The following antibodies were employed: histone H3 antibody (Abcam, ab1791), Histone H3 (di methyl K9) antibody (Abcam, ab1220), ChIPAb+ Trimethyl-Histone H3 (Lys4) (Millipore, 17-614), Anti-acetyl-Histone H4 antibody (Millipore, 06-866), RNA polymerase II CTD repeat YSPTSPS antibody [4H8] - ChIP Grade (Abcam, ab5408), anti-histone H3 monomethyl K4 antibody (Abcam, ab8895), anti-histone H3 acetyl K9 antibody (Abcam, ab4441) , anti-histone H3 trimethyl K9 antibody (Abcam, ab8898), anti-trimethyl-histone 3 (Lys27) (Millipore, 07-449), anti-histone H3 (acetyl K27) antibody (Abcam, ab4729), and anti-Flag M2 antibody (Sigma, F1804).

ChIP-sequencing. Briefly, cells were incubated as above and at the indicated times following stimulation or viral infection were treated with 1% formaldehyde for 10 minutes. Fixation was terminated with the addition of glycine to a final concentration of 0.125M. Cells were then washed serially with PBS/0.5% FCS and collected. Cells were then lysed to isolate chromatin and sonicated for 10-20 min (depending on cell type) using a Bioruptor (Diagenode). Fragmentation of sonicated chromatin to lengths of 200-500 bp was confirmed by agarose gel electrophoresis.

For immunoprecipitation, beads were prepared with 7-10µg of antibody coupled to M-280 mouse or rabbit Dynabeads (Invitrogen) for 8 hours as per the manufacturer's instructions. Beads were then washed with PBS/0.5% FBS on a magnet and 20-50µg sonicated chromatin was added and incubated overnight on a rotator. Following immunoprecipitation, beads were washed in modified RIPA wash buffer (50 mM HEPES-KOH pH 7.6, 100 or 300 mM LiCl, 1 mM EDTA pH 8.0, 1% NP-40, 0.7% Na-Deoxycholate) and then in TE wash buffer (10 mM Tris-HCl pH 8.0, 1 mM EDTA pH 8.0, 50 mM NaCl). DNA was then eluted at 65°C for 40 min in elution buffer (50 mM Tris-HCl pH 8.0, 10 mM EDTA pH 8.0, 1% SDS). Crosslinks were reversed overnight and protein and RNA were digested. For validation of ChIP-seq, subsequent purified DNA was analyzed via qPCR.

For ChIP-seq library preparation, blunt-end DNA was prepared using the End-It End Repair Kit (Epicentre), “A” bases were added using Klenow fragment (NEB), and adapters for sequencing (Illumina) were ligated using T4 DNA ligase (NEB). Adapter-ligated DNA was then amplified using PE primers 1.0 and 2.0 (Illumina) and Phusion polymerase (ThermoScientific). Libraries were analyzed via agarose gel electrophoresis, a NanoDrop spectrophotometer, on an Agilent Bioanalyzer for integrity, appropriate size, and the presence of adapter dimers or primer dimers. Libraries were then loaded onto the Illumina HiSeq 2000 according to Illumina protocols.

RNA-sequencing. RNA was isolated in TriZOL reagent (Invitrogen) and purified according to the manufacturer’s instructions. Purified RNA was quantified on a NanoDrop spectrophotometer (Agilent). Total RNA was depleted of small RNAs (miRNA, tRNA) using the cleanup protocol of the RNeasy Mini Kit (Qiagen) and again checked for purity on a Nanodrop and the Agilent Bioanalyzer. Ribosomal RNA was depleted from 10µg total RNA using the Ribo-Zero Magnetic Kit (Epicentre). Ribo-depleted RNA was then fragmented with subsequent synthesis of cDNA and strand-specific library generation using the Script-Seq V2 Kit (Epicentre) and the FailSafe PCR enzyme mix, both used in accordance with the manufacturer’s instructions. Libraries were then loaded onto the Illumina HiSeq 2000 according to standard Illumina protocols.

Analysis of sequencing data. For all alignments, reads were aligned to the mm9 build of the mouse genome, downloaded from the UCSC Genome Browser. For ChIP-seq data,

reads were aligned at 36bp (H3K4me3 and RNAPII) or 51bp (all others), allowing for only unique alignments with 2 mismatches using Bowtie v0.12.7. Sequencing reads from replicate ChIP experiments were combined for final analyses. For RNA-seq data, reads were 101bp and were aligned using Tophat v2.0. Reads were segmented to 25bp and 2 mismatches were allowed. Junctions were supplied from RefSeq annotations. Peak calling was performed as follows: MACS v1.4 was used for peak calling for p300 and CCAT3.0 for all others. Suitable inputs or controls were used for all analyses. Scores 60 and higher were used for MACS and FDR values of 0.05 or less were used for CCAT3.0. For profiling of ChIP-seq and RNA-seq data, reads were extended 100bp from the 3' end to account for the expected size of the fragments and binned into 100bp windows. Windows upstream and downstream of indicated features were queried for 5kb, or the distances indicated. In libraries where the rate of duplication was high, duplicates were removed to avoid biasing profiles. Profiles are reported as reads per million mapped reads per bin/window size (100bp). Fragments-per-kilobase-per-million-mapped-reads values were calculated from alignment data for the intervals/peaks regions specified. A pseudocount of 1 read per 100M aligned reads per kilobase was used to avoid division-by-zero errors.

Enhancer definition. To qualify as an enhancer, p300 peaks (with score 60 from MACS) were assessed based on the following criteria. A p300 peak could not intersect with a H3K4me3 peak called for any condition (L0/L4/2D0/2D4), could not be within 1kb of a RefSeq gene start site (TSS) or 2kb from the start site (TSS) of any spliced EST entries

downloaded from the UCSC genome browser, and must intersect with a H3K4me1 peak location from any of the conditions. Intragenic enhancers were defined as those p300 peaks that passed these criteria that were contained within the transcriptional unit for RefSeq genes. Extragenic enhancers were those remaining enhancers that were not within 5kb of the transcription end site, to avoid strong RNAPII from biasing profiling signal. For eRNA profiling, additional filtering was performed to eliminate potentially un-annotated genes, repetitive sequence or other problematic features. As the characteristic profiles of eRNAs are short, less than 2kb transcripts in the region 2kb downstream on the plus strand and 2kb upstream on the minus strand were considered. The following were excluded: any transcript for which the ratio of reads contained on the forward strand 2kb downstream of the p300 peak summit to reads on the minus strand 2kb upstream was more than 5; any transcript for which the signal in the region +2-4kb or -2-4kb was higher than 2kb immediately upstream or downstream (to eliminate potential long/genic transcripts); any high signal over 1 FPKM that constituted a small fraction of loci with an aberrantly high number of alignments potentially due to repetitive signal; any loci with homology to any ribosomal RNA sequence. Inducible enhancers were defined as follows: Enhancers were deemed to be induced if H4ac or H3K9ac peaks were found in the poly I:C stimulated condition using the respective unstimulated H4ac or H3K9ac library as a control, using CCAT3.0 with an FDR < 0.1. These peaks had to intersect enhancers that passed all aforementioned criteria.

Chromatin state analysis. ChromHMM was used to determine chromatin states. 29 states were specified, with the indicated target samples being used. Proper control libraries were used. The software models potential states using a hidden Markov model to determine likely combinations of enriched regions. Enriched regions for each target are then assessed for the representation in the various potential chromatin states. Target regions, such as genes, enhancers and other genomic loci can then be queried to ascertain the predominant chromatin states present at those loci.

References

Agalioti, T., Lomvardas, S., Parekh, B., Yie, J., Maniatis, T., and Thanos, D. (2000). Ordered recruitment of chromatin modifying and general transcription factors to the IFN-beta promoter. Cell *103*, 667-678.

Anand, R., and Marmorstein, R. (2007). Structure and mechanism of lysine-specific demethylase enzymes. The Journal of biological chemistry *282*, 35425-35429.

Apostolou, E., and Thanos, D. (2008). Virus Infection Induces NF-kappaB-dependent interchromosomal associations mediating monoallelic IFN-beta gene expression. Cell *134*, 85-96.

Bannister, A.J., and Kouzarides, T. (2005). Reversing histone methylation. Nature *436*, 1103-1106.

Barski, A., Cuddapah, S., Cui, K., Roh, T.Y., Schones, D.E., Wang, Z., Wei, G., Chepelev, I., and Zhao, K. (2007). High-resolution profiling of histone methylations in the human genome. Cell *129*, 823-837.

Belotserkovskaya, R., Oh, S., Bondarenko, V.A., Orphanides, G., Studitsky, V.M., and Reinberg, D. (2003). FACT facilitates transcription-dependent nucleosome alteration. Science *301*, 1090-1093.

Berger, S.L. (2007). The complex language of chromatin regulation during transcription. Nature *447*, 407-412.

Beyer, S., Kristensen, M.M., Jensen, K.S., Johansen, J.V., and Staller, P. (2008). The histone demethylases JMJD1A and JMJD2B are transcriptional targets of hypoxia-inducible factor HIF. The Journal of biological chemistry *283*, 36542-36552.

Bowie, A.G., and Unterholzner, L. (2008). Viral evasion and subversion of pattern-recognition receptor signalling. Nature reviews Immunology *8*, 911-922.

Bulger, M., and Groudine, M. (2010). Enhancers: the abundance and function of regulatory sequences beyond promoters. Developmental biology *339*, 250-257.

Calo, E., and Wysocka, J. (2013). Modification of enhancer chromatin: what, how, and why? Molecular cell *49*, 825-837.

Chen, Z., Zang, J., Whetstine, J., Hong, X., Davrazou, F., Kutateladze, T.G., Simpson, M., Mao, Q., Pan, C.H., Dai, S*., et al.* (2006). Structural insights into histone demethylation by JMJD2 family members. Cell *125*, 691-702.

Chi, P., Allis, C.D., and Wang, G.G. (2010). Covalent histone modifications--miswritten, misinterpreted and mis-erased in human cancers. Nature reviews Cancer *10*, 457-469.

Cloos, P.A., Christensen, J., Agger, K., Maiolica, A., Rappsilber, J., Antal, T., Hansen, K.H., and Helin, K. (2006). The putative oncogene GASC1 demethylates tri- and dimethylated lysine 9 on histone H3. Nature *442*, 307-311.

Creyghton, M.P., Cheng, A.W., Welstead, G.G., Kooistra, T., Carey, B.W., Steine, E.J., Hanna, J., Lodato, M.A., Frampton, G.M., Sharp, P.A*., et al.* (2010). Histone H3K27ac separates active from poised enhancers and predicts developmental state. Proceedings of the National Academy of Sciences of the United States of America *107*, 21931-21936.

De Santa, F., Barozzi, I., Mietton, F., Ghisletti, S., Polletti, S., Tusi, B.K., Muller, H., Ragoussis, J., Wei, C.L., and Natoli, G. (2010). A large fraction of extragenic RNA Pol II transcription sites overlap enhancers. PLoS biology *8*, e1000384.

De Santa, F., Totaro, M.G., Prosperini, E., Notarbartolo, S., Testa, G., and Natoli, G. (2007). The histone H3 lysine-27 demethylase Jmjd3 links inflammation to inhibition of polycomb-mediated gene silencing. Cell *130*, 1083-1094.

Egelhofer, T.A., Minoda, A., Klugman, S., Lee, K., Kolasinska-Zwierz, P., Alekseyenko, A.A., Cheung, M.S., Day, D.S., Gadel, S., Gorchakov, A.A*., et al.* (2011). An assessment of histone-modification antibody quality. Nature structural & molecular biology *18*, 91-93.

El Gazzar, M., Yoza, B.K., Hu, J.Y., Cousart, S.L., and McCall, C.E. (2007). Epigenetic silencing of tumor necrosis factor alpha during endotoxin tolerance. The Journal of biological chemistry *282*, 26857-26864.

Ernst, J., Kheradpour, P., Mikkelsen, T.S., Shoresh, N., Ward, L.D., Epstein, C.B., Zhang, X., Wang, L., Issner, R., Coyne, M*., et al.* (2011). Mapping and analysis of chromatin state dynamics in nine human cell types. Nature *473*, 43-49.

Fang, R., Barbera, A.J., Xu, Y., Rutenberg, M., Leonor, T., Bi, Q., Lan, F., Mei, P., Yuan, G.C., Lian, C*., et al.* (2010). Human LSD2/KDM1b/AOF1 regulates gene transcription by modulating intragenic H3K4me2 methylation. Molecular cell *39*, 222-233.

Fang, T.C., Schaefer, U., Mecklenbrauker, I., Stienen, A., Dewell, S., Chen, M.S., Rioja, I., Parravicini, V., Prinjha, R.K., Chandwani, R*., et al.* (2012). Histone H3 lysine 9 di-methylation as an epigenetic signature of the interferon response. The Journal of experimental medicine *209*, 661-669.

Fodor, B.D., Kubicek, S., Yonezawa, M., O'Sullivan, R.J., Sengupta, R., Perez-Burgos, L., Opravil, S., Mechtler, K., Schotta, G., and Jenuwein, T. (2006). Jmjd2b antagonizes H3K9 trimethylation at pericentric heterochromatin in mammalian cells. Genes & development *20*, 1557-1562.

Fortschegger, K., de Graaf, P., Outchkourov, N.S., van Schaik, F.M., Timmers, H.T., and Shiekhattar, R. (2010). PHF8 targets histone methylation and RNA polymerase II to activate transcription. Molecular and cellular biology *30*, 3286-3298.

Ghisletti, S., Barozzi, I., Mietton, F., Polletti, S., De Santa, F., Venturini, E., Gregory, L., Lonie, L., Chew, A., Wei, C.L*., et al.* (2010). Identification and characterization of enhancers controlling the inflammatory gene expression program in macrophages. Immunity *32*, 317-328.

Gibcus, J.H., and Dekker, J. (2013). The hierarchy of the 3D genome. Molecular cell *49*, 773-782.

Gilchrist, D.A., Dos Santos, G., Fargo, D.C., Xie, B., Gao, Y., Li, L., and Adelman, K. (2010). Pausing of RNA polymerase II disrupts DNA-specified nucleosome organization to enable precise gene regulation. Cell *143*, 540-551.

Goldberg, A.D., Banaszynski, L.A., Noh, K.M., Lewis, P.W., Elsaesser, S.J., Stadler, S., Dewell, S., Law, M., Guo, X., Li, X*., et al.* (2010). Distinct factors control histone variant H3.3 localization at specific genomic regions. Cell *140*, 678-691.

Hallikas, O., Palin, K., Sinjushina, N., Rautiainen, R., Partanen, J., Ukkonen, E., and Taipale, J. (2006). Genome-wide prediction of mammalian enhancers based on analysis of transcription-factor binding affinity. Cell *124*, 47-59.

Hampsey, M., and Reinberg, D. (2003). Tails of intrigue: phosphorylation of RNA polymerase II mediates histone methylation. Cell *113*, 429-432.

Heintzman, N.D., Hon, G.C., Hawkins, R.D., Kheradpour, P., Stark, A., Harp, L.F., Ye, Z., Lee, L.K., Stuart, R.K., Ching, C.W*., et al.* (2009). Histone modifications at human enhancers reflect global cell-type-specific gene expression. Nature *459*, 108-112.

Heintzman, N.D., and Ren, B. (2009). Finding distal regulatory elements in the human genome. Current opinion in genetics & development *19*, 541-549.

Horton, J.R., Upadhyay, A.K., Qi, H.H., Zhang, X., Shi, Y., and Cheng, X. (2010). Enzymatic and structural insights for substrate specificity of a family of jumonji histone lysine demethylases. Nature structural & molecular biology *17*, 38-43.

Jamai, A., Puglisi, A., and Strubin, M. (2009). Histone chaperone spt16 promotes redeposition of the original h3-h4 histones evicted by elongating RNA polymerase. Molecular cell *35*, 377-383.

Jang, M.K., Mochizuki, K., Zhou, M., Jeong, H.S., Brady, J.N., and Ozato, K. (2005). The bromodomain protein Brd4 is a positive regulatory component of P-TEFb and stimulates RNA polymerase II-dependent transcription. Molecular cell *19*, 523-534.

Jenuwein, T., and Allis, C.D. (2001). Translating the histone code. Science *293*, 1074-1080.

Jin, C., Zang, C., Wei, G., Cui, K., Peng, W., Zhao, K., and Felsenfeld, G. (2009). H3.3/H2A.Z double variant-containing nucleosomes mark 'nucleosome-free regions' of active promoters and other regulatory regions. Nature genetics *41*, 941-945.

Kharchenko, P.V., Alekseyenko, A.A., Schwartz, Y.B., Minoda, A., Riddle, N.C., Ernst, J., Sabo, P.J., Larschan, E., Gorchakov, A.A., Gu, T.*, et al.* (2011). Comprehensive analysis of the chromatin landscape in Drosophila melanogaster. Nature *471*, 480-485.

Kidder, B.L., Hu, G., and Zhao, K. (2011). ChIP-Seq: technical considerations for obtaining high-quality data. Nature immunology *12*, 918-922.

Kim, T.K., Hemberg, M., Gray, J.M., Costa, A.M., Bear, D.M., Wu, J., Harmin, D.A., Laptewicz, M., Barbara-Haley, K., Kuersten, S.*, et al.* (2010). Widespread transcription at neuronal activity-regulated enhancers. Nature *465*, 182-187.

Klose, R.J., Kallin, E.M., and Zhang, Y. (2006). JmjC-domain-containing proteins and histone demethylation. Nature reviews Genetics *7*, 715-727.

Klose, R.J., and Zhang, Y. (2007). Regulation of histone methylation by demethylimination and demethylation. Nature reviews Molecular cell biology *8*, 307-318.

Kouzarides, T. (2007). Chromatin modifications and their function. Cell *128*, 693-705.

Kraus, W.L. (2008). Transcriptional control by PARP-1: chromatin modulation, enhancer-binding, coregulation, and insulation. Current opinion in cell biology *20*, 294-302.

Krieg, A.J., Rankin, E.B., Chan, D., Razorenova, O., Fernandez, S., and Giaccia, A.J. (2010). Regulation of the histone demethylase JMJD1A by hypoxia-inducible factor 1 alpha enhances hypoxic gene expression and tumor growth. Molecular and cellular biology *30*, 344-353.

Krishnan, S., Horowitz, S., and Trievel, R.C. (2011). Structure and Function of Histone H3 Lysine 9 Methyltransferases and Demethylases. Chembiochem : a European journal of chemical biology.

Kwon, S.H., Florens, L., Swanson, S.K., Washburn, M.P., Abmayr, S.M., and Workman, J.L. (2010). Heterochromatin protein 1 (HP1) connects the FACT histone chaperone complex to the phosphorylated CTD of RNA polymerase II. Genes & development *24*, 2133-2145.

Li, C.C., Ramirez-Carrozzi, V.R., and Smale, S.T. (2006). Pursuing gene regulation 'logic' via RNA interference and chromatin immunoprecipitation. Nature immunology *7*, 692-697.

Liu, X.Y., Chen, W., Wei, B., Shan, Y.F., and Wang, C. (2011). IFN-induced TPR protein IFIT3 potentiates antiviral signaling by bridging MAVS and TBK1. Journal of immunology *187*, 2559-2568.

Loh, Y.H., Zhang, W., Chen, X., George, J., and Ng, H.H. (2007). Jmjd1a and Jmjd2c histone H3 Lys 9 demethylases regulate self-renewal in embryonic stem cells. Genes & development *21*, 2545-2557.

Mamanova, L., Coffey, A.J., Scott, C.E., Kozarewa, I., Turner, E.H., Kumar, A., Howard, E., Shendure, J., and Turner, D.J. (2010). Target-enrichment strategies for next-generation sequencing. Nature methods *7*, 111-118.

Martin, C., and Zhang, Y. (2005). The diverse functions of histone lysine methylation. Nature reviews Molecular cell biology *6*, 838-849.

Maston, G.A., Evans, S.K., and Green, M.R. (2006). Transcriptional regulatory elements in the human genome. Annual review of genomics and human genetics *7*, 29-59.

Medzhitov, R., and Horng, T. (2009). Transcriptional control of the inflammatory response. Nature reviews Immunology *9*, 692-703.

Metzger, E., and Schule, R. (2007). The expanding world of histone lysine demethylases. Nature structural & molecular biology *14*, 252-254.

Mito, Y., Henikoff, J.G., and Henikoff, S. (2007). Histone replacement marks the boundaries of cis-regulatory domains. Science *315*, 1408-1411.

Mortazavi, A., Williams, B.A., McCue, K., Schaeffer, L., and Wold, B. (2008). Mapping and quantifying mammalian transcriptomes by RNA-Seq. Nature methods *5*, 621-628.

Mosammaparast, N., and Shi, Y. (2010). Reversal of histone methylation: biochemical and molecular mechanisms of histone demethylases. Annual review of biochemistry *79*, 155-179.

Natoli, G., and Andrau, J.C. (2012). Noncoding transcription at enhancers: general principles and functional models. Annual review of genetics *46*, 1-19.

Nicodeme, E., Jeffrey, K.L., Schaefer, U., Beinke, S., Dewell, S., Chung, C.W., Chandwani, R., Marazzi, I., Wilson, P., Coste, H.*, et al.* (2010). Suppression of inflammation by a synthetic histone mimic. Nature *468*, 1119-1123.

Nottke, A., Colaiacovo, M.P., and Shi, Y. (2009). Developmental roles of the histone lysine demethylases. Development *136*, 879-889.

Okada, Y., Scott, G., Ray, M.K., Mishina, Y., and Zhang, Y. (2007). Histone demethylase JHDM2A is critical for Tnp1 and Prm1 transcription and spermatogenesis. Nature *450*, 119-123.

Ong, C.T., and Corces, V.G. (2011). Enhancer function: new insights into the regulation of tissue-specific gene expression. Nature reviews Genetics *12*, 283-293.

Panne, D., Maniatis, T., and Harrison, S.C. (2004). Crystal structure of ATF-2/c-Jun and IRF-3 bound to the interferon-beta enhancer. The EMBO journal *23*, 4384-4393.

Panne, D., Maniatis, T., and Harrison, S.C. (2007). An atomic model of the interferon-beta enhanceosome. Cell *129*, 1111-1123.

Perissi, V., Jepsen, K., Glass, C.K., and Rosenfeld, M.G. (2010). Deconstructing repression: evolving models of co-repressor action. Nature reviews Genetics *11*, 109-123.

Pichlmair, A., Lassnig, C., Eberle, C.A., Gorna, M.W., Baumann, C.L., Burkard, T.R., Burckstummer, T., Stefanovic, A., Krieger, S., Bennett, K.L.*, et al.* (2011). IFIT1 is an antiviral protein that recognizes 5'-triphosphate RNA. Nature immunology *12*, 624-630.

Pray-Grant, M.G., Daniel, J.A., Schieltz, D., Yates, J.R., 3rd, and Grant, P.A. (2005). Chd1 chromodomain links histone H3 methylation with SAGA- and SLIK-dependent acetylation. Nature *433*, 434-438.

Rada-Iglesias, A., Bajpai, R., Swigut, T., Brugmann, S.A., Flynn, R.A., and Wysocka, J. (2011). A unique chromatin signature uncovers early developmental enhancers in humans. Nature *470*, 279-283.

Ramirez-Carrozzi, V.R., Braas, D., Bhatt, D.M., Cheng, C.S., Hong, C., Doty, K.R., Black, J.C., Hoffmann, A., Carey, M., and Smale, S.T. (2009). A unifying model for the selective regulation of inducible transcription by CpG islands and nucleosome remodeling. Cell *138*, 114-128.

Rea, S., Eisenhaber, F., O'Carroll, D., Strahl, B.D., Sun, Z.W., Schmid, M., Opravil, S., Mechtler, K., Ponting, C.P., Allis, C.D.*, et al.* (2000). Regulation of chromatin structure by site-specific histone H3 methyltransferases. Nature *406*, 593-599.

Roh, T.Y., Cuddapah, S., Cui, K., and Zhao, K. (2006). The genomic landscape of histone modifications in human T cells. Proceedings of the National Academy of Sciences of the United States of America *103*, 15782-15787.

Rosenfeld, M.G., Lunyak, V.V., and Glass, C.K. (2006). Sensors and signals: a coactivator/corepressor/epigenetic code for integrating signal-dependent programs of transcriptional response. Genes & development *20*, 1405-1428.

Ruthenburg, A.J., Li, H., Patel, D.J., and Allis, C.D. (2007). Multivalent engagement of chromatin modifications by linked binding modules. Nature reviews Molecular cell biology *8*, 983-994.

Saccani, S., and Natoli, G. (2002). Dynamic changes in histone H3 Lys 9 methylation occurring at tightly regulated inducible inflammatory genes. Genes & development *16*, 2219-2224.

Schall, T.J., Bacon, K., Toy, K.J., and Goeddel, D.V. (1990). Selective attraction of monocytes and T lymphocytes of the memory phenotype by cytokine RANTES. Nature *347*, 669-671.

Scheu, S., Dresing, P., and Locksley, R.M. (2008). Visualization of IFNbeta production by plasmacytoid versus conventional dendritic cells under specific stimulation conditions in vivo. Proceedings of the National Academy of Sciences of the United States of America *105*, 20416-20421.

Sen, G.L., Webster, D.E., Barragan, D.I., Chang, H.Y., and Khavari, P.A. (2008). Control of differentiation in a self-renewing mammalian tissue by the histone demethylase JMJD3. Genes & development *22*, 1865-1870.

Shen, Y., Yue, F., McCleary, D.F., Ye, Z., Edsall, L., Kuan, S., Wagner, U., Dixon, J., Lee, L., Lobanenkov, V.V.*, et al.* (2012). A map of the cis-regulatory sequences in the mouse genome. Nature *488*, 116-120.

Shi, Y. (2007). Histone lysine demethylases: emerging roles in development, physiology and disease. Nature reviews Genetics *8*, 829-833.

Shi, Y., Lan, F., Matson, C., Mulligan, P., Whetstine, J.R., Cole, P.A., Casero, R.A., and Shi, Y. (2004). Histone demethylation mediated by the nuclear amine oxidase homolog LSD1. Cell *119*, 941-953.

Shi, Y., and Whetstine, J.R. (2007). Dynamic regulation of histone lysine methylation by demethylases. Molecular cell *25*, 1-14.

Shin, S., and Janknecht, R. (2007). Activation of androgen receptor by histone demethylases JMJD2A and JMJD2D. Biochemical and biophysical research communications *359*, 742-746.
Shin, S., and Janknecht, R. (2007). Diversity within the JMJD2 histone demethylase family. Biochemical and biophysical research communications *353*, 973-977.

Simonatto, M., Barozzi, I., and Natoli, G. (2013). Non-coding transcription at cis-regulatory elements: Computational and experimental approaches. Methods.

Smale, S.T., and Fisher, A.G. (2002). Chromatin structure and gene regulation in the immune system. Annual review of immunology *20*, 427-462.

Stadler, M.B., Murr, R., Burger, L., Ivanek, R., Lienert, F., Scholer, A., van Nimwegen, E., Wirbelauer, C., Oakeley, E.J., Gaidatzis, D*., et al.* (2011). DNA-binding factors shape the mouse methylome at distal regulatory regions. Nature *480*, 490-495.

Stetson, D.B., and Medzhitov, R. (2006). Type I interferons in host defense. Immunity *25*, 373-381.

Strahl, B.D., and Allis, C.D. (2000). The language of covalent histone modifications. Nature *403*, 41-45.

Su, A.I., Wiltshire, T., Batalov, S., Lapp, H., Ching, K.A., Block, D., Zhang, J., Soden, R., Hayakawa, M., Kreiman, G*., et al.* (2004). A gene atlas of the mouse and human protein-encoding transcriptomes. Proceedings of the National Academy of Sciences of the United States of America *101*, 6062-6067.

Tachibana, M., Ueda, J., Fukuda, M., Takeda, N., Ohta, T., Iwanari, H., Sakihama, T., Kodama, T., Hamakubo, T., and Shinkai, Y. (2005). Histone methyltransferases G9a and GLP form heteromeric complexes and are both crucial for methylation of euchromatin at H3-K9. Genes & development *19*, 815-826.

Tarakhovsky, A. (2010). Tools and landscapes of epigenetics. Nature immunology *11*, 565-568.

Tateishi, K., Okada, Y., Kallin, E.M., and Zhang, Y. (2009). Role of Jhdm2a in regulating metabolic gene expression and obesity resistance. Nature *458*, 757-761.

Taverna, S.D., Li, H., Ruthenburg, A.J., Allis, C.D., and Patel, D.J. (2007). How chromatin-binding modules interpret histone modifications: lessons from professional pocket pickers. Nature structural & molecular biology *14*, 1025-1040.

Teperino, R., Schoonjans, K., and Auwerx, J. (2010). Histone methyl transferases and demethylases; can they link metabolism and transcription? Cell metabolism *12*, 321-327.

Teytelman, L., Ozaydin, B., Zill, O., Lefrancois, P., Snyder, M., Rine, J., and Eisen, M.B. (2009). Impact of chromatin structures on DNA processing for genomic analyses. PloS one *4*, e6700.

Thanos, D., and Maniatis, T. (1995). Virus induction of human IFN beta gene expression requires the assembly of an enhanceosome. Cell *83*, 1091-1100.

Thanos, D., and Maniatis, T. (1996). In vitro assembly of enhancer complexes. Methods in enzymology *274*, 162-173.

Vakoc, C.R., Mandat, S.A., Olenchock, B.A., and Blobel, G.A. (2005). Histone H3 lysine 9 methylation and HP1gamma are associated with transcription elongation through mammalian chromatin. Molecular cell *19*, 381-391.

Vakoc, C.R., Sachdeva, M.M., Wang, H., and Blobel, G.A. (2006). Profile of histone lysine methylation across transcribed mammalian chromatin. Molecular and cellular biology *26*, 9185-9195.

Verhelst, J., Parthoens, E., Schepens, B., Fiers, W., and Saelens, X. (2012). Interferon-inducible protein Mx1 inhibits influenza virus by interfering with functional viral ribonucleoprotein complex assembly. Journal of virology *86*, 13445-13455.

Villeneuve, L.M., Reddy, M.A., Lanting, L.L., Wang, M., Meng, L., and Natarajan, R. (2008). Epigenetic histone H3 lysine 9 methylation in metabolic memory and inflammatory phenotype of vascular smooth muscle cells in diabetes. Proceedings of the National Academy of Sciences of the United States of America *105*, 9047-9052.

Visel, A., Blow, M.J., Li, Z., Zhang, T., Akiyama, J.A., Holt, A., Plajzer-Frick, I., Shoukry, M., Wright, C., Chen, F*., et al.* (2009). ChIP-seq accurately predicts tissue-specific activity of enhancers. Nature *457*, 854-858.

Whetstine, J.R., Nottke, A., Lan, F., Huarte, M., Smolikov, S., Chen, Z., Spooner, E., Li, E., Zhang, G., Colaiacovo, M.*, et al.* (2006). Reversal of histone lysine trimethylation by the JMJD2 family of histone demethylases. Cell *125*, 467-481.

Yamane, K., Toumazou, C., Tsukada, Y., Erdjument-Bromage, H., Tempst, P., Wong, J., and Zhang, Y. (2006). JHDM2A, a JmjC-containing H3K9 demethylase, facilitates transcription activation by androgen receptor. Cell *125*, 483-495.

Zentner, G.E., Tesar, P.J., and Scacheri, P.C. (2011). Epigenetic signatures distinguish multiple classes of enhancers with distinct cellular functions. Genome research *21*, 1273-1283.

Zhao, M., Zhang, J., Phatnani, H., Scheu, S., and Maniatis, T. (2012). Stochastic expression of the interferon-beta gene. PLoS biology *10*, e1001249.

Zhu, Y., van Essen, D., and Saccani, S. (2012). Cell-type-specific control of enhancer activity by H3K9 trimethylation. Molecular cell *46*, 408-423.